Analysis and Fabrication of Grating Assisted Optical Components

Hui Zhang

A Thesis

in

The Department

of

Electrical & Computer Engineering

Presented in Partial Fulfilment of the Requirements

for the Degree of Master of Applied Science at

Concordia University

Montreal, Quebec, Canada

January, 1994

ISBN 0-315-90902-1

To

Andi and Jenny

Abstract

Analysis and Fabrication of Grating Assisted Optical Components

Hui Zhang

Optical wave propagation in a grating assisted coupler is analyzed and simulated. Grating assisted waveguides fabricated by proton-exchange in X cut Y propagation $LiNbO_3$ are experimentally investigated.

Marcatili's method is used to obtain the wave propagation constants and the field distributions. The dependence of power exchange on waveguide parameters in grating assisted couplers are analyzed using a matrix description. A computer software was developed using MATLAB to evaluate the properties of wave propagation in slab waveguides, channel waveguides, codirectional couplers and grating assisted couplers.

A two-step proton-exchange process was used to produce waveguides and gratings in lithium niobate. In both steps mixtures of lithium benzoate and benzoic acid were used. The grating masks with submicrometer periodicity were fabricated by means of a two-layer photoresist process. The photoresist was exposed holographically using a HeCd laser. The fabricated components were characterized and, in particular, the light intensity diffracted out into the air by the grating was measured.

Acknowledgments

I would like to thank my co-supervisor, Prof. O. Schwelb, for his guidance and patience throughout the duration of my research work and study towards Master degree, and his financial support. I also thank my co-supervisor, Prof. S. Iraj Najafi, for his supervising my research work and giving me financial support.

I am particularly gratitude to Dr. M.J. Li, for introducing me to waveguide fabrication and measurement procedures when I started the experiment, and for his many helpful suggestions and discussions during the early period of my laboratory work. I must thank Dr. W.J. Wang for his help, suggestions and discussions during all my experimental work. I also appreciate the valuable suggestions and discussions of Dr. Seppo Honkanen. All my colleagues, Paul Lefebvre, Jian-yao Chen, Guang Wen Zhang, Dr. Qing He, gave me their helpful discussions and cooperations. I would express my gratitude to them.

In addition, I would like to take this opportunity to thank Dr. J.D. Dai for his help and discussions during my study.

My indebtedness is for my parents and my brother for the most important support in this period.

My thanks must be given especially to Jenny H. Zhou, for her understanding, help and important support.

I shall remain grateful forever to Xianshu Huang, for her understanding and constant encouragement in those years.

Contents

List of Tables

List of Figures

Chapter 1

INTRODUCTION

The technology of integrated optics has been investigated and developed well and rapidly since S.E. Miller proposed the term *Integrated Optics* in 1969[11]. The basic concept of integrated optics is that planar technology can be applied to fabricate optical components. This technique leads to the possibility of an integrated optical circuit (IOC) that combines basic optical components on a single substrate. Through integration, a more compact, reliable, and functional optical system with high mechanical and thermal stability and low power consumption can be expected.

Realizability of numerous components for integrated optics have been demonstrated. Typical components include mode splitters, power dividers, filters, wavelength division multiplexers/demultiplexers, directional couplers, modulators, detectors, switches, lasers and amplifiers. Grating assisted waveguide is one of the most important elements for integrated optical circuit construction. They are used as various passive components (e.g., couplers, deflectors, reflectors, etc.), and they have many applications for functional devices of optical wave control. The grating affects the wave propagation in the waveguide through a deformation of the permittivity in the guiding

region. The grating can be made by various techniques. A periodic-corrugated grating layer, which was made photolithographically, was demonstrated by Dakss[2] and Kogelnik.[3] The periodic corrugation or topographic grating is usually made by etching of the waveguide surface.[4,5] The periodic modulation of the refractive index in the wave-guiding layer which is usually done by two diffusion steps is also an effective method to fabricate a grating.[5,6] The grating produced through acousto-optic and electro-optic effects have been widely used in various IOC components, such as modulators,[7] DFB (distributed feed-back) lasers,[8] etc.

The directional coupler is another important component used in IOC. Here the power is exchanged between two waveguides. A coupler with two identical waveguides is capable of complete power transfer in a broad frequency band. For some applications such as frequency filters, grating assisted couplers made using nonsynchronous waveguides are able to achieve frequency selective and narrow band power transfer.[9,10]

The substrate materials used in IOC include glass, compound semiconductors such as GaAs and InP, and ferroelectric crystals such as $LiNbO_3$ and $LiTaO_3$. Lithium niobate ($LiNbO_3$) has been and will continue to be a prime candidate for many integrated optics applications due to its excellent electrooptic, acoustooptic and waveguiding properties as well as its relative maturity in terms of device performance, fabrication technology, and packaging. Optical dielectric waveguides have been made by a variety of fabrication methods in lithium niobate. To achieve waveguiding, the refractive index in the guide region n_g must be greater than that of the substrate n_s and the superstrate which is generally air. The feasibility of a wide range of devices formed on lithium niobate such

as modulators, switches, polarization controllers, and ring resonators has been demonstrated in the last few years.

Proton exchange in lithium niobate was first used to fabricate optical waveguides by Jackel et al.[111] It has advantages such as low processing temperature, simple fabrication method and obtaining large surface refractive index change. The optical devices obtained by this processing method have high optical qualities, low inplane scattering, good electro-optic property and can support TM modes in Z-cut material and TE modes in X- or Y-cut material.

This thesis consists of two parts: theoretical and experimental. In the theoretical part, the grating assisted coupler is analyzed. The grating assisted coupler is treated as a four-port device and a transfer matrix description is used to relate the output power flow to input power flow. The coupling coefficient matrix contains all the information on coupling in the device. To evaluate the coupling coefficients, first the field distribution is evaluated. Next the coupling coefficients are computed by evaluating the overlap between the fields of the coupled guides. A computer program which is developed in MATLAB is used to evaluate the coupling coefficients and the output power of the grating assisted coupler.

In the experimental part, the fabrication and testing of the grating assisted waveguide made in X cut $LiNbO_3$ substrate using a two-step proton exchange technique are demonstrated. A holographic set-up is used to generate the submicron grating mask. The diffraction angles between the normal of the substrate surface and the diffracted beam are measured and the refractive indices are calculated using those values. The results are

found to be comparable with those obtained from prism coupling. This latter method is used to estimate the refractive index of channel waveguides.

Chapter 2

THEORETICAL PART

Analysis & Simulation of Grating Assisted Coupler

To understand the properties of grating assisted coupler, a theoretical analysis and computer simulation are presented in this chapter. We start from the analysis of slab waveguide with a structure of three biaxially anisotropic layers. Following Marcatili's method, the wave propagation constants and field distributions of a channel waveguide are derived. The coefficients of mode coupling in a codirectional coupler and in a grating assisted rectangular waveguide are obtained with coupled mode theory based on those results obtained in the analysis of a channel waveguide. A scattering representation for the grating assisted coupler which relates the relative power output to the coupling coefficients is given. A computer software is developed using MATLAB to evaluate the power output and its dependence on the waveguide parameters in grating assisted coupler. This computer software is also able to analyze the properties of slab waveguide, channel waveguide and codirectional coupler for given structure parameters and material parameters.

2.1 Wave propagation in step-index planar waveguides

A slab waveguide is the simplest optical component. The behaviour of the guided-wave solution of slab waveguides in anisotropic material will be discussed first because of its simple geometry. It is helpful in gaining an understanding of the waveguiding properties of more complicated structures. In this section, the field distribution and the dispersion relations of the slab waveguide are derived. The proton-exchanged slab waveguide in Z cut $LiNbO_3$ is used as the example for a numerical evaluation.

2.1.1 Wave equation

A general case in which a planar waveguide consists of three *biaxially anisotropic* layers, each aligned along their principal axes, is considered here. The permittivity tensor of each layer is *diagonal*,

$$[\varepsilon_\alpha] = \varepsilon_0 \begin{bmatrix} \varepsilon_{\alpha xx} & 0 & 0 \\ 0 & \varepsilon_{\alpha yy} & 0 \\ 0 & 0 & \varepsilon_{\alpha zz} \end{bmatrix} = \varepsilon_0 \begin{bmatrix} n_{\alpha xx}^2 & 0 & 0 \\ 0 & n_{\alpha yy}^2 & 0 \\ 0 & 0 & n_{\alpha zz}^2 \end{bmatrix} \qquad (2.1)$$

where $\varepsilon_{\omega i}$ $(i = x, y, z)$ are relative permittivity and $n_{\omega i}$ $(i = x, y, z)$ are refractive indices in x, y, z directions in region α, where $\alpha = s, f, c$ for substrate, guiding film and cover, respectively. We shall assume wave propagation in the z direction, uniformity in the y direction and a $e^{j\omega t}$ harmonic time dependence. The time dependence will be suppressed. With these assumptions, the time independent Maxwell equations in a nonmagnetic dielectric can be written as

$$j\beta E_y = -j\omega\mu_0 H_x \tag{2.2}$$

$$j\beta E_x + \frac{\partial E_z}{\partial x} = j\omega\mu_0 H_y \tag{2.3}$$

$$\frac{\partial E_y}{\partial x} = -j\omega\mu_0 H_z \tag{2.4}$$

$$j\beta H_y = j\omega\varepsilon_0\varepsilon_{xx} E_x \tag{2.5}$$

$$j\beta H_x + \frac{\partial H_z}{\partial x} = -j\omega\varepsilon_0\varepsilon_{yy} E_y \tag{2.6}$$

$$\frac{\partial H_y}{\partial x} = j\omega\varepsilon_0\varepsilon_{zz} E_z \tag{2.7}$$

The planar waveguide geometry is as shown in Fig. 2.1. The field distribution can be expressed in the form

$$\begin{bmatrix} \boldsymbol{E}(x,z) \\ \boldsymbol{H}(x,z) \end{bmatrix} = \begin{bmatrix} \boldsymbol{E}(x) \\ \boldsymbol{H}(x) \end{bmatrix} \exp[-j\beta z] \tag{2.8}$$

These equations give rise to mutually orthogonal TE and TM polarization states. The TE mode consists of the field components E_y, H_x and H_z while the TM mode has nonzero E_x, H_y and E_z. The Helmholtz equations for the TE and TM modes for anisotropic media are given in Table 2.1. The field solutions and the boundary conditions at the interface $x = 0$ and $x = d$ lead to eigenvalue equations that determine the propagation characteristics of the TE and TM modes.

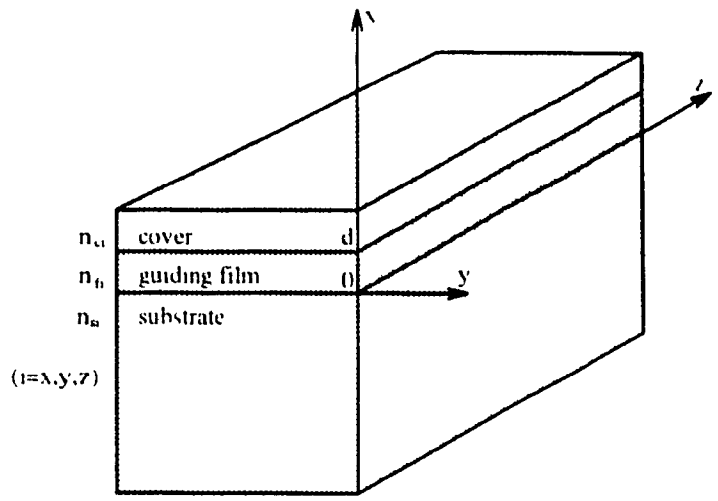

Fig.2.1 Asymmetric planar waveguide geometry

Table 2.1: Helmholtz equations and field components for TE and TM modes

TE mode $E_z = H_x = E_y = 0$	TM mode $H_z = H_x = E_y = 0$
$\frac{\partial^2 E_y}{\partial x^2} + (k_0^2 \varepsilon_{yy} - \beta^2) E_y = 0$	$\frac{\partial^2 H_y}{\partial x^2} + (k_0^2 \varepsilon_{zz} - \frac{\varepsilon_{zz}}{\varepsilon_{xx}} \beta^2) H_y = 0$
$H_x = -\frac{\beta}{\omega \mu_0} E_y$	$E_x = \frac{\beta}{\omega \varepsilon_0 \varepsilon_{xx}} H_y$
$H_z = -\frac{1}{j\omega \mu_0} \frac{\partial E_y}{\partial x}$	$E_z = \frac{1}{j\omega \varepsilon_0 \varepsilon_{zz}} \frac{\partial H_y}{\partial x}$

$\left(k_0 = \omega\sqrt{\mu_0 \varepsilon_0} = 2\pi / \lambda_0\right)$

2.1.2 Dispersion characteristics of guided modes

TM modes (H_z=0)

For guided modes, we require that the power be confined largely to the central layer of the guide. The form of the Helmholtz equation in Table 2.1 implies that the confinement will be satisfied for an oscillatory solution in the guiding film region with evanescent "tails" in the cover and substrate regions when

$$\begin{cases} k_0^2 n_{fzz}^2 - \dfrac{n_{fzz}^2}{n_{fxx}^2}\beta^2 > 0 \\ k_0^2 n_{\alpha zz}^2 - \dfrac{n_{\alpha zz}^2}{n_{\alpha xx}^2}\beta^2 < 0 \end{cases} \tag{2.9}$$

where α is either s (substrate) or c (cover), and $k_0 = \omega^2\mu_0\varepsilon_0$ is the vacuum wavenumber. These inequalities give the guidance conditions for the TM mode

$$k_0^2 n_{fxx}^2 > \beta^2 > k_0^2 n_{\alpha xx}^2 \tag{2.10}$$

From the above considerations, the field solutions are obtained by solving the Helmholtz equation in the three regions of interest

$$H_y = \begin{cases} A_1 \exp(\alpha_s x) & x \le 0 \quad \text{(substrate)} \\ B_1 \cos(k_x x + \phi) & 0 \le x \le d \quad \text{(film)} \\ C_1 \exp[\alpha_c (d - x)] & x \ge d \quad \text{(cover)} \end{cases} \tag{2.11}$$

where A_1, B_1 and C_1 are constant coefficients, the propagation and attenuation constants in the x direction in the three regions are

$$k_x^2 = k_0^2 n_{fzz}^2 - \frac{n_{fzz}^2}{n_{fxx}^2}\beta^2 \quad \text{(film)} \tag{2.12}$$

$$\alpha_s^2 = \frac{n_{szz}^2}{n_{sxx}^2}\beta^2 - k_0^2 n_{szz}^2 \qquad \text{(substrate)} \tag{2.13}$$

$$\alpha_c^2 = \frac{n_{czz}^2}{n_{cxx}^2}\beta^2 - k_0^2 n_{czz}^2 \qquad \text{(cover)} \tag{2.14}$$

respectively. The boundary condition for the tangential field component H_y at $x = 0$ and $x = d$ requires that

$$\begin{cases} A_1 = B_1 \cos(\phi) & \text{at } x=0 \\ C_1 = B_1 \cos(k_x d+\phi) & \text{at } x=d \end{cases} \tag{2.15}$$

Substitution of (2.15) into (2.11) results in

$$H_y = \begin{cases} B_1 \cos(\phi)\exp(\alpha_s x) & x \le 0 \quad \text{(substrate)} \\ B_1 \cos(k_x x+\phi) & 0 \le x \le d \quad \text{(film)} \\ B_1 \cos(k_x d+\phi)\exp[\alpha_c(d-x)] & x \ge d \quad \text{(cover)} \end{cases} \tag{2.16}$$

From the appropriate column of Table 2.1

$$E_z = \begin{cases} \dfrac{\alpha_s B_1 \cos(\phi)}{j\omega\varepsilon_0^2 n_{szz}^2}\exp(\alpha_s x) & x \le 0 \quad \text{(substrate)} \\ -\dfrac{B_1 k_x}{j\omega\varepsilon_0 n_{fzz}^2}\sin(k_x x+\phi) & 0 \le x \le d \quad \text{(film)} \\ -\dfrac{\alpha_c B_1 \cos(k_x d+\phi)}{j\omega\varepsilon_0 n_{czz}^2}\exp(\alpha_c(d-x)) & x \ge d \quad \text{(cover)} \end{cases} \tag{2.17}$$

Applying continuity of E_z at $x = 0$ and $x = d$ we find that

$$\begin{cases} \dfrac{\alpha_s B_1 \cos(\phi)}{j\omega\varepsilon_0 n_{szz}^2} = -\dfrac{k_x B_1 \sin(\phi)}{j\omega\varepsilon_0 n_{fzz}^2} & \text{at } x=0 \\ -\dfrac{B_1 k_x \sin(k_x d+\phi)}{j\omega\varepsilon_0 n_{fzz}^2} = -\dfrac{\alpha_c B_1 \cos(k_x d+\phi)}{j\omega\varepsilon_0 n_{czz}^2} & \text{at } x=d \end{cases} \tag{2.18}$$

This leads to

$$\phi = -\tan^{-1}\left(\frac{n_{fzz}^2 \alpha_s}{n_{szz}^2 k_x}\right) \tag{2.19}$$

and

$$k_x d + \phi = \tan^{-1}\left(\frac{n_{fzz}^2 \alpha_c}{n_{czz}^2 k_x}\right) \tag{2.20}$$

Using the trigonometric identity,

$$\tan(x) = \tan(x \pm m\pi) \tag{2.21}$$

where m is an integer, the TM dispersion relation for the three-layer anisotropic geometry can be obtained as,

$$\tan^{-1}\left\{\frac{n_{fzz}^2 \alpha_c}{n_{czz}^2 k_x}\right\} + \tan^{-1}\left\{\frac{n_{fzz}^2 \alpha_s}{n_{szz}^2 k_x}\right\} + m\pi = k_x d \tag{2.22}$$

Expression (2.22) which can be written as

$$2k_x d - 2\phi_c - 2\phi_s = 2m\pi \tag{2.23}$$

is the phase condition of transverse oscillations in the slab waveguide, where $2k_x d$, $-2\phi_c$ and $-2\phi_s$ are, respectively, the phase delays suffered in the film region upon reflection at the cover and upon reflection at the substrate interface.

TE mode (E_z=0)

The guidance conditions for TE mode is easily obtained

$$k_0^2 n_{fyy}^2 > \beta^2 > k_0^2 n_{\alpha yy}^2 \tag{2.24}$$

where $\alpha = s, c$ for substrate or cover. Following a similar procedure as that in the TM case, the TE field is obtained as

$$E_y = \begin{cases} B_2 \cos(\phi) \exp(\alpha_s x) & x \le 0 \quad \text{(substrate)} \\ B_2 \cos(k_x x + \phi) & 0 \le x \le d \quad \text{(film)} \\ B_2 \cos(k_x d + \phi) \exp[\alpha_c (d - x)] & x \ge d \quad \text{(cover)} \end{cases} \tag{2.25}$$

where B_2 is a constant, the propagation, attenuation and phase constants are

$$k_x^2 = k_0^2 n_{fyy}^2 - \beta^2 \qquad \text{(film)} \tag{2.26}$$

$$\alpha_s^2 = \beta^2 - k_0^2 n_{syy}^2 \qquad \text{(substrate)} \tag{2.27}$$

$$\alpha_c^2 = \beta^2 - k_0^2 n_{cyy}^2 \qquad \text{(cover)} \tag{2.28}$$

and

$$\phi = -\tan^{-1}\left(\frac{\alpha_s}{k_x}\right) \tag{2.29}$$

The dispersion relation for TE mode is,

$$\tan^{-1}\left\{\frac{\alpha_s}{k_x}\right\} + \tan^{-1}\left\{\frac{\alpha_c}{k_x}\right\} + m\pi = k_x d \tag{2.30}$$

Once again (2.30) is recognized as the phase condition for transverse resonance. By simply interchanging n_{xx} and n_{yy} (or ε_{xx} and ε_{yy}), all the results (TE and TM) in this

section can also be used if the coordinate system as shown in y slab guide in Fig. 2.5 in Section 2.2.2 is chosen. These results will be used in the channel waveguide analysis.

2.1.3 Dispersion relation of proton-exchanged $LiNbO_3$ slab waveguide

$LiNbO_3$ being uniaxial its permittivity tensor for the substrate and the proton-exchanged film region is given by,

$$[\varepsilon_\alpha] = \varepsilon_0 \begin{bmatrix} \varepsilon_{\alpha XX} & 0 & 0 \\ 0 & \varepsilon_{\alpha XX} & 0 \\ 0 & 0 & \varepsilon_{\alpha ZZ} \end{bmatrix} = \varepsilon_0 \begin{bmatrix} n_{\alpha o}^2 & 0 & 0 \\ 0 & n_{\alpha o}^2 & 0 \\ 0 & 0 & n_{\alpha e}^2 \end{bmatrix} \tag{2.31}$$

where $\alpha = s, f$ for substrate and film, respectively. The subscripts X, Y, Z refer to crystal coordinates.

Here, we consider the case where the proton exchanged waveguide is made on Z cut $LiNbO_3$. The refractive indices in the substrate and film are such that $n_{fe} > n_{se}$, and $n_{fo} < n_{so}$. If we substitute these inequality relations into (2.10) and (2.24), we find that only the TM mode can be guided in this waveguide. Rotating the crystal coordinates 90° about the y axis we get, in laboratory coordinates

$$[\varepsilon_\alpha] = \varepsilon_0 \begin{bmatrix} \varepsilon_{\alpha ZZ} & 0 & 0 \\ 0 & \varepsilon_{\alpha XX} & 0 \\ 0 & 0 & \varepsilon_{\alpha XX} \end{bmatrix} = \varepsilon_0 \begin{bmatrix} n_{\alpha e}^2 & 0 & 0 \\ 0 & n_{\alpha o}^2 & 0 \\ 0 & 0 & n_{\alpha o}^2 \end{bmatrix} \tag{2.32}$$

From (2.22) or (2.23), the dispersion relation for this structure with air cover is,

$$\phi_{s,m} + \phi_{c,m} + m\pi = \frac{n_{fo}}{n_{fe}} k_0 d \sqrt{n_{fe}^2 - n_{eff,m}^2} \tag{2.33}$$

where

$$\phi_{s,m} = \tan^{-1}\left[\frac{n_{fo} n_{fe}}{n_{so} n_{se}} \sqrt{\frac{n_{eff,m}^2 - n_{se}^2}{n_{fe}^2 - n_{eff,m}^2}} \right] \tag{2.34}$$

$$\phi_{c,m} = \tan^{-1}\left[\frac{n_{fo} n_{fe}}{n_o} \sqrt{\frac{n_{eff,m}^2 - n_0^2}{n_{fe}^2 - n_{eff,m}^2}} \right] \tag{2.35}$$

and

$$n_{eff,m} = \frac{\beta}{k_0} \tag{2.36}$$

where $n_{eff,m}$ is the effective index of refraction for mode order m. Using n_{se}=2.200, and n_{so}=2.287, $\Delta n_e = n_{fe} - n_{se} = 0.12$, $\Delta n_o = n_{fo} - n_{so} = -0.04$ and $n_c = 1$, one can generate dispersion curves for the step index planar waveguide as shown in Fig. 2.2a. The cut-off thickness normalized to the vacuum wavelength (d/λ_0) for the TM_m mode is given by,

$$\left(\frac{d}{\lambda_0}\right)_m^{TM} = \frac{1}{2\pi \frac{n_{fo}}{n_{fe}} \sqrt{n_{fe}^2 - n_{se}^2}} \left\{ m\pi + \tan^{-1}\left[\frac{n_{fo} n_{fe}}{n_0^2} \sqrt{\frac{n_{se}^2 - n_0^2}{n_{fe}^2 - n_{se}^2}} \right] \right\} \tag{2.37}$$

The region between the two dotted lines in Fig. 2.2a is the single mode region. From (2.33) - (2.36), one can find the total number of modes ($M = m + 1$) supported by a given waveguide of core dimension d

$$M = \mathrm{Int}\left\{1 + \frac{1}{\pi}\left[\frac{n_{fo}}{n_{fe}} k_0 d\sqrt{n_{fe}^2 - n_{se}^2} - \tan^{-1}\left(\frac{n_{fo} n_{fe}}{n_0^2}\sqrt{\frac{n_{se}^2 - n_0^2}{n_{fe}^2 - n_{se}^2}}\right)\right]\right\} \quad \textbf{(2.38)}$$

where Int refers to integer part. From (2.37), the width of the single mode range is given by

$$\Delta\left(\frac{d}{\lambda_0}\right) = \frac{1}{2}\frac{n_{fe}/n_{fo}}{\sqrt{n_{fe}^2 - n_{se}^2}} \quad \textbf{(2.39)}$$

For the parameters given above, $\Delta(d/\lambda_0) = 0.7$.

For X cut $LiNbO_3$, the index tensor is

$$[n_\alpha] = \begin{bmatrix} n_{\alpha o}^2 & 0 & 0 \\ 0 & n_{\alpha e}^2 & 0 \\ 0 & 0 & n_{\alpha o}^2 \end{bmatrix} \quad \textbf{(2.40)}$$

This configuration can support only TE modes. The dispersion curves are shown in Fig. 2.2b

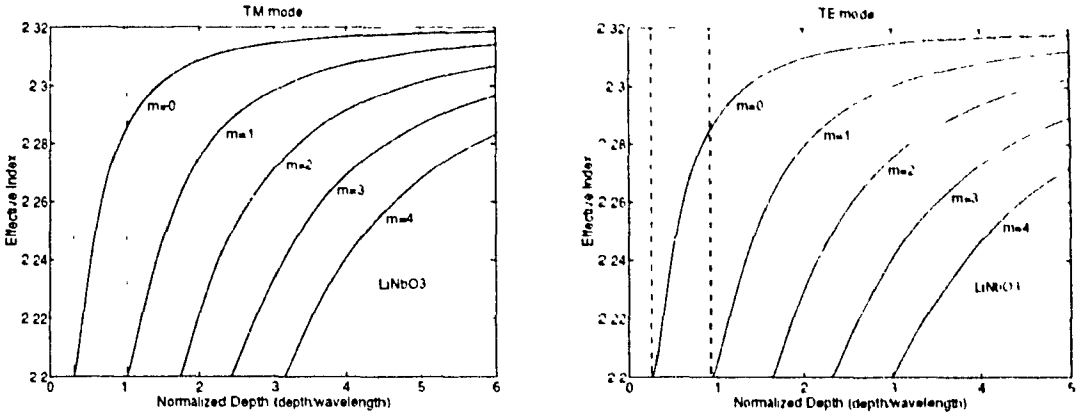

(a) (b)

Fig. 2.2 Dispersion curves for step-index $LiNbO_3$ slab waveguide. $\Delta n_e = 0.12$, $\Delta n_o = -0.04$. (a) TM mode in Z cut (b) TE mode in X cut

2.2 Wave propagation in dielectric channel waveguides

In this section, the wave propagation in dielectric channel waveguides is discussed. Marcatili's method is applied in the analysis. The guiding modes are divided into two groups, namely E^{x}_{pq} modes (polarized in x direction) and E^{y}_{pq} modes (polarized in y direction). Expressions for dispersion and field distribution are given. Numerical results for $LiNbO_3$ are presented as an example.

2.2.1 Introduction

In most integrated optics applications it is expected that optical waveguides consist of a rectangular or a near rectangular dielectric core embedded in a dielectric medium of slightly lower refractive index. Fig. 2.3 shows the geometry of a rectangular dielectric channel waveguide. This kind of waveguide can serve not only as a transmission medium to confine and to transmit optical signals, but also as the basic building block for components in integrated optical circuits such as filters, directional couplers, y junctions, etc.

An exact analytical treatment of this waveguide is made difficult by the boundary matching requirement at the corners of the channel. Approximate numerical solutions have been obtained by Marcatili,[12] Goell,[13] Schlosser,[14] and others. Marcatili developed an approximate analytical approach with sinusoidal variation in the core region and exponentially decaying fields in the adjacent medium, neglecting the regions shown in Fig. 2.4 which are shaded. This method is therefore called the method of field shadows.

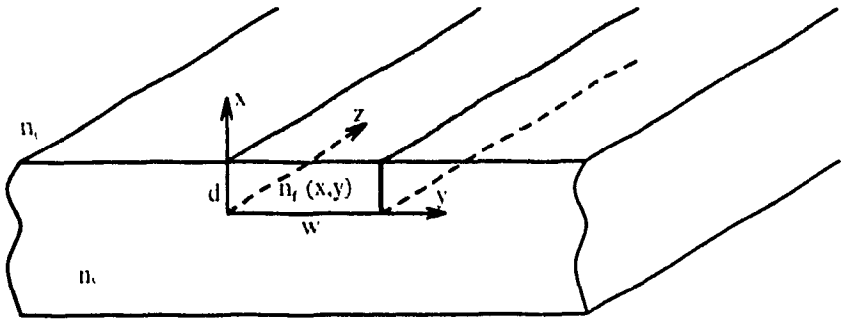

Fig. 2.3 Dielectric channel waveguide geometry

In each region of Fig. 2.4, a single propagating mode is used, and the tangential field components are matched at boundaries. This method is relatively simple to formulate for numerical evaluation. As a result of this assumption, Marcatili's approximation loses its validity near cut-off, where the field distribution extends deep into the regions surrounding the core. When the waveguide is far from cut-off, the results of Marcatili's method is sufficiently accurate for most practical purposes[10,13]. Some improvement can be used to increase the accuracy especially when the modes are near cut-off.[13,19]

In this section, we shall follow Marcatili's method using the results obtained in

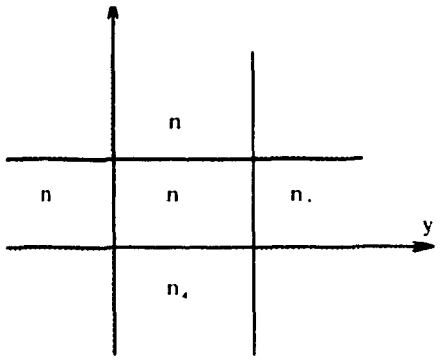

Fig. 2.4 Regions of a channel waveguide in Marcatili's analysis

Section 2.1. To analyze the characteristics of a channel waveguide, its cross-section is subdivided into nine regions, as shown in Fig. 2.4. In accordance with Marcatili's basic assumption, the energy flow in the shaded regions will be neglected. We shall investigate a channel waveguide fabricated in Z cut $LiNbO_3$, a uniaxial, anisotropic medium, oriented so that the principal axes of the crystal coincide with the axes of the laboratory coordinates. For simplification of analysis, the index profile of the waveguide is chosen as a step profile and the material is assumed lossless.

2.2.2 Marcatili's method of field shadows

Let us consider an embedded channel waveguide of rectangular cross section as shown in Fig. 2.3. First we consider the case of biaxial media and the refractive index tensor only has diagonal non-zero components

$$n_\alpha = \begin{bmatrix} n_{\alpha xx} & 0 & 0 \\ 0 & n_{\alpha yy} & 0 \\ 0 & 0 & n_{\alpha zz} \end{bmatrix} \tag{2.41}$$

in which $\alpha = c, f, s$ for cover, guiding film layer and substrate, respectively. The solution to this channel waveguide is assumed to be the superposition of solutions of the orthogonal slab waveguides shown in Fig. 2.5. One is x slab guide, where the interface normal is in the x direction. Another is y slab guide with the interface normal in the y direction. In the x slab guide, the refractive indices for the substrate, film and cover are given by

$$n^x(x) = \begin{cases} n_s & x \le 0 \\ n_f & 0 \le x \le d \\ n_0 & x \ge d \end{cases} \qquad (2.42)$$

where n_s, n_f and n_0 are diagonal matrices of the form given by (2.41). Similarly in y slab guide

$$n^y(y) = \begin{cases} n_s & y \le 0 \\ n_f & 0 \le y \le w \\ n_s & y \ge w \end{cases} \qquad (2.43)$$

Superscripts x and y refer to the x and y slab guides, respectively. The appropriate refractive index of each region of the channel waveguide can be obtained by superposing the indices of the two slab guides. Thus

$$n^2(x,y) \approx [n^x(x)]^2 + [n^y(y)]^2 - n_f^2 \qquad (2.44)$$

where $n^2(x,y)$ is also a diagonal matrix, whose three components are

$$\begin{aligned} n_1^2 &= [n_{xx}^x]^2 + [n_{xx}^y]^2 - n_{fxx}^2 \\ n_2^2 &= [n_{yy}^x]^2 + [n_{yy}^y]^2 - n_{fyy}^2 \\ n_3^2 &= [n_{zz}^x]^2 + [n_{zz}^y]^2 - n_{fzz}^2 \end{aligned} \qquad (2.45)$$

The refractive indices in the shadow regions are unspecified and the fields in these regions are disregarded.

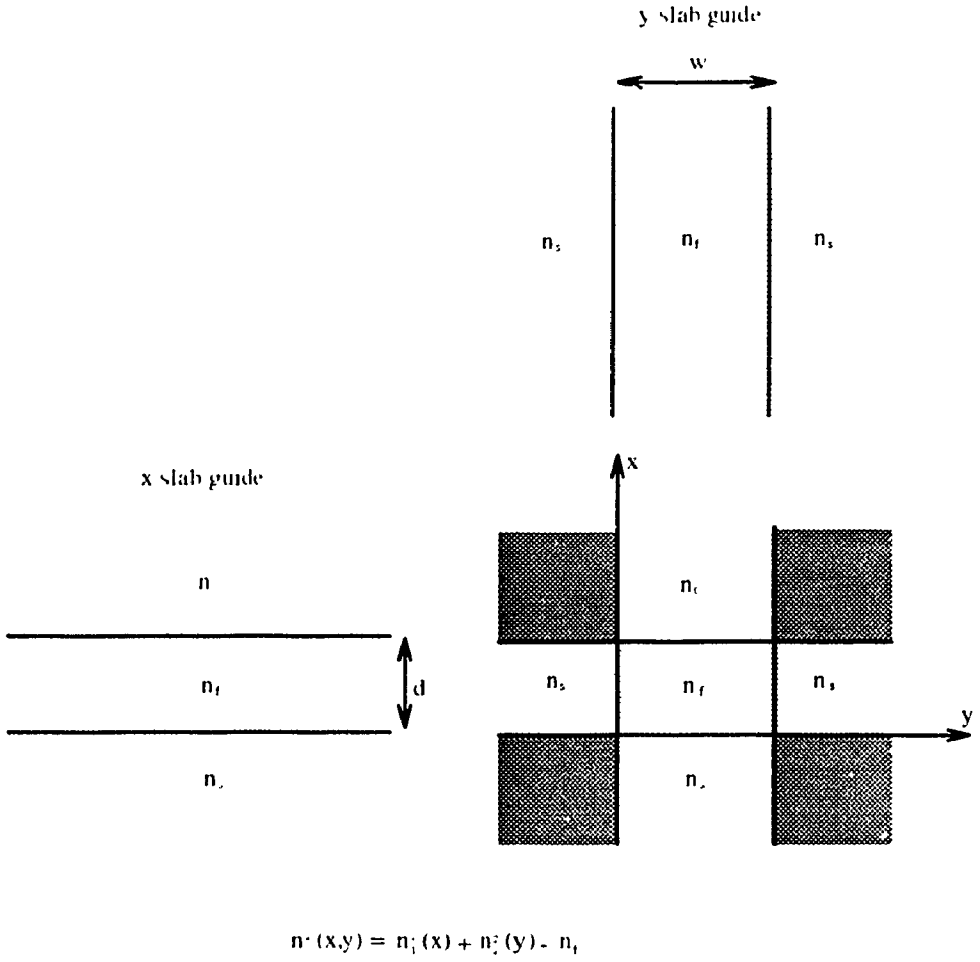

Fig. 2.5 Subdivision of the channel waveguide into slab waveguides according to the method of field shadows. The surface normals of x and y slab guides are in the x and y directions, respectively.

The modes supported by the waveguide with the structure mentioned above are hybrid modes, and can be grouped into two sets, E^y_{pq} modes and E^y_{pq} modes, by satisfying the boundary conditions in the channel waveguide. E^x_{pq} modes polarize predominantly in the x direction and the principal field components are E_x and H_y. E^y_{pq} modes polarize predominantly in the y direction with principal field components E_y and H_x. In both cases

the subscripts x and y refer to the x and y directions and the subscripts p, q refer to mode number, respectively. In the following we analyze the propagation properties of E^{x}_{pq} modes, and find the expressions of field distributions. The results of E^{y}_{pq} modes are also given and they are obtained by the similar analysis method for E^{x}_{pq}.

E^{x}_{pq} modes (polarized in x direction)

The principal transverse field components of E^{x}_{pq} modes are E_x and H_y with E_y 0. We will find the expressions of the fields, E_x, H_y, H_x, E_z and H_z through solving Helmholtz equations in both x and y directions.

When the channel waveguide is subdivided into x and y slab guides, it can be found that E^{x}_{pq} modes are corresponding to the TM modes in the x slab guide, and to the TE modes in y slab guide. By using separation of variables, the field function E_x is written as a product of plane wave solutions. Thus

$$\begin{aligned} E_x(x,y,z) &= E_x(x,y)\, e^{-j\beta z} \\ &= e_x^x(x)\, e_x^y(y)\, e^{-j\beta z} \end{aligned} \tag{2.46}$$

$e_x^{x}(x)$ and $e_x^{y}(y)$ satisfy the equations,

$$\left\{ \frac{d^2}{dx^2} + \left[k_0^2 \left(n_{zz}^x\right)^2 - \frac{\left(n_{zz}^x\right)^2}{\left(n_{xx}^x\right)^2} (\beta^x)^2 \right] \right\} e_x^x(x) = 0 \quad \text{(in x slab)} \tag{2.47}$$

and

$$\left\{\frac{d^2}{dy^2} + \left[k_0^2(n_{xx}^y)^2 - (\beta^y)^2\right]\right\} e_x^y(y) = 0 \qquad \text{(in y slab)} \tag{2.48}$$

obtained from solving Maxwell's equations as in the Appendix, and using (2.45). In these expressions, $e_x^x(x)$ and $e_x^y(y)$ are the waveguide modes and β^x and β^y are the corresponding z directed propagation constants in the x and y slab guides, respectively. The propagation constant β of the channel waveguide in the z direction can be determined from β^x and β^y using the expression

$$\beta^2 = (\beta^x)^2 + (\beta^y)^2 - k_0 n_{fxx}^2 \tag{2.49}$$

From the results in Section 2.1.2, the solutions of the Helmholtz equations (2.47), (2.48) are

$$e_x^x(x) = \begin{cases} B^x \cos(\phi^x) \exp(\alpha_s^x x) & x \le 0 \\ B^x \cos(k_x x + \phi^x) & 0 \le x \le d \\ B^x \cos(k_x d + \phi^x) \exp(\alpha_c^x (d-x)) & x \ge d \end{cases} \tag{2.50}$$

for x slab guide,

$$e_x^y(y) = \begin{cases} B^y \cos(\phi^y) \exp(\alpha_s^y y) & y \le 0 \\ B^y \cos(k_y y + \phi^y) & 0 \le y \le w \\ B^y \cos(k_y w + \phi^y) \exp\left[\alpha_c^y (w-y)\right] & y \ge w \end{cases} \tag{2.51}$$

for y slab guide, where the attenuation constants α_c^x, α_s^x, α_c^y, α_s^y and propagation constants k_x, k_y, are defined, respectively, by

$$(\alpha_\alpha^x)^2 = \frac{n_{\alpha zz}^2}{n_{\alpha xx}^2}(\beta^x)^2 - k_0^2 n_{\alpha zz}^2 \tag{2.52}$$

$$(\alpha_s^y)^2 = (\alpha_c^y)^2 = (\beta^y)^2 - k_0^2 n_{sxx}^2 \tag{2.53}$$

for the covers and substrate, subscript $\alpha = c, s$, and

$$k_x^2 = k_0^2 n_{fzz}^2 - \frac{n_{fzz}^2}{n_{fxx}^2}(\beta^x)^2 \tag{2.54}$$

$$k_y^2 = k_0^2 n_{fxx}^2 - (\beta^y)^2 \tag{2.55}$$

for the guiding film regions. The phase parameters ϕ^x and ϕ^y are obtained from the complex reflection coefficient of the boundary as in section 2.1. Thus

$$\phi^x = -\tan^{-1}\left(\frac{n_{fzz}^2 \alpha_s^x}{n_{szz}^2 k_x}\right) \tag{2.56}$$

$$\phi^y = -\tan^{-1}\left(\frac{\alpha_s^y}{k_y}\right) \tag{2.57}$$

The propagation constants β^x and β^y are the solutions of the transcendental equations which can be found by matching boundary conditions at $x = 0, d$, and $y = 0, w$,

$$\tan^{-1}\left\{\frac{n_{fzz}^2 \alpha_c^x}{n_{czz}^2 k_x}\right\} + \tan^{-1}\left\{\frac{n_{fzz}^2 \alpha_s^x}{n_{szz}^2 k_x}\right\} + p\pi = k_x d \tag{2.58}$$

$$2\tan^{-1}\left\{\frac{\alpha_s^y}{k_y}\right\} + q\pi = k_y w \tag{2.59}$$

The guidance condition for the channel waveguide is obtained from (2.52) - (2.55) by the condition that the modal field in x and y slab guides should be oscillatory in the guiding

region and evanescent in the cover and substrate. This condition requires that

$$k_0^2 n_{axx}^2 < (\beta^x)^2,\ (\beta^y)^2 < k_0^2 n_{fxx}^2 \tag{2.60}$$

The effective index n_{eff} of channel guide is obtained by

$$\begin{aligned} n_{eff}^2 &= \frac{(\beta^x)^2}{k_0^2} + \frac{(\beta^y)^2}{k_0^2} - n_{fxx}^2 \\ &= (n_e^x)^2 + (n_e^y)^2 - n_{fxx}^2 \end{aligned} \tag{2.61}$$

where n_e^x and n_e^y are the effective indices in x and y slab guides, respectively. Using (2.50) and (2.51), the modal field of the channel guide $E_x(x,y)$ is obtained by

$$E_x(x,y) = E_{x0}\Psi(x,y) \tag{2.62}$$

where E_{x0} is the amplitude constant with unit of V/m and the field pattern function is

$$\Psi(x,y) = \begin{cases} \cos(k_x x+\phi^x)\cos(k_y y+\phi^y) & \nu=1 \\ \cos(k_x d+\phi^x)\cos(k_y y+\phi^y)\exp[\alpha_c^x(d-x)] & \nu=2 \\ \cos(k_y w+\phi^y)\cos(k_x x+\phi^x)\exp[\alpha_s^y(w-y)] & \nu=3 \\ \cos(\phi^x)\cos(k_y y+\phi^y)\exp(\alpha_s^x x) & \nu=4 \\ \cos(\phi^y)\cos(k_x x+\phi^x)\exp(\alpha_s^y y) & \nu=5 \end{cases} \tag{2.63}$$

where $\nu = 1 \sim 5$ represents the five regions as in Fig. 2.4. All other field components are obtained from E_x through Maxwell's equations:

$$E_z = -\frac{jn_1^2}{\beta n_3^2}\frac{\partial E_x}{\partial x} \tag{2.64}$$

$$H_x = \frac{1}{\beta\omega\mu_0}\frac{\partial^2 E_x}{\partial x \partial y} \tag{2.65}$$

$$H_y = \frac{1}{\beta \omega \mu_0}\left(k_0^2 n_1^2 E_x + \frac{\partial^2 E_x}{\partial y^2}\right) \tag{2.66}$$

$$H_z = \frac{1}{j\omega\mu_0}\frac{\partial E_x}{\partial y} \tag{2.67}$$

where n_1 and n_3 are defined in (2.45). Since $\{k_x, k_z\} << \{\beta, \omega\mu_0\}$, the longitudinal field components E_z and H_z and transverse component H_x are much smaller than the transverse components E_x and H_y.

E^y_{pq} modes (polarized in y direction)

The principal transverse field components of the E^y_{pq} modes are E_y and H_x with $E_x = 0$. These modes correspond to TE modes in the x slab guide, and to TM modes in y slab guide. The similar expressions are obtained by the same method as that for E^x_{pq} modes. Here the expressions are listed directly.

Using the same procedures as in the previous section, the modal field pattern for $E_y(x,y)$ of the channel guide is given by (2.63), while the attenuation and the propagation constants α_c^y, α_s^y, α_c^y, α_s^y, k_x, k_y, and the phase parameters ϕ^y, ϕ^y are defined in (2.52) - (2.55), except that x and y, and d and w are interchanged. β^y and β^y are the solutions of the transcendental equations

$$\tan^{-1}\left\{\frac{\alpha_c^x}{k_x}\right\} + \tan^{-1}\left\{\frac{\alpha_s^x}{k_x}\right\} + p\pi = k_x d \tag{2.68}$$

$$2\tan^{-1}\left\{\frac{n_{fzz}^2\alpha_s^y}{n_{szz}^2 k_y}\right\} + q\pi = k_y w \tag{2.69}$$

The propagation constants β^x, β^y and effective indices n_e^x, n_e^y of slab guides determine the corresponding quantities β and n_{eff} of the channel guide by

$$\beta^2 = (\beta^x)^2 + (\beta^y)^2 - k_0^2 n_{fyy}^2 \tag{2.70}$$

$$n_{eff}^2 = \left(n_e^x\right)^2 + \left(n_e^y\right)^2 - n_{fyy}^2 \tag{2.71}$$

The guidance condition is

$$k_0^2 n_{\alpha yy}^2 < (\beta^x)^2,\ (\beta^y)^2 < k_0^2 n_{fyy}^2 \tag{2.72}$$

The other four field components are obtained from $E_y(x,y)$ through Maxwell's equations,

$$E_z = -\frac{jn_2^2}{\beta n_3^2}\frac{\partial E_y}{\partial y} \tag{2.73}$$

$$H_x = -\frac{1}{\beta\omega\mu_0}\left(k_0^2 n_2^2 E_y + \frac{\partial^2 E_y}{\partial x^2}\right) \tag{2.74}$$

$$H_y = -\frac{1}{\beta\omega\mu_0}\frac{\partial^2 E_y}{\partial x \partial y} \tag{2.75}$$

$$H_z = \frac{1}{j\omega\mu_0}\frac{\partial E_y}{\partial x} \tag{2.76}$$

Here also $\{E_z, H_z, H_y\} << \{E_y, H_x\}$

2.2.3 Normalization of the modal field

The normalization for the modal field for E^{y}_{pq} modes is discussed here. Similar results for E^{x}_{pq} modes can be obtained from the same procedures.

The power carried in the z direction by the E^{y}_{pq} mode is obtained from the surface integral

$$P = \frac{1}{2}\int_{-\infty}^{\infty}\int_{-\infty}^{\infty} E_x(x,y)\cdot H_y(x,y)\,dxdy \tag{2.77}$$

Substituting (2.62) and (2.66) into (2.77) and using (2.45), we have

$$P = \frac{E_{x0}^2}{2\omega\mu_0\beta}\int_{-\infty}^{\infty}\int_{-\infty}^{\infty} \Psi\left(k_0^2 n_1^2\Psi + \frac{\partial^2\Psi}{\partial y^2}\right) dxdy \tag{2.78}$$

where P is in the unit of W, and E_{x0} is in V/m. The integrand can be simplified. From (2.45), the index distribution is

$$n_1^2 = \begin{cases} n_{fxx}^2+n_{fxx}^2-n_{fxx}^2 = n_{fxx}^2 & \nu=1 \\ n_{cxx}^2+n_{fxx}^2-n_{fxx}^2 = n_{cxx}^2 & \nu=2 \\ n_{fxx}^2+n_{sxx}^2-n_{fxx}^2 = n_{sxx}^2 & \nu=3 \\ n_{sxx}^2+n_{fxx}^2-n_{fxx}^2 = n_{sxx}^2 & \nu=4 \\ n_{fxx}^2+n_{sxx}^2-n_{fxx}^2 = n_{sxx}^2 & \nu=5 \end{cases} \tag{2.79}$$

where ν is the waveguide region index. The field distribution pattern can be separated in x and y directions into functions determined by $\partial^2\Psi(x,y)/\partial y^2 = -k_{y\nu}^2\Psi(x,y)$. Then using (2.53), (2.55) and (2.63), the attenuation and propagation constants in y direction are found to be

$$k_{yv}^2 = k_0^2 \begin{cases} n_{fxx}^2 - (n_e^{yv})^2 & v = 1, 2, 4 \\ (n_e^{yv})^2 - n_{sxx}^2 & v = 3, 5 \end{cases} \tag{2.80}$$

Subtracting (2.80) from (2.79),

$$k_0^2 n_1^2 - k_{yv}^2 = (\beta^{yv})^2 C_{0v} \tag{2.81}$$

where

$$(\beta^{yv})^2 = k_0^2 (n_e^{yv})^2 \tag{2.82}$$

and

$$C_{0v} = \begin{cases} 1 & v = 1 \\ 1 - \dfrac{n_{fxx}^2 - n_{cxx}^2}{(n_e^{yv})^2} & v = 2 \\ -1 + 2\dfrac{n_{sxx}^2}{(n_e^{yv})^2} & v = 3 \\ 1 - \dfrac{n_{fxx}^2 - n_{sxx}^2}{(n_e^{yv})^2} & v = 4 \\ -1 + 2\dfrac{n_{sxx}^2}{(n_e^{yv})^2} & v = 5 \end{cases} \tag{2.83}$$

C_{0v} is a constant in each range. As a result, (2.78) can be expressed as

$$P = \frac{(\beta^{yv})^2}{2\omega\mu_0\beta} E_{x0}^2 \int_{-\infty}^{\infty}\int_{-\infty}^{\infty} C_{0v} \Psi^2 \, dxdy \tag{2.84}$$

The normalized field coefficient is

$$E_{x0}^2 = \frac{2\omega\mu_0\beta' P}{(\beta')^2 \int_{-\infty}^{\infty}\int_{-\infty}^{\infty} C_{0v}\Psi^2\, dxdy} \qquad (2.85)$$

As the width of the channel waveguide tends to infinity, $\beta' \rightarrow \beta$ and (2.85) converges to the result obtained for the slab waveguide.

For E'_{pq} modes, a similar result for E_{y0} can be obtained using the expressions (2.83) to (2.85) and replacing n_{fx}, n_{sx}, n_{cx}, n_e' and β' with n_{fy}, n_{sy}, n_{cy}, n_e' and β', respectively.

2.2.4 Dispersion curve of proton exchanged waveguide in $LiNbO_3$

We study the properties of a waveguide in Z cut $LiNbO_3$. From the guidance conditions described in Section 2.2.2, and from the considerations given in section 2.1.3, we know that only E'_{pq} modes exist in Z cut $LiNbO_3$. Using (2.32) and letting $n_c = n_0 = 1$, we can simplify the results obtained above. Thus for the E'_{pq} mode, the attenuation and propagation constants as well as the phase constants in x and y slab guides are

$$\alpha_a^x = k_0 \frac{n_{ao}}{n_{ae}} \sqrt{(n_e^x)^2 - n_{ae}^2} \qquad (2.86)$$

$$k_x = k_0 \frac{n_{fo}}{n_{fe}} \sqrt{n_{fe}^2 - (n_e^x)^2} \qquad (2.87)$$

$$\phi^x = -\tan^{-1}\left(\frac{n_{fe}n_{fo}}{n_{se}n_{so}}\sqrt{\frac{(n_e^x)^2-n_{se}^2}{n_{fe}^2-(n_e^x)^2}} \right) \tag{2.88}$$

$$\alpha_s^y = k_0\sqrt{(n_e^y)^2 - n_{se}^2} \tag{2.89}$$

$$k_y = k_0\sqrt{n_{fe}^2 - (n_e^y)^2} \tag{2.90}$$

$$\phi^y = -\tan^{-1}\left(\sqrt{\frac{(n_e^y)^2-n_{se}^2}{n_{fe}^2-(n_e^y)^2}} \right) \tag{2.91}$$

in which n_e^x and n_e^y are solutions of the transcendental equations

$$\begin{aligned} \frac{n_{fo}}{n_{fe}}\sqrt{n_{fe}^2-(n_e^x)^2}\,k_0 d = p\pi &+ \tan^{-1}\left\{ \frac{n_{fe}n_{fo}}{n_{se}n_{so}}\sqrt{\frac{(n_e^x)^2-n_{se}^2}{n_{fe}^2-(n_e^x)^2}} \right\} \\ &+ \tan^{-1}\left\{ n_{fe}n_{fo}\sqrt{\frac{(n_e^x)^2-1}{n_{fe}^2-(n_e^x)^2}} \right\} \end{aligned} \tag{2.92}$$

$$\sqrt{n_{fe}^2-(n_e^y)^2}\,k_0 w = q\pi + 2\tan^{-1}\left\{ \sqrt{\frac{(n_e^y)^2-n_{se}^2}{n_{fe}^2-(n_e^y)^2}} \right\} \tag{2.93}$$

The numerical results are given using the parameters $n_{se} = 2.200$, $n_{so} = 2.287$, $\Delta n_e = n_{fe} - n_{se} = 0.12$, and $\Delta n_o = n_{fo} - n_{so} = -0.04$. Fig. 2.6(a,b,c) are the dispersion curves for different modes for the waveguide width to depth ratio $R = w/d = 1$, 2, and 4. Fig. 2.6d shows the dispersion curves of the fundamental mode ($p,q = 0,0$) for $R = 1$, 2, 4, 10, and ∞. It is obvious that, when $R \geq 10$, the dispersion relation of a rectangular waveguide is very close to that of a slab waveguide. Fig. 2.7(a,b) show the modal field pattern in the cross-section of the waveguide for modes $p,q = 0,0$ and $p,q = 0,1$ with $d = \lambda$ and $R = 2$.

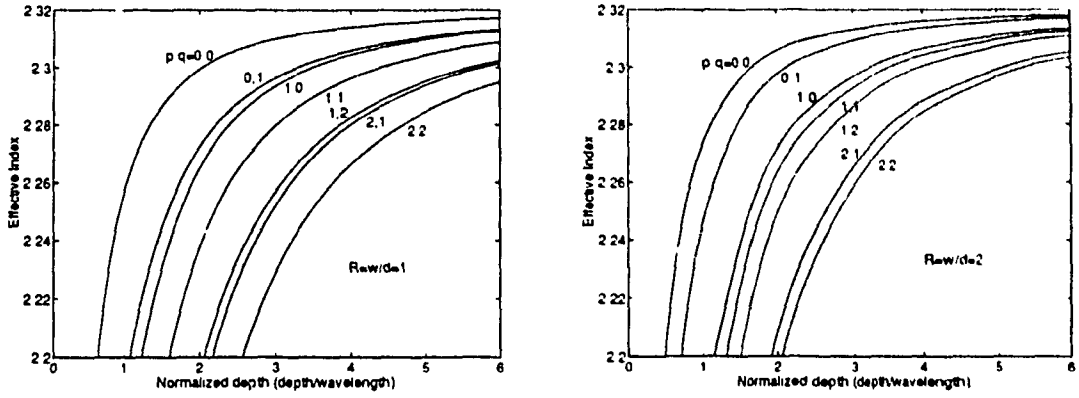

(a) (b)

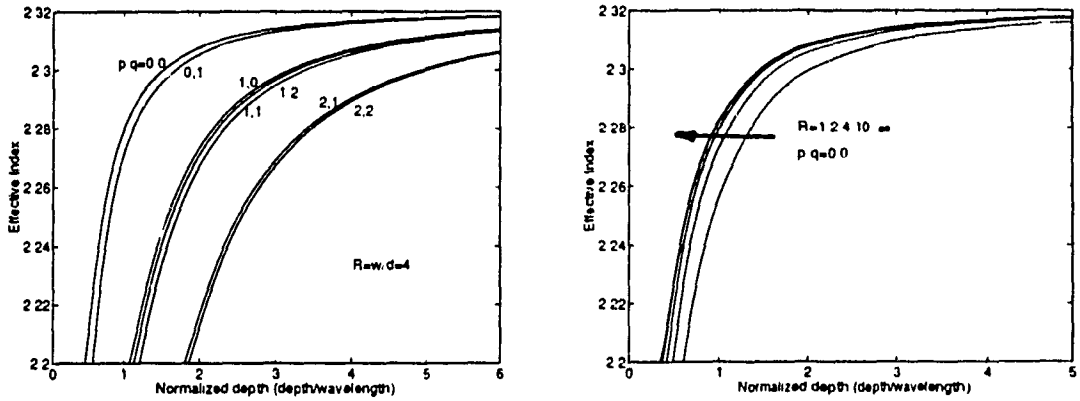

(c) (d)

Fig. 2.6 Dispersion curves for channel waveguides p,q mode in Z cut $LiNbO_3$, $\Delta n_e = 0.12$, $\Delta n_o = -0.04$: (a) $R = 1$, (b) $R = 2$, (c) $R = 4$, and (d) $p,q = 0,0$, $R = 1, 2, 4, 10$ and ∞

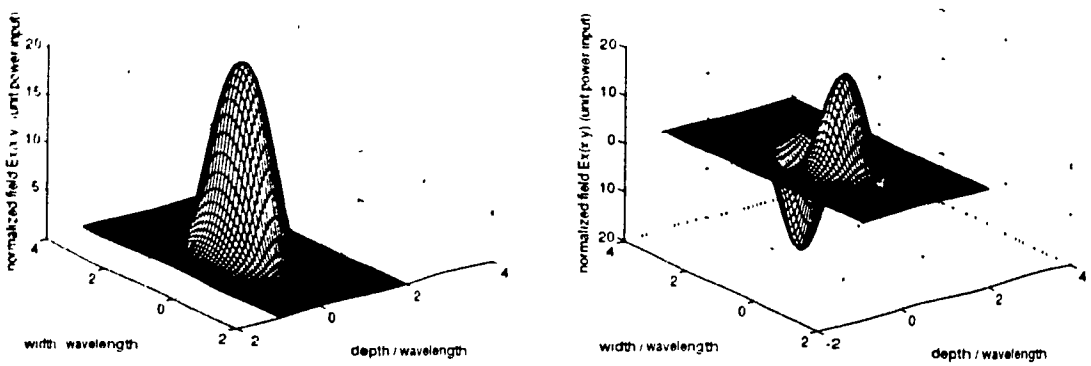

(a) (b)

Fig. 2.7 Modal field pattern in a channel waveguide, $d=\lambda$, $R=w/d=2$:
(a) $p,q = 0,0$ (b) $p,q = 0,1$

2.3 Mode coupling between two parallel channel waveguides

Let us consider two fundamental modes in both waveguides A and B as shown in Fig. 2.8a. When they are sufficiently separated from each other, the fundamental modes, A and B, propagate independently with field patterns $\boldsymbol{E}_A(x,y)$ and $\boldsymbol{E}_B(x,y)$, and with propagation constants β_A and β_B, respectively. Here subscripts A and B refer to guiding modes A and B. When the waveguides are brought into proximity, than the overlay of evanescent field will cause interferential coupling. As a result the power of the guided mode will be coupled from one guide to the adjacent guide.

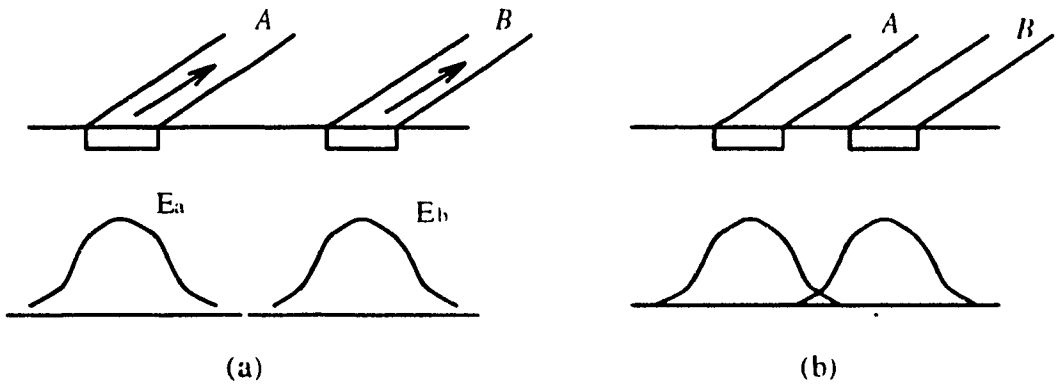

Fig. 2.8 Guided modes in two parallel waveguides in the absence and presence of coupling

The wave propagation in such a composite structure can be represented by the exact solutions of the guided modes from Maxwell's equations, or wave equations. To solve the wave equation for a composite waveguide structure is usually difficult, and the closed form solution is often not available. An easier way to get the solution for a weakly perturbed system is from the coupled-mode analysis (or perturbation theory). Here the electric field is represented by a linear combination of the unperturbed guided modes with varying amplitudes. Variation of the amplitudes with distance indicates the

transfer of energy between the unperturbed modes. In this section, the mode coupling between two parallel rectangular waveguides is treated by coupled-mode theory. Let $\boldsymbol{E}_A(x,y)\exp[i(\omega t-\beta_A z)]$ and $\boldsymbol{E}_B(x,y)\exp[i(\omega t-\beta_B z)]$ be the modes of propagation of the individual waveguides when they are far apart, where electric field distributions $\boldsymbol{E}_A(x,y)$, $\boldsymbol{E}_B(x,y)$ and propagation constants β_A, β_B were obtained in the previous section for a given waveguide (i.e., fixed dimensions, refractive indices). Assuming that waves propagate only in the forward direction, the electric field in the coupled-guide structure can be approximated by a linear combination of the two independent original modes[20,21]

$$\begin{aligned}\boldsymbol{E}(x,y,z,t) = {} & A(z)\,\boldsymbol{E}_A(x,y)\,e^{j(\omega t-\beta_A z)} \\ & + B(z)\,\boldsymbol{E}_B(x,y)\,e^{j(\omega t-\beta_B z)}\end{aligned} \tag{2.94}$$

provided the two waveguides are not too close to each other. If coupling between guides A and B is reduced to zero, $A(z)$ and $B(z)$ are reduced to two constants and the coupled modes are reduced to two independent original modes. The refractive index distribution in this structure is presented as

$$n^2(x,y) = n_s^2 + \Delta n_A^2(x,y) + \Delta n_B^2(x,y) \tag{2.95}$$

where $\Delta n_A^2(x,y)$ and $\Delta n_B^2(x,y)$ represents the presence of waveguides A and B and both vanish except at the cores of waveguides A and B, respectively, as shown in Fig. 2.9. The local transverse field distribution of the guided modes $E_{A,B}$ and the local propagation constants $\beta_{A,B}$ are linked by the equation of

$$\left[\nabla_T^2 + k_0^2\left(n_s^2 + \Delta n_\alpha^2\right)\right]\boldsymbol{E}_\alpha(x,y) = \beta_\alpha^2\,\boldsymbol{E}_\alpha(x,y) \tag{2.96}$$

where subscript $\alpha = A, B$ and $\nabla_T^2 = \partial^2/\partial x^2 + \partial^2/\partial y^2$. The total electric field (2.94) must

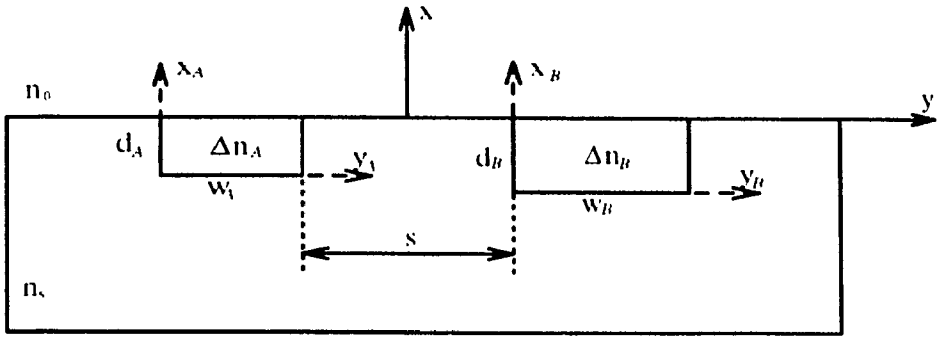

Fig. 2.9 Coupled dissimilar channel waveguide geometry

obey the scalar wave equation

$$\left[\nabla^2 + k_0^2\left(n_s^2(x,y) + \Delta n_A^2(x,y) + \Delta n_B^2(x,y)\right)\right]\boldsymbol{E}(x,y,z) = 0 \qquad (2.97)$$

The coupling between the two waveguides can be described by the coupled equations for the varying amplitudes which can be obtained by substitution of (2.95) and (2.96) into the three dimensional Helmholtz equation (2.97),[20] and by using the assumption of slow variation of mode amplitudes over z. After some manipulation, these lead to

$$\begin{aligned} &-2j\beta_A\frac{dA(z)}{dz}E_A(x,y)\,e^{j(\omega t-\beta_A z)} - 2j\beta_B\frac{dB(z)}{dz}E_B(x,y)\,e^{j(\omega t-\beta_B z)} \\ &= -k_0^2\left[\Delta n_B^2(x,y)\,A(z)\,E_A(x,y)\,e^{j(\omega t-\beta_A z)} - \Delta n_A^2(x,y)\,B(z)\,E_B(x,y)\,e^{j(\omega t-\beta_B z)}\right] \end{aligned} \qquad (2.98)$$

Then taking the scalar product of (2.98) with $\boldsymbol{E}_A^*(x,y)$ and $\boldsymbol{E}_B^*(x,y)$, respectively, and integrating over all x and y leads to the coupled mode equations

$$\begin{cases} \dfrac{dA(z)}{dz} = -j\kappa_{AB}B(z)\,e^{j(\beta_A-\beta_B)z} - j\kappa_{AA}A(z) \\ \dfrac{dB(z)}{dz} = -j\kappa_{BA}A(z)\,e^{-j(\beta_A-\beta_B)z} - j\kappa_{BB}B(z) \end{cases} \qquad (2.99)$$

where

$$\kappa_{ij} = \frac{k_0^2}{2\beta_i} \frac{\iint \boldsymbol{E}_i^*(x,y) \cdot \Delta n_i^2(x,y)\, \boldsymbol{E}_j(x,y)\, dxdy}{\int_{-\infty}^{\infty}\int_{-\infty}^{\infty} \boldsymbol{E}_i^2(x,y)\, dxdy} \tag{2.100}$$

where $i, j = A, B$. κ_{AA} and κ_{BB} represent the self-coupling of the guides, while κ_{AB} and κ_{BA} describe the mutual coupling between the guides. The integrations in the numerator of (2.100) are carried out in the areas defined by $\Delta n_A(x,y)$ and $\Delta n_B(x,y)$.

As we have seen in previous sections, Z-cut $LiNbO_3$ supports only $\boldsymbol{E}^x_{pq}$ modes. Therefore, the y component, $E_y(x,y) = 0$ in each individual guide. When $\Delta n_A = \Delta n_B = \Delta n$,

$$\Delta n = \begin{bmatrix} \Delta n_e & 0 & 0 \\ 0 & \Delta n_o & 0 \\ 0 & 0 & \Delta n_o \end{bmatrix} \tag{2.101}$$

and considering that E_{AB_x} are the dominant field components, $\Delta n_o^2 E_z << \Delta n_e^2 E_x$, the coupling coefficients are approximately rewritten as

$$\kappa_{AB} = \frac{k_0^2 \Delta n_e^2}{2\beta_A} \frac{\iint_A \boldsymbol{E}_{Ax}^*(x,y) \cdot \boldsymbol{E}_{Bx}(x,y)\, dxdy}{\int_{-\infty}^{\infty}\int_{-\infty}^{\infty} \boldsymbol{E}_{Ax}^2(x,y)\, dxdy} \tag{2.102}$$

$$\kappa_{BA} = \frac{k_0^2 \Delta n_e^2}{2\beta_B} \frac{\iint_B \boldsymbol{E}_{Bx}^*(x,y) \cdot \boldsymbol{E}_{Ax}(x,y)\, dxdy}{\int_{-\infty}^{\infty}\int_{-\infty}^{\infty} \boldsymbol{E}_{Bx}^2(x,y)\, dxdy} \tag{2.103}$$

$$\kappa_{AA} = \frac{k_0^2 \Delta n_e^2}{2\beta_A} \frac{\iint_A E_{Ax}^2(x,y)\,dxdy}{\int_{-\infty}^{\infty}\int_{-\infty}^{\infty} E_{Ax}^2(x,y)\,dxdy} \tag{2.104}$$

$$\kappa_{BB} = \frac{k_0^2 \Delta n_e^2}{2\beta_B} \frac{\iint_B E_{Bx}^2(x,y)\,dxdy}{\int_{-\infty}^{\infty}\int_{-\infty}^{\infty} E_{Bx}^2(x,y)\,dxdy} \tag{2.105}$$

where the integrations in the numerators of (2.102) to (2.105) are carried out over the guiding area corresponding to where the index change occurred.

For the waveguides which support only E^y_{pq} modes (for example, in X or Y cut $LiNbO_3$), we can let $E_x(x,y) = 0$. Then with $\Delta n_A = \Delta n_B = \Delta n$,

$$\Delta n = \begin{bmatrix} \Delta n_o & 0 & 0 \\ 0 & \Delta n_e & 0 \\ 0 & 0 & \Delta n_o \end{bmatrix} \tag{2.106}$$

and because now E_{AB_y} are the dominant components, $\Delta n_o^2 E_z << \Delta n_e^2 E_y$, we can obtain the coupling coefficients for the E^y_{pq} mode as in (2.102) - (2.105) after substituting E_{AB_y} for E_{AB_x}.

To use the results obtained in the previous sections, we need a coordinate shift as shown in Fig. 2.9, namely

$$\begin{cases} x_A = x + d_A \\ y_A = y + (\frac{S}{2} + w_A) \end{cases} \tag{2.107}$$

$$\begin{cases} x_B = x + d_B \\ y_B = y - \dfrac{s}{2} \end{cases} \tag{2.108}$$

where x_A and y_A are local coordinates for guiding mode A while x_B and y_B are local coordinates for guiding mode B, s is the separation between the two guides, $d_{A,B}$ and $w_{A,B}$ are the depth and width of the guides. After using the coordinate shift, the expressions of the field pattern function in section 2.2 can be substituted into (2.102) - (2.105) directly.

Numerical results for the normalized coupling coefficients are given in Table 2.2 for three specific values of the normalized depth d_A/λ. In all cases, $d_A = w_A = d_B = s$, $w_B = 1.001 d_B$ and $\Delta n_c = 0.12$. Fig. 2.10 shows the variation of coupling coefficients with the normalized separation (s/λ) between the two guides for the fundamental 0,0 mode with $d_A = w_A = d_B = \lambda$, $w_B = 1.5\lambda$. Since the plot in Fig. 2.10 is made using semi-logarithmic scales, the y-axis is ln while the x-axis is linear, it is obvious that an exponential relationship exists between the coupling coefficients and the separation between the guides.

Table 2.2: Coupler characterization

d/λ	$n_{effB} - n_{effA}$	$\lambda\kappa_{AA}$	$\lambda\kappa_{AB}$	$\lambda\kappa_{BA}$	$\lambda\kappa_{BB}$
0.7	0.000005	6.7623×10^{-6}	2.4757×10^{-4}	2.4796×10^{-4}	6.7419×10^{-6}
1.0	0.00004	1.9333×10^{-7}	3.4969×10^{-5}	3.6018×10^{-5}	1.9272×10^{-7}
2.0	0.00002	2.6503×10^{-12}	7.0794×10^{-8}	7.0854×10^{-8}	2.6426×10^{-12}

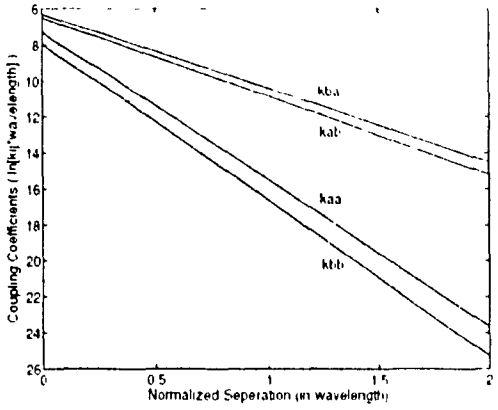

Fig.2.10 Coupling coefficients as a function of guide separation. y-axis is *ln* while x-axis is linear. Δn_a=0.12, Δn_b=-0.04, $d_a=w_a=d_f=s=\lambda$, w_b=1.5λ

2.4 Mode coupling in periodically perturbed channel waveguides

An optical waveguide with grating is a very useful element for optical integrated circuits construction. It can be used for coupling, deflecting, reflecting, wavelength filtering, and mode conversion. The properties of such a component has been studied by a number of workers.[20-25] The results quoted and justified here are for the evaluation of the grating assisted coupler to be discussed in the next section.

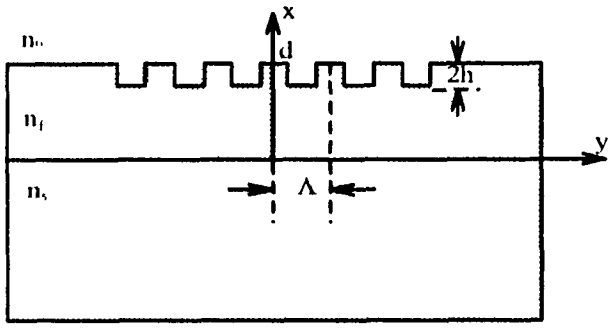

Fig. 2.11. Grating geometry

The geometry of a grating is shown in Fig. 2.11. It is assumed that the nonuniformity of the index distribution is small so that the grating only slightly perturbs the field distribution. The perturbation properties of the grating are analyzed using coupled mode method. The general expressions of the coupling coefficients are derived from the coupled equations first. Then those expressions are applied to the grating mentioned above.

Due to their orthogonality, the guided modes of a channel waveguide propagate independently of each other when no perturbation exists, that is, when the index distribution $n(x,y)$ remains independent of propagation direction z. If a grating, a

perturbation of the refractive index along the z axis, is imposed onto the waveguide, the refractive index acquires a z-dependence.

Let us consider the mode coupling between two linearly independent modes, a forward mode and a backward mode. Then the perturbed field can be expressed in terms of a linear combination of the two unperturbed eigenmodes

$$\boldsymbol{E}(x,y,z) = F(z)\,\boldsymbol{E}_f(x,y)\,e^{-j\beta_f z} + B(z)\,\boldsymbol{E}_b(x,y)\,e^{j\beta_b z} \qquad (2.109)$$

where $F(z)$ and $B(z)$ are the amplitudes and β_f and β_b are the propagation constants of forward and backward modes, respectively. $\boldsymbol{E}$, $\boldsymbol{E}_f$ and $\boldsymbol{E}_b$ have unit of V/m, while F and B are non-dimensional variables. If there is no dielectric perturbation F and B reduce to constants. The z variation in F and B indicates that the power is exchanged between the two modes $\boldsymbol{E}_f$ and $\boldsymbol{E}_b$.

We consider the dielectric perturbation caused by a "shallow" grating, represented by a small perturbing term. The refractive index distribution is approximately

$$n^2(x,y,z) = n_s^2(x,y) + \Delta n_f^2(x,y) + \Delta n_g^2(x,y)\,P(z) \qquad (2.110)$$

where $n_s(x,y)$ is the refractive index of the substrate and $\Delta n_f(x,y)$ represents the presence of the waveguide, $\Delta n_g(x,y)$ is the perturbed term of the refractive index in the grating area, which depends on the cross sectional geometry of the grating and the index change in the grating area, and $P(z)$ is a periodic function of z. According to the coupled-mode theory[20,21] which was used in the last section, the substitution of (2.109) and (2.110) into the three dimensional Helmholtz equation, and considering that the variation of the mode amplitudes over z is slow, lead to

$$2\beta_f \frac{dF(z)}{dz} E_f(x,y)\, e^{-j\beta_f z} - 2\beta_b \frac{dB(z)}{dz} E_b(x,y)\, e^{-j\beta_b z}$$
$$= -jk_0^2 \Delta n_\eta^2(x,y)\, P(z)\left[F(z)\, E_f(x,y)\, e^{-j\beta_f z} + B(z)\, E_f(x,y)\, e^{j\beta_b z}\right] \qquad \textbf{(2.111)}$$

$P(z)$ is chosen as a periodic square wave function. In one period,

$$P(z) = \begin{cases} 1 & |z| < \frac{\Lambda}{4} \\ 0 & \frac{\Lambda}{4} < z < \frac{3\Lambda}{4} \end{cases} \qquad \textbf{(2.112)}$$

where Λ is the period of the grating. $P(z)$ can be expanded into the Fourier series

$$P(z) = \frac{1}{2} + \frac{2}{\pi}\cos\left(\frac{2\pi}{\Lambda}\right)z - \frac{2}{3\pi}\cos\left(\frac{6\pi}{\Lambda}z\right) + \ldots + \frac{2}{m\pi}\sin\left(\frac{m\pi}{2}\right)\cos\left(\frac{2m\pi}{\Lambda}z\right) + \ldots \qquad \textbf{(2.113)}$$

where m is an odd integer (m = 1, 3, 5, ...). The first term in (2.113) represents average value of $P(z)$. The harmonic terms represent the perturbation. The influence of each harmonic term may be analyzed individually and the final result obtained by summing the effects of all terms. Here we only consider the mth harmonic, or mth order Bragg coupling.

$$P_m(z) = \frac{2}{m\pi}\sin\left(\frac{m\pi}{2}\right)\cos\left(\frac{2m\pi}{\Lambda}z\right) = \frac{2}{m\pi}\sin\left(\frac{m\pi}{2}\right)\cos(K_m z) \qquad \textbf{(2.114)}$$

where K_m is the constant spatial frequency for the mth harmonic. Substitution of (2.114) into (2.111) leads to

$$2\beta_f \frac{dF(z)}{dz} E_f(x,y)\, e^{-j\beta_f z} - 2\beta_b \frac{dB(z)}{dz} E_b(x,y)\, e^{j\beta_b z}$$

$$= -jk_0^2 \Delta n_g^2(x,y) \frac{2\sin\left(\frac{m\pi}{2}\right)}{m\pi} \cos(K_m z) \tag{2.115}$$

$$\times \left[F(z)\, E_f(x,y)\, e^{-j\beta_f z} + B(z)\, E_b(x,y)\, e^{j\beta_b z}\right]$$

If we use $\cos(K_m z) = \frac{1}{2}[\exp(jK_m z) + \exp(-jK_m z)]$, and take the inner product between E_f^* and (2.115), and then integrate over the whole xy plane, the equation describing the growth of the mode $F(z)$ may be written as

$$\frac{dF(z)}{dz} = -j \frac{k_0^2 \sin\left(\frac{m\pi}{2}\right)}{2m\pi\beta_f \int_{-\infty}^{\infty}\int_{-\infty}^{\infty} E_f^2(x,y)\, dxdy} \left[F(z)\, e^{j K_z z} \iint_G \Delta n_g^2(x,y)\, E_f^*(x,y)\, dxdy \right.$$

$$+ F(z)\, e^{-jK_z z} \iint_G \Delta n_g^2(x,y)\, E_f^2(x,y)\, dxdy \tag{2.116}$$

$$+ B(z)\, e^{j(K_z+\beta_f+\beta_b)z} \iint_G E_f^*(x,y) \cdot \Delta n_q^2(x,y)\, E_b(x,y)\, dxdy$$

$$\left. + B(z)\, e^{-j(K_z-\beta_f-\beta_b)z} \iint_G E_f^*(x,y) \cdot \Delta n_q^2(x,y)\, E_b(x,y)\, dxdy \right]$$

in the square brackets of the r.h.s. of (2.116), the first three terms are rapidly oscillating and do not contribute to the rate of change of $F(z)$. Those three terms can be neglected. The last term, however, represents a slow variation when

$$K_m - \beta_f - \beta_b = \Delta\beta \tag{2.117}$$

is zero or relatively small. So (2.116) can be simplified to

$$\frac{dF(z)}{dz} = -j\kappa_{fb} e^{-j\Delta\beta z} B(z) \tag{2.118}$$

with

$$\kappa_{fb} = \frac{k_0^2 \sin\left(\frac{m\pi}{2}\right)}{2m\pi\beta_f} \frac{\iint_G E_f^*(x,y) \cdot \Delta n_g^2(x,y) E_b(x,y)\, dxdy}{\int_{-\infty}^{\infty}\int_{-\infty}^{\infty} E_f^2(x,y)\, dxdy} \tag{2.119}$$

Taking the inner product between E_b^*(x,y) and (2.115), similar results can be obtained. The coupling coefficient κ_{bf} is

$$\kappa_{bf} = \frac{k_0^2 \sin\left(\frac{m\pi}{2}\right)}{2m\pi\beta_b} \frac{\iint_G E_b^*(x,y) \cdot \Delta n_g^2(x,y) E_f(x,y)\, dxdy}{\int_{-\infty}^{\infty}\int_{-\infty}^{\infty} E_b^2(x,y)\, dxdy} \tag{2.120}$$

The coupling between the forward and backward waves can thus be represented by the coupled equations

$$\begin{cases} \dfrac{dF(z)}{dz} = -j\kappa_{fb} e^{-j\Delta\beta z} B(z) \\ \dfrac{dB(z)}{dz} = j\kappa_{bf} e^{j\Delta\beta z} F(z) \end{cases} \tag{2.121}$$

Considering a grating assisted waveguide as shown in Fig. 2.11, the refractive index change in the grating area can be expressed as

$$\Delta n_g^2(x,y) = \begin{cases} n_f^2 - n_c^2 & d-2h < x < d \\ 0 & \text{otherwise} \end{cases} \tag{2.122}$$

Substitution of (2.122) into (2.119) and (2.120) produces

$$\kappa_{fb} = \frac{k_0^2 (n_f^2 - n_c^2) \sin\left(\frac{m\pi}{2}\right)}{2m\pi\beta_f} \frac{\int_{d-2h}^{d}\int_{-\infty}^{\infty} E_f^*(x,y)\cdot E_b(x,y)\,dxdy}{\int_{-\infty}^{\infty}\int_{-\infty}^{\infty} E_f^2(x,y)\,dxdy} \qquad (2.123)$$

and

$$\kappa_{bf} = \frac{k_0^2 (n_f^2 - n_c^2) \sin\left(\frac{m\pi}{2}\right)}{2m\pi\beta_b} \frac{\int_{d-2h}^{d}\int_{-\infty}^{\infty} E_b^*(x,y)\cdot E_f(x,y)\,dxdy}{\int_{-\infty}^{\infty}\int_{-\infty}^{\infty} E_b^2(x,y)\,dxdy} \qquad (2.124)$$

The coupling coefficients are proportional to the index change in the grating area. When the grating groove depth is much smaller than the thickness of the guiding layer ($2h << d$), the field functions in the integral in the numerator of (2.123), (2.124) can be approximated by the values at $x = d$. Thus $E_{fh}(x,y) \approx E_{fh}(d,y)$.

2.5 Grating assisted coupler and its characterization

In this section, a scattering representation of four-port devices and the relationship between the output power from each of the four ports to the input power at a given port are given. An analytic solution of the codirectional coupler is derived from the matrix description. Some numerical evaluations are given to demonstrate the characterizations of the grating assisted coupler.

2.5.1 General theory of matrix description for four-port devices

The grating assisted reverse coupler can be considered as a four-port device as shown in Fig. 2.12 (a),(b). It is assumed that each waveguide supports only a single forward mode and a single backward mode, $\mathbf{a}_1$ (forward mode) and $\mathbf{a}_2$ (backward mode) in guide A, $\mathbf{a}_3$ (forward mode) and $\mathbf{a}_4$ (backward mode) in guide B. It is also assumed that these modes are linearly polarized. In the coupling region (length L), the evanescent fields of the modes overlap and energy exchange occurs. A grating is placed over both guides along the entire length of the coupling region. The grating period is Λ. The energy exchange in this composite structure includes two kinds of Bragg coupling. The first one is **direct Bragg coupling**, where a mode is reflected back into the same guide to exchange energy with a mode travelling in the opposite direction, for example, the coupling between the modes $\mathbf{a}_1$ and $\mathbf{a}_2$, or $\mathbf{a}_3$ and $\mathbf{a}_4$. The second one is **exchange Bragg coupling**, where a mode is reflected back into the opposite guide and thus exchanges energy with a mode travelling in the opposite direction in the opposite guide, for example,

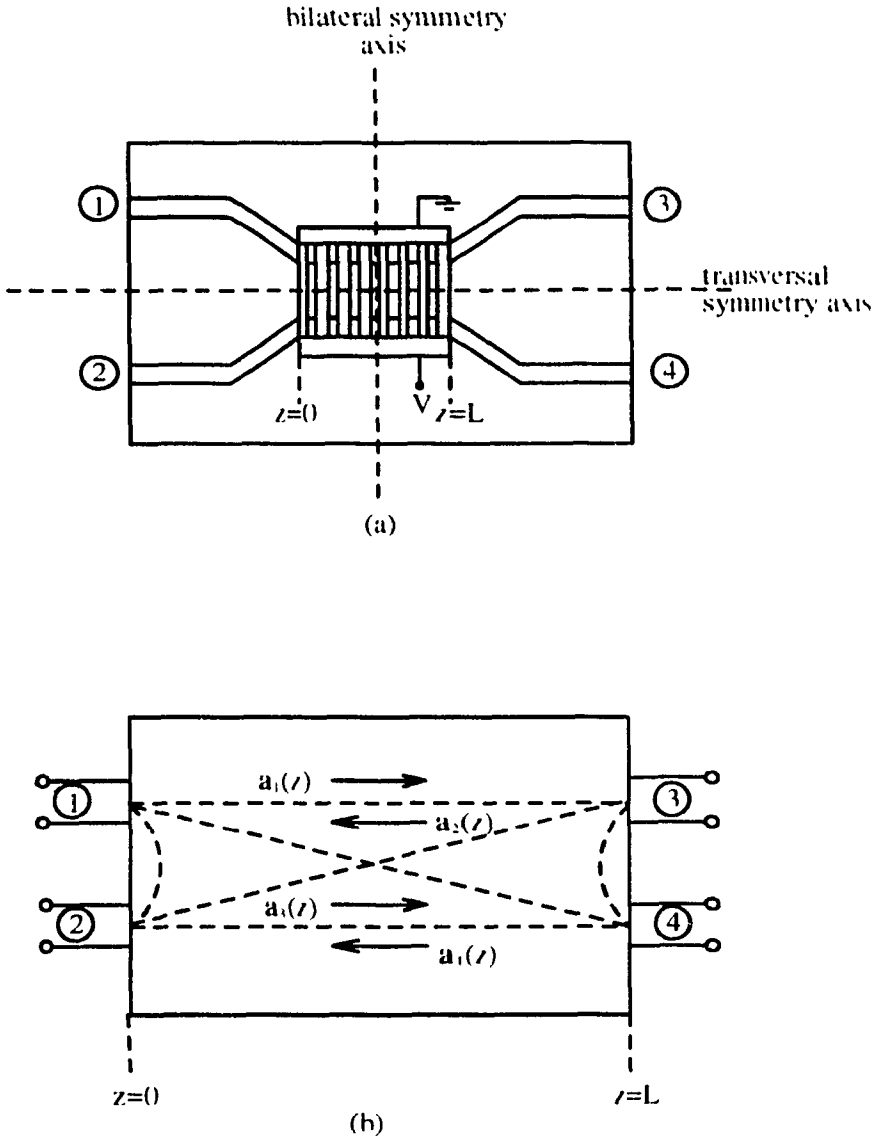

Fig. 2.12 Geometry of a grating assisted coupler (a) and the equivalent four port (b)

the coupling between the modes $\mathbf{a}_1$ and $\mathbf{a}_4$, or $\mathbf{a}_2$ and $\mathbf{a}_3$. The mode vector can be expressed as:

$$\boldsymbol{a}(z) = \begin{bmatrix} a_1(z) \\ a_2(z) \\ a_3(z) \\ a_4(z) \end{bmatrix} \tag{2.125}$$

According to coupled mode theory, we use the first order differential vector coupled equation to describe the rate of change of the mode amplitudes in terms of the coupling constants. The differential vector coupled equation is

$$\frac{d\boldsymbol{a}(z)}{dz} = -j\boldsymbol{R}\boldsymbol{a}(z) \tag{2.126}$$

where $\boldsymbol{R}$ is the coupling coefficient matrix which can be calculated directly from the properties of the guides and the grating as mentioned in last two sections. It will be further discussed in Section 2.5.2. The terminal vectors at z=0 and z=L are expressed as

$$\begin{aligned} \boldsymbol{a}(0) &= [a_1(0),\ a_2(0),\ a_3(0),\ a_4(0)]^t \\ &\triangleq [a_1,\ b_1,\ a_2,\ b_2]^t \end{aligned} \tag{2.127}$$

and

$$\begin{aligned} \boldsymbol{a}(L) &= [a_1(L),\ a_2(L),\ a_3(L),\ a_4(L)]^t \\ &\triangleq [b_3,\ a_3,\ b_4,\ a_4]^t \end{aligned} \tag{2.128}$$

respectively. The superscript t refers to the transpose of the vectors. The linear relationship between $\boldsymbol{a}(L)$ and $\boldsymbol{a}(0)$ is

$$\boldsymbol{a}(L) = \boldsymbol{M}(L)\,\boldsymbol{a}(0) \tag{2.129}$$

where

$$\begin{aligned} \boldsymbol{M}(L) &= e^{-j\boldsymbol{R}L} \\ &= \boldsymbol{U}\, diag\left[e^{-j\beta_1 L},\ e^{-j\beta_2 L}, e^{-j\beta_3 L}, e^{-j\beta_4 L}\right] \boldsymbol{U}^{-1} \end{aligned} \tag{2.130}$$

is the scattering transfer matrix, $\boldsymbol{U}$ is the common modal matrix of $\boldsymbol{M}(L)$ and $\boldsymbol{R}$, and β_i (i = 1 to 4) are the eigenvalues of $\boldsymbol{R}$. In order to compute the scattering matrix of the coupler we define the "tilde" transform

$$\tilde{\boldsymbol{M}} = \pi_{23}\, \boldsymbol{M}\, \pi_{23} \tag{2.131}$$

where π_{23} is a permutation matrix

$$\pi_{23} = \begin{bmatrix} 1 & 0 & 0 & 0 \\ 0 & 0 & 1 & 0 \\ 0 & 1 & 0 & 0 \\ 0 & 0 & 0 & 1 \end{bmatrix} \tag{2.132}$$

By partitioning the 4×4 $\tilde{\boldsymbol{M}}$ matrix into 2×2 submatrixes

$$\tilde{\boldsymbol{M}} = \begin{bmatrix} \tilde{M}_A & \tilde{M}_B \\ \tilde{M}_C & \tilde{M}_D \end{bmatrix} \tag{2.133}$$

we obtain the scattering matrix of the four-port device, defined by

$$\boldsymbol{b} = [b_1\ b_2\ b_3\ b_4]^t = \boldsymbol{S}\boldsymbol{a} = \boldsymbol{S}\,[a_1\ a_2\ a_3\ a_4]^t \tag{2.134}$$

through the transformation equation

$$\boldsymbol{S} = \begin{bmatrix} -\tilde{M}_D^{-1}\tilde{M}_C & \tilde{M}_D^{-1} \\ \tilde{M}_A - \tilde{M}_B\tilde{M}_D^{-1}\tilde{M}_C & \tilde{M}_B\tilde{M}_D^{-1} \end{bmatrix} \tag{2.135}$$

2.5.2 Coupling coefficient matrix of grating assisted coupler

To evaluate the mode properties of the waves propagating in a grating assisted coupler, the coupling coefficient matrix $\boldsymbol{R}$ must be found first. For simplification, we assume (1) that the grating assisted coupler only supports two confined forward modes and two backward modes, and (2) that the same grating covers both waveguides as shown in Fig. 2.12a. The field modes in this structure take the form of

$$\begin{cases} A_1(z)\,\boldsymbol{E}_1(x,y)\,e^{-j\beta_1 z} & \text{(forward mode in guide } A\text{)} \\ A_2(z)\,\boldsymbol{E}_2(x,y)\,e^{j\beta_2 z} & \text{(backward mode in guide } A\text{)} \\ A_3(z)\,\boldsymbol{E}_3(x,y)\,e^{-j\beta_3 z} & \text{(forward mode in guide } B\text{)} \\ A_4(z)\,\boldsymbol{E}_4(x,y)\,e^{j\beta_4 z} & \text{(backward mode in guide } B\text{)} \end{cases} \tag{2.136}$$

The variation in the mode amplitudes A_i indicates that power is exchanged between the four modes. To study the mode coupling, the refractive index profile can be approximately expressed as

$$\begin{aligned} n^2(x,y,z) = {} & n_S^2(x,y) + \Delta n_A^2(x,y) + \Delta n_B^2(x,y) \\ & + \Delta n_g^2(x,y)\,P(z) \end{aligned} \tag{2.137}$$

where $n_s(x,y)$ is the refractive index distribution of the substrate, $\Delta n_A(x,y)$ and $\Delta n_B(x,y)$ represent the presence of guide A and B, and vanish outside the guiding regions. $\Delta n_g(x,y)$ represents the refractive index variation caused by the geometry of the corrugation in the grating region, $P(z)$, a periodic function of z given in (2.112), represents the periodic dielectric perturbation of the grating.

The field patterns of $\boldsymbol{E}_i$ should satisfy Helmholtz equation when no dielectric perturbation exists.

$$\left[\nabla_T^2 + k_0^2 (n_s^2 + \Delta n_A^2) - \beta_{1,2}^2\right] \boldsymbol{E}_{1,2} = 0 \tag{2.138}$$

$$\left[\nabla_T^2 + k_0^2 (n_s^2 + \Delta n_B^2) - \beta_{3,4}^2\right] \boldsymbol{E}_{3,4} = 0 \tag{2.139}$$

In a grating assisted coupler structure, the total field is the sum of the forward- and backward-modes

$$\begin{aligned} \boldsymbol{E}(x,y,z) &= A_1(z)\boldsymbol{E}_1(x,y)e^{-j\beta_1 z} + A_2(z)\boldsymbol{E}_2(x,y)e^{j\beta_2 z} \\ &+ A_3(z)\boldsymbol{E}_3(x,y)e^{-j\beta_3 z} + A_4(z)\boldsymbol{E}_4(x,y)e^{j\beta_4 z} \end{aligned} \tag{2.140}$$

Substituting (2.136), (2.137) and (2.140) into the three dimensional Helmholtz equation and eliminating terms by using (2.138) and (2.139) as well as neglecting slowly varying terms, we obtain

$$\begin{aligned} & 2\beta_1 \frac{dA_1}{dz}\boldsymbol{E}_1 e^{-j\beta_1 z} - 2\beta_2 \frac{dA_2}{dz}\boldsymbol{E}_2 e^{j\beta_2 z} + 2\beta_3 \frac{dA_3}{dz}\boldsymbol{E}_3 e^{-j\beta_3 z} - 2\beta_4 \frac{dA_4}{dz}\boldsymbol{E}_4 e^{j\beta_4 z} \\ = & -jk_0^2 \Delta n_B^2 A_1 \boldsymbol{E}_1 e^{-j\beta_1 z} - jk_0^2 \Delta n_g^2 P(z) A_1 \boldsymbol{E}_1 e^{-j\beta_1 z} \\ & -jk_0^2 \Delta n_B^2 A_2 \boldsymbol{E}_2 e^{j\beta_2 z} - jk_0^2 \Delta n_g^2 P(z) A_2 \boldsymbol{E}_2 e^{j\beta_2 z} \\ & -jk_0^2 \Delta n_A^2 A_3 \boldsymbol{E}_3 e^{-j\beta_3 z} - jk_0^2 \Delta n_g^2 P(z) A_3 \boldsymbol{E}_3 e^{-j\beta_3 z} \\ & -jk_0^2 \Delta n_A^2 A_4 \boldsymbol{E}_4 e^{j\beta_4 z} - jk_0^2 \Delta n_g^2 P(z) A_4 \boldsymbol{E}_4 e^{j\beta_4 z} \end{aligned} \tag{2.141}$$

Let all propagation constants β_i be close to a reference value K/2, where K is the constant spatial frequency of the grating, $K = 2\pi/\Lambda$. The periodic function $P(z)$ can be expanded into a Fourier series as in (2.113) and only the mth harmonic term is considered which is given in (2.114). Substituting (2.114) into (2.141), equating the terms of which the modes propagate in $+z$ direction and in $-z$ direction individually with zero and neglecting higher diffraction orders, two equations can be obtained

$$
\begin{aligned}
&2\beta_1\frac{dA_1}{dz}\boldsymbol{E}_1 e^{-j\beta_1 z} + 2\beta_3\frac{dA_3}{dz}\boldsymbol{E}_3 e^{-j\beta_3 z} \\
&\quad = -jk_0^2\Delta n_B^2 A_1\boldsymbol{E}_1 e^{-j\beta_1 z} - jk_0^2\Delta n_A^2 A_3\boldsymbol{E}_3 e^{-j\beta_3 z} \\
&\quad -j\frac{k_0^2 n_g^2}{m\pi}\sin\left(\frac{m\pi}{2}\right)A_2\boldsymbol{E}_2 e^{-j(K_m-\beta_2)z} \\
&\quad -j\frac{k_0^2 n_g^2}{m\pi}\sin\left(\frac{m\pi}{2}\right)A_4\boldsymbol{E}_4 e^{-j(K_m-\beta_4)z}
\end{aligned}
\tag{2.142}
$$

and

$$
\begin{aligned}
&-2\beta_2\frac{dA_2}{dz}\boldsymbol{E}_2 e^{j\beta_2 z} - 2\beta_4\frac{dA_4}{dz}\boldsymbol{E}_4 e^{j\beta_4 z} \\
&\quad = -jk_0^2\Delta n_B^2 A_2\boldsymbol{E}_2 e^{j\beta_2 z} - jk_0^2\Delta n_A A_4\boldsymbol{E}_4 e^{j\beta_4 z} \\
&\quad -j\frac{k_0^2\Delta n_g^2}{m\pi}\sin\left(\frac{m\pi}{2}\right)A_1\boldsymbol{E}_1 e^{j(K_m-\beta_1)z} \\
&\quad -j\frac{k_0^2\Delta n_g^2}{m\pi}\sin\left(\frac{m\pi}{2}\right)A_3\boldsymbol{E}_3 e^{j(K_m-\beta_3)z}
\end{aligned}
\tag{2.143}
$$

Now taking the inner product between (2.142) and the modal field $\boldsymbol{E}_l^*$ and integrating over the whole xy plane.

$$
\begin{aligned}
\frac{dA_1}{dz} &= -j\left[\kappa_{11}A_1 + \kappa_{12}e^{-j(K_m-\beta_1-\beta_2)z}A_2\right. \\
&\quad \left. + \kappa_{13}e^{j(\beta_1-\beta_3)z}A_3 + \kappa_{14}e^{-j(K_m-\beta_1-\beta_4)z}A_4\right]
\end{aligned}
\tag{2.144}
$$

where κ_{ij} are the coupling coefficients. The amplitude change rate of A_1 is determined by all of the mode amplitudes through the coupling coefficients κ_{ij}. A_3 can affect the amplitude change rate of A_1 through κ_{13} only under the satisfaction of the phase match condition $\beta_1 - \beta_3 \approx 0$. The period of grating Λ can be chosen properly to satisfy either the phase match condition $K_m - \beta_1 - \beta_2 \approx 0$ to get the strong coupling between A_1 and A_2, or

the phase match condition $K_m - \beta_1 - \beta_2 \approx 0$ to obtain the strong coupling between A_1 and A_4. Three similar equations can be obtained by taking the inner products between (2.142) and modal field $\boldsymbol{E}_3^*$, and between (2.143) and the modal fields $\boldsymbol{E}_2^*$ and $\boldsymbol{E}_4^*$, separately, and integrating over the whole xy plane. The coupling coefficients can be calculated from the properties of the guides and the gratings. Thus

$$\kappa_{ij} = \frac{k_0^2}{2\beta_i} \frac{\iint_B \boldsymbol{E}_i^*(x,y) \cdot \Delta n_B^2(x,y) \boldsymbol{E}_j(x,y)\, dxdy}{\int_{-\infty}^{\infty}\int_{-\infty}^{\infty} \boldsymbol{E}_i^2(x,y)\, dxdy} \tag{2.145}$$

for the elements of $[i,j] = [1,1], [2,2], [3,1], [4,2]$ and the integration in the numerator is carried out over the cross section area of waveguide B, and

$$\kappa_{ij} = \frac{k_0^2}{2\beta_i} \frac{\iint_A \boldsymbol{E}_i^*(x,y) \cdot \Delta n_A^2(x,y) \boldsymbol{E}_j(x,y)\, dxdy}{\int_{-\infty}^{\infty}\int_{-\infty}^{\infty} \boldsymbol{E}_i^2(x,y)\, dxdy} \tag{2.146}$$

for the elements of $[i,j] = [1,3], [2,4], [3,3], [4,4]$ and the integration in the numerator is carried out over the cross section area of waveguide A. For the remaining elements of the coupling matrix

$$\kappa_{ij} = \frac{k_0^2 \sin\left(\frac{m\pi}{2}\right)}{2m\pi\beta_i} \frac{\iint_G \boldsymbol{E}_1^*(x,y) \cdot \Delta n_g^2(x,y) \boldsymbol{E}_j(x,y)\, dxdy}{\int_{-\infty}^{\infty}\int_{-\infty}^{\infty} \boldsymbol{E}_i^2(x,y)} \tag{2.147}$$

where the integration in the numerator is carried out over the grating area. The four coupled equations can be written as a matrix vector equation

$$\frac{d\hat{\mathbf{a}}(z)}{dz} = -j\hat{\mathbf{R}}(z)\,\hat{\mathbf{a}}(z) \tag{2.148}$$

with

$$\hat{\mathbf{a}}(z) = [A_1(z) \quad A_2(z) \quad A_3(z) \quad A_4(z)]^t \tag{2.149}$$

and

$$\hat{\boldsymbol{R}}(z) = \begin{pmatrix} \kappa_{11} & \kappa_{12}e^{-j(K_m-\beta_1-\beta_2)z} & \kappa_{13}e^{j(\beta_1-\beta_3)z} & \kappa_{14}e^{-j(K_m-\beta_1-\beta_4)z} \\ -\kappa_{21}e^{j(K_m-\beta_1-\beta_2)z} & -\kappa_{22} & -\kappa_{23}e^{j(K_m-\beta_2-\beta_3)z} & -\kappa_{24}e^{-j(\beta_2-\beta_4)z} \\ \kappa_{31}e^{-j(\beta_1-\beta_3)z} & \kappa_{32}e^{-j(K_m-\beta_2-\beta_3)z} & \kappa_{33} & \kappa_{34}e^{-j(K_m-\beta_3-\beta_4)z} \\ -\kappa_{41}e^{j(K_m-\beta_1-\beta_4)z} & -\kappa_{42}e^{j(\beta_2-\beta_4)z} & -\kappa_{43}e^{j(K_m-\beta_3-\beta_4)z} & -\kappa_{44} \end{pmatrix} \tag{2.150}$$

Note that this coupling coefficient matrix is a function of z while the **R** matrix in (2.126) is a constant matrix. To be able to apply the theory discussed in Section 2.5.1 to the differential equation (2.148), we must first transform the coefficient matrix (2.150) to a constant matrix. To this end we define the transformation

$$\hat{\mathbf{a}}(z) = \boldsymbol{T}(z)\,\boldsymbol{a}(z) \tag{2.151}$$

with the transform matrix

$$\boldsymbol{T}(z) = \begin{bmatrix} e^{j\delta_1 z} & 0 & 0 & 0 \\ 0 & e^{j\delta_2 z} & 0 & 0 \\ 0 & 0 & e^{j\delta_3 z} & 0 \\ 0 & 0 & 0 & e^{j\delta_4 z} \end{bmatrix} \tag{2.152}$$

and apply it to (2.148) to yield a new differential equation,

$$\frac{d\boldsymbol{a}(z)}{dz} = -j\boldsymbol{R}\boldsymbol{a}(z) \tag{2.153}$$

where

$$\boldsymbol{R} = \boldsymbol{T}^{-1}(z)\left[\hat{\boldsymbol{R}}(z) - j\frac{d\boldsymbol{T}(z)}{dz}\boldsymbol{T}^{-1}(z)\right]\boldsymbol{T}(z) \tag{2.154}$$

Substitution of (2.150) and (2.152) into (2.154),

$$\boldsymbol{R} = \begin{pmatrix} \cdot\cdot + \delta_1 & \kappa_{12}e^{-j(K_m-\beta_1-\beta_2+\delta_1-\delta_2)z} & \kappa_{13}e^{j(\beta_1-\beta_3-\delta_1+\delta_3)z} & \kappa_{14}e^{-j(K_m-\beta_1-\beta_4+\delta_1-\delta_4)z} \\ -\kappa_{21}e^{j(K_m-\beta_1-\beta_2-\delta_2+\delta_1)z} & -(\kappa_{22}-\delta_2) & -\kappa_{23}e^{j(K_m-\beta_2-\beta_3-\delta_2+\delta_3)z} & -\kappa_{24}e^{-j(\beta_2-\beta_4+\delta_2-\delta_4)z} \\ \kappa_{31}e^{-j(\beta_1-\beta_3+\delta_3-\delta_1)z} & \kappa_{32}e^{-j(K_m-\beta_2-\beta_3+\delta_3-\delta_2)z} & \kappa_{33}+\delta_3 & \kappa_{34}e^{-j(K_m-\beta_3-\beta_4+\delta_3-\delta_4)z} \\ -\kappa_{41}e^{j(K_m-\beta_1-\beta_4-\delta_4+\delta_1)z} & -\kappa_{42}e^{j(\beta_2-\beta_4-\delta_4+\delta_2)z} & -\kappa_{43}e^{j(K_m-\beta_3-\beta_4-\delta_4+\delta_3)z} & -(\kappa_{33}-\delta_4) \end{pmatrix} \tag{2.155}$$

Now setting

$$\delta_1 = -\frac{K_m}{2} + \beta_1 \tag{2.156}$$

$$\delta_2 = \frac{K_m}{2} - \beta_2 \tag{2.157}$$

$$\delta_3 = -\frac{K_m}{2} + \beta_3 \tag{2.158}$$

$$\delta_4 = \frac{K_m}{2} - \beta_4 \tag{2.159}$$

where $K_m/2$ is the reference value of the propagation constants. The $\boldsymbol{R}$ matrix (2.155) can be reduced by using (2.156) to (2.159), to the constant matrix

$$\boldsymbol{R} = \begin{pmatrix} \kappa_{11}+\delta_1 & \kappa_{12} & \kappa_{13} & \kappa_{14} \\ -\kappa_{21} & -(\kappa_{22}-\delta_2) & -\kappa_{23} & -\kappa_{24} \\ \kappa_{31} & \kappa_{32} & \kappa_{33}+\delta_3 & \kappa_{34} \\ -\kappa_{41} & -\kappa_{42} & -\kappa_{43} & -(\kappa_{44}-\delta_3) \end{pmatrix} \tag{2.160}$$

In deriving the remaining equations, the lower case r_{ij} are used in the matrix as

$$\boldsymbol{R} = \begin{pmatrix} r_{11} & r_{12} & r_{13} & r_{14} \\ -r_{21} & -r_{22} & -r_{23} & -r_{24} \\ r_{31} & r_{32} & r_{33} & r_{34} \\ -r_{41} & -r_{42} & -r_{43} & -r_{44} \end{pmatrix} \tag{2.161}$$

with

$$\begin{cases} r_{ij} = \kappa_{ij} & (i \neq j) \\ r_{ii} = \kappa_{ii} + (-1)^{i-1}\delta_i \end{cases} \tag{2.162}$$

where i = 1 to 4. In (2.161), the coupling constants r_{13}, r_{31}, r_{24}, r_{42} are associated with all codirectional energy interchanges; the coupling constants r_{12}, r_{21}, r_{34}, r_{43} are associated with all direct Bragg interchanges; the coupling constants r_{14}, r_{41}, r_{23}, r_{32} are associated with all exchange Bragg interchanges and indicate the reflection to the opposite waveguide and opposite directions. Now we can solve the differential equation (2.151) with constant coefficient matrix $\boldsymbol{R}$ (2.161) and can calculate the modal field distributions in the grating assisted coupler by using the formulations described in Section 2.5.1. When the $\boldsymbol{R}$ matrix has the form of (2.161) with a general case, an analytic solution would normally prove difficult. The numerical method is efficient to evaluate the properties of mode propagation in such a structure. Under certain geometrical symmetry, the $\boldsymbol{R}$ matrix may be simplified. Five simplifying assumptions are analyzed.

(1) No grating. In this case there is no back reflection. This is the case of the codirectional coupler. Only codirectional energy interchanges exist in the composite structure. If the structure is uniform and bilaterally symmetric, the coupling coefficient matrix has the form

$$\boldsymbol{R} = \begin{pmatrix} r_{11} & 0 & r_{13} & 0 \\ 0 & -r_{11} & 0 & -r_{13} \\ r_{31} & 0 & r_{33} & 0 \\ 0 & -r_{31} & 0 & -r_{33} \end{pmatrix} \tag{2.163}$$

If the coupler is also reciprocal, the matrix in (2.163) is reduced to

$$\boldsymbol{R} = \begin{pmatrix} r_{11} & 0 & r_{13} & 0 \\ 0 & -r_{11} & 0 & -r_{13} \\ r_{13} & 0 & r_{33} & 0 \\ 0 & -r_{13} & 0 & -r_{33} \end{pmatrix} \tag{2.164}$$

(2) Waveguides far apart. In this case no exchange Bragg coupling will occur. This is the case for a reflection grating placed over a single straight waveguide. The coupling coefficient matrix can be obtained by considering that the interaction between the two guides is negligible. If the guide is reciprocally and bilaterally symmetric, from (2.161)

$$\boldsymbol{R} = \begin{pmatrix} r_{11} & r_{12} & 0 & 0 \\ -r_{12} & -r_{11} & 0 & 0 \\ 0 & 0 & r_{33} & r_{34} \\ 0 & 0 & -r_{34} & -r_{33} \end{pmatrix} \tag{2.165}$$

(3) Bilaterally symmetric general case. In this case (2.161) reduces to

$$\boldsymbol{R} = \begin{pmatrix} r_{11} & r_{12} & r_{13} & r_{14} \\ -r_{12} & -r_{11} & -r_{14} & -r_{13} \\ r_{31} & r_{32} & r_{33} & r_{34} \\ -r_{32} & -r_{31} & -r_{34} & -r_{33} \end{pmatrix} \tag{2.166}$$

A grating assisted coupler with bilaterally symmetric but with two dissimilar waveguides is an example of this case.

(4) Bilaterally symmetric and reciprocal case. In this case the coupling matrix assumes the form

$$\boldsymbol{R} = \begin{pmatrix} r_{11} & r_{12} & r_{13} & r_{14} \\ -r_{12} & -r_{11} & -r_{14} & -r_{13} \\ r_{13} & r_{14} & r_{33} & r_{34} \\ -r_{14} & -r_{13} & -r_{34} & -r_{33} \end{pmatrix} \tag{2.167}$$

(5) Bilaterally, transversely symmetric and reciprocal case. In this case the coupling coefficient matrix is much more simple as

$$\boldsymbol{R} = \begin{pmatrix} r_{11} & r_{12} & r_{13} & r_{14} \\ -r_{12} & -r_{11} & -r_{14} & -r_{13} \\ r_{13} & r_{14} & r_{11} & r_{12} \\ -r_{14} & -r_{13} & -r_{12} & -r_{11} \end{pmatrix} \tag{2.168}$$

A grating assisted coupler with two identical waveguides is an example of this case.

A transversely symmetric coupler supports symmetric and antisymmetric modes which are defined as

$$\begin{cases} a_{sf} = a_1 + a_3 \\ a_{sb} = a_2 + a_4 \\ a_{af} = a_1 - a_3 \\ a_{ab} = a_2 - a_4 \end{cases} \tag{2.169}$$

where the a_{sf} is the symmetric forward mode, a_{sb} is the symmetric backward mode, a_{af} is the antisymmetric forward mode, and a_{ab} is the antisymmetric backward mode. (2.169) can be expressed in matrix form

$$a' = Wa \tag{2.170}$$

with

$$a' = \begin{bmatrix} a_{sf} \\ a_{sb} \\ a_{af} \\ a_{ab} \end{bmatrix} \quad \text{and} \quad W = \begin{bmatrix} 1 & 0 & 1 & 0 \\ 0 & 1 & 0 & 1 \\ 1 & 0 & -1 & 0 \\ 0 & 1 & 0 & -1 \end{bmatrix} \tag{2.171}$$

Rewriting (2.170) as $a = W^{-1}a'$, and substituting it into the differential equation (2.153) and using (2.168), the coupling coefficient matrix R' for symmetric and antisymmetric modes is

$$R' = WRW^{-1} = \begin{bmatrix} r_{11}+r_{13} & r_{12}+r_{14} & 0 & 0 \\ -r_{12}-r_{14} & -r_{11}-r_{13} & 0 & 0 \\ 0 & 0 & r_{11}-r_{13} & r_{12}-r_{14} \\ 0 & 0 & -r_{12}+r_{14} & -r_{11}+r_{13} \end{bmatrix} \tag{2.172}$$

2.5.3 Uniform coupler without grating

Normally, an optical coupler without grating is codirectional. This means that only outputs of the device (as shown in Fig. 2.12) at ports 3 and 4 exist for input at port 1 and/or 2. If the codirectional coupler is uniform and bilaterally symmetric but not necessarily reciprocal, then its coupling coefficient matrix can be obtained from (2.161)

$$\boldsymbol{R} = \begin{bmatrix} r_{11} & 0 & r_{13} & 0 \\ 0 & -r_{11} & 0 & -r_{13} \\ r_{31} & 0 & r_{33} & 0 \\ 0 & -r_{31} & 0 & -r_{33} \end{bmatrix} \tag{2.173}$$

The eigenvalues β_i of $\boldsymbol{R}$ are obtained from the determinantal equation

$$|\boldsymbol{R} - \beta \boldsymbol{I}| = 0 \tag{2.174}$$

Expanding (2.174) results in

$$\beta^4 - (r_{11}^2 + r_{33}^2 + 2r_{13}r_{31})\beta^2 + (r_{11}r_{33} - r_{13}r_{31})^2 = 0 \tag{2.175}$$

yielding the four solutions

$$\begin{cases} \beta_1 = \beta_0 + \dfrac{\Delta\beta}{2} & \beta_2 = -\beta_1 \\ \beta_3 = \beta_0 - \dfrac{\Delta\beta}{2} & \beta_4 = -\beta_3 \end{cases} \tag{2.176}$$

where

$$\begin{cases} \beta_0 = \dfrac{r_{11} + r_{33}}{2} & \Delta\beta = 2\sqrt{\beta_d^2 + \beta_c^2} \\ \beta_d = \dfrac{r_{11} - r_{33}}{2} & \beta_c = \sqrt{r_{13}r_{31}} \end{cases} \tag{2.177}$$

The eigenvectors may be found by solving

$$\begin{bmatrix} r_{11} & 0 & r_{13} & 0 \\ 0 & -r_{11} & 0 & -r_{13} \\ r_{31} & 0 & r_{33} & 0 \\ 0 & -r_{31} & 0 & -r_{33} \end{bmatrix} \begin{bmatrix} U_1 \\ U_2 \\ U_3 \\ U_4 \end{bmatrix} = \beta \begin{bmatrix} U_1 \\ U_2 \\ U_3 \\ U_4 \end{bmatrix} \tag{2.178}$$

The eigenvector matrix can be written as

$$\boldsymbol{U} = \begin{bmatrix} 1 & 0 & 1 & 0 \\ 0 & 1 & 0 & 1 \\ \dfrac{\beta_1 - r_{11}}{r_{13}} & 0 & \dfrac{\beta_3 - r_{11}}{r_{13}} & 0 \\ 0 & \dfrac{\beta_1 - r_{11}}{r_{13}} & 0 & \dfrac{\beta_3 - r_{11}}{r_{13}} \end{bmatrix} \tag{2.179}$$

Substitution of (2.179) into (2.130) yields the $\boldsymbol{M}$ matrix

$$\boldsymbol{M} = \begin{bmatrix} m_{11} & 0 & m_{13} & 0 \\ 0 & m_{11}^* & 0 & m_{13}^* \\ m_{31} & 0 & m_{33} & 0 \\ 0 & m_{31}^* & 0 & m_{33}^* \end{bmatrix} \tag{2.180}$$

where

$$\begin{cases} m_{11} = -\dfrac{1}{\beta_1 - \beta_3}\left[(\beta_3 - r_{11})\, e^{-j\beta_1 L} - (\beta_1 - r_{11})\, e^{-j\beta_3 L}\right] \\ m_{13} = \dfrac{r_{13}}{\beta_1 - \beta_3}\left[e^{-j\beta_1 L} - e^{-j\beta_3 L}\right] \\ m_{31} = -\dfrac{r_{31}}{\beta_1 - \beta_3}\left[e^{-j\beta_1 L} - e^{-j\beta_3 L}\right] \\ m_{33} = \dfrac{1}{\beta_1 - \beta_3}\left[(\beta_1 - r_{11}) e^{-j\beta_1 L} - (\beta_3 - r_{11}) e^{j\beta_3 L}\right] \end{cases} \tag{2.181}$$

By writing the exponential form in sinusoidal function and using (2.176), the m_{ij} can be rewritten as

$$\begin{cases} m_{11} = \left[\cos\left(\frac{\Delta\beta L}{2}\right) - j\frac{2\beta_d}{\Delta\beta}\sin\left(\frac{\Delta\beta L}{2}\right)\right] e^{-j\beta_0 L} \\ m_{13} = -j\frac{2r_{13}}{\Delta\beta}\sin\left(\frac{\Delta\beta L}{2}\right) e^{-j\beta_0 L} \\ m_{31} = -j\frac{2r_{31}}{\Delta\beta}\sin\left(\frac{\Delta\beta L}{2}\right) e^{-j\beta_0 L} \\ m_{33} = \left[\cos\left(\frac{\Delta\beta L}{2}\right) + j\frac{2\beta_d}{\Delta\beta}\sin\left(\frac{\Delta\beta L}{2}\right)\right] e^{-j\beta_0 L} \end{cases} \quad (2.182)$$

$\tilde{\boldsymbol{M}}$ can be obtained by substituting (2.180) into (2.131)

$$\tilde{\boldsymbol{M}} = \begin{bmatrix} m_{11} & m_{13} & 0 & 0 \\ m_{31} & m_{33} & 0 & 0 \\ 0 & 0 & m_{11}^* & m_{13}^* \\ 0 & 0 & m_{31}^* & m_{33}^* \end{bmatrix} = \begin{bmatrix} \tilde{M}_A & \tilde{M}_B \\ \tilde{M}_C & \tilde{M}_D \end{bmatrix} \quad (2.183)$$

By Substituting (2.182) into (2.183), it can be proven that

$$\tilde{M}_A = \tilde{M}_D^{-1} \quad (2.184)$$

Finally, the scattering matrix of the coupler is obtained from (2.135) as

$$\boldsymbol{S} = \begin{bmatrix} 0 & 0 & m_{11} & m_{13} \\ 0 & 0 & m_{31} & m_{33} \\ m_{11} & m_{13} & 0 & 0 \\ m_{31} & m_{33} & 0 & 0 \end{bmatrix} \quad (2.185)$$

For an input into a single port, for example, port 1,

$$\boldsymbol{a} = [a_1, 0, 0, 0] \quad (2.186)$$

and therefore

$$b_1 = 0, \quad b_2 = 0, \quad b_3 = m_{11}a_1, \quad b_4 = m_{31}a_1 \tag{2.187}$$

The waves in the two waveguides exchange power periodically. From (2.182) and (2.187), the fraction of output power at port 4 of the total output power is

$$\frac{|b_4|^2}{|b_3|^2 + |b_4|^2} = \frac{4r_{31}^2}{\Delta\beta^2\cot^2\left(\frac{\Delta\beta L}{2}\right) + 4\beta_d^2 + 4r_{31}^2} \tag{2.188}$$

When two waveguides are not in synchronism, the power exchange is incomplete. Such an incomplete power exchange of the waves in a nonsynchronous directional coupler in Z cut $LiNbO_3$ is shown in Fig. 2.13. The indices of the waveguides are $n_{w} = 2.200$, $n_{w'} = 2.287$, $n_{f} = 2.320$, and $n_{f'} = 2.247$. The dimensions of the waveguides are, $d_A = w'_A = d_B = s = \lambda$, $w'_B = 1.001\lambda$. From this figure. it can be seen that the power exchange is very weak when the two waveguides are not identical, even though the difference between the width of the two waveguides is very small ($\Delta w' = w'_A - w'_B = 0.001\lambda$ for Fig. 2.13).

The fractional output power at port 4 reaches the first maximum when the grating length $L = \pi/\Delta\beta$ and its value, obtained from (2.188), is

$$\frac{|b_4|^2}{|b_3|^2+|b_4|^2} = \frac{r_{31}^2}{\beta_d^2 + r_{31}^2} \tag{2.189}$$

When the coupled waveguides are identical and operate in full synchronism, it is possible to obtain complete transfer of power from one channel to the other. In this case, $\delta_1 = 0$, $\delta_3 = 0$, $r_{11} = \kappa_0 + \delta_1 = \kappa_0$, $r_{33} = \kappa_0 + \delta_3 = \kappa_0$, $r_{13} = r_{31} = \kappa$. From (2.175), $\beta_0 = \kappa_0$, $\beta_d = 0$, $\beta_c = \kappa$, and $\Delta\beta = 2\kappa$. Thus

$$\begin{cases} b_3 = \cos(\kappa L)\, e^{-j\kappa_0 L} \\ b_4 = -j\sin(\kappa L)\, e^{-j\kappa_0 L} \end{cases} \tag{2.190}$$

Both output amplitudes depend on κL sinusoidally. The 100% power exchange occurs at

$$L = \frac{n\pi}{2\kappa} \quad (n\text{=odd}) \tag{2.191}$$

An example of the power exchange of synchronous waves is shown in Fig. 2.14 for the coupler parameters of: $n_{sA} = 2.200$, $n_{sB} = 2.287$, $n_{fc} = 2.320$, and $n_{fo} = 2.247$, $d_A = w_A = d_B = w_B = s = \lambda$.

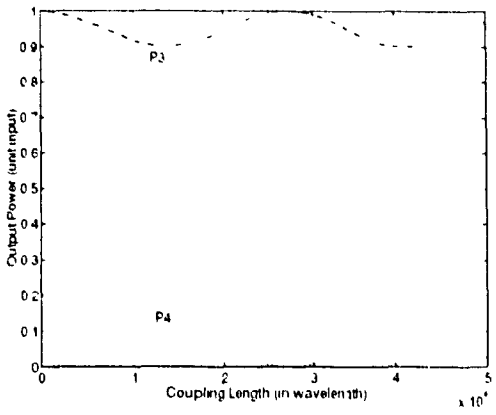

Fig. 2.13 Incomplete power exchange in a nonsynchronous codirectional coupler in Z cut $LiNbO_3$. $\Delta n_e = 0.12$, $\Delta n_o = -0.04$, $d_a = w_a = d_b = s = \lambda$, $w_b = 1.001\lambda$

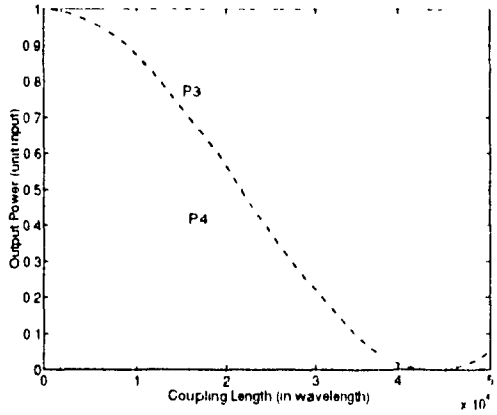

Fig. 2.14 Complete power exchange in a synchronous codirectional coupler in Z cut $LiNbO_3$. $\Delta n_e = 0.12$, $\Delta n_o = -0.04$, $d_a = w_a = d_b = s = \lambda$, $w_b = 1.001\lambda$

2.5.4 Reciprocal, bilaterally symmetric grating assisted coupler

Here we consider a simple case where a device is simultaneously reciprocal and bilaterally symmetric but nonuniform. The two waveguides are not the same, but the grating imposed nonuniformity is common to both waveguides because the grating straddles the entire coupler, so that the reflection in both guides are the same and $r_{34} = r_{12}$. For this case, the coupling coefficient matrix has the form of (2.167) rewritten here:

$$\boldsymbol{R} = \begin{bmatrix} r_{11} & r_{12} & r_{13} & r_{14} \\ -r_{12} & -r_{11} & -r_{14} & -r_{13} \\ r_{13} & r_{14} & r_{33} & r_{12} \\ -r_{14} & -r_{13} & -r_{12} & -r_{33} \end{bmatrix} \tag{2.192}$$

The eigenvalues are obtained by setting the determinantal equation to zero. The expanded determinantal equation is

$$\beta^4 + b\beta^2 + c = 0 \tag{2.193}$$

where

$$\begin{aligned} b &= 2\left(r_{13}^2 - r_{12}^2 - r_{14}^2\right) + \left(r_{11}^2 + r_{33}^2\right) \\ c &= \left(r_{12}^4 + r_{13}^4 + r_{14}^4\right) - 2\left(r_{12}^2 r_{13}^2 + r_{13}^2 r_{14}^2 + r_{14}^2 r_{12}^2\right) \\ &\quad - 2r_{11}r_{33}\left(r_{13}^2 + r_{14}^2\right) - \left(r_{11}^2 + r_{33}^2\right)r_{12}^2 + r_{11}^2 r_{33}^2 \\ &\quad + 4r_{12}r_{13}r_{14}\left(r_{11} + r_{33}\right) \end{aligned} \tag{2.194}$$

The solution of (2.193) gives the propagation constants of the general, asynchronous, grating assisted coupler

$$\beta_i = \pm \left[\frac{r_{11}^2+r_{33}^2}{2} + r_{13}^2 - r_{12}^2 - r_{14}^2 \pm 2\sqrt{\left(\frac{r_{11}+r_{33}}{2}\right)^2 r_{13}^2 - \left(\frac{r_{11}-r_{33}}{2}\right)^2 r_{14}^2 + \left(\frac{r_{11}^2-r_{33}^2}{4}\right)^2 - (r_{11}+r_{33})\, r_{12} r_{13} r_{14} + r_{12}^2 r_{14}^2} \right]^{\frac{1}{2}} \quad \textbf{(2.195)}$$

where i = 1 to 4. In practice, $r_{11} = \kappa_0 + \delta_1 + \delta_e$ (for the upper guide in Fig.2.12a) and $r_{33} = \kappa_0 + \delta_3 - \delta_e$ (for the lower guide in Fig.2.12a), where δ_1 and δ_3 are the dephasing due to the change in wavelength, while δ_e is the effect on the wavenumber caused by the electric field applied to the dielectric via the electrodes.

When the coupler is also transversely symmetric, i.e., the two guides are identical and no electric field is applied ($\delta_e = 0$), $r_{33} = r_{11} = \kappa_0 + \delta_1$, and $r_{13} = r_{31} = \kappa$, (2.195) can be reduced to the form of

$$\begin{aligned} \beta_{1,2} &= \pm\sqrt{(\kappa_0+\delta_1+\kappa)^2 - (r_{12}+r_{14})^2} \\ \beta_{3,4} &= \pm\sqrt{(\kappa_0+\delta_1-\kappa)^2 - (r_{12}-r_{14})^2} \end{aligned} \quad \textbf{(2.196)}$$

corresponding to an asynchronous condition. At full synchronous condition ($\delta_1 = 0$) and assuming $\kappa_0 << \kappa$, the propagation constants are

$$\begin{aligned} \beta_{1,2} &= \pm\sqrt{\kappa^2 - (r_{12}+r_{14})^2} \\ \beta_{3,4} &= \pm\sqrt{\kappa^2 - (r_{12}-r_{14})^2} \end{aligned} \quad \textbf{(2.197)}$$

With no grating ($r_{12} = r_{14} = 0$), (2.195) is reduced to (2.176), the solution for the codirectional coupler.

Figure 2.15 shows the numerical evaluation of the four output powers ($P1$, $P2$, $P3$ and $P4$ at ports 1, 2, 3, and 4, separately) of a reciprocal, bilaterally and transversely symmetric grating assisted coupler as a function of the normalized coupling length (L/λ)

for unit input power at port 1. The waveguide parameters are: n_{sc} = 2.200, n_{s0} = 2.287, n_{fc} = 2.320, and n_{f0} = 2.247, $d_A = w_A = d_B = w_B = s = \lambda$, and the grating period $\Lambda = 0.5\lambda$. The depth of the gratings h are different for the three plots.

In Fig. 2.15a, $h = 0.001\lambda$, it is close to the characteristics of a codirectional coupler because of the small effect of the grating. The outputs at port 1 and 2 are very small. The variations of P3 and P4 are nearly sinusoidal functions of the normalized coupling length.

Fig. 2.15b is for a depth of grating $h = 0.0025\lambda$. As h increases, the maximum amplitude that P4 can reach decreases. The other two outputs, namely $P1$ and $P2$ rise because the Bragg coupling increases (r_{12} and r_{14} increase). One quarter of the output power is obtained at all of the four ports for certain coupling length.

In Fig. 2.15c, $h = 0.005\lambda$. We see that most of the power is reflected back to port 1. The direct Bragg coupling r_{12} is stronger when the large grating depth is used.

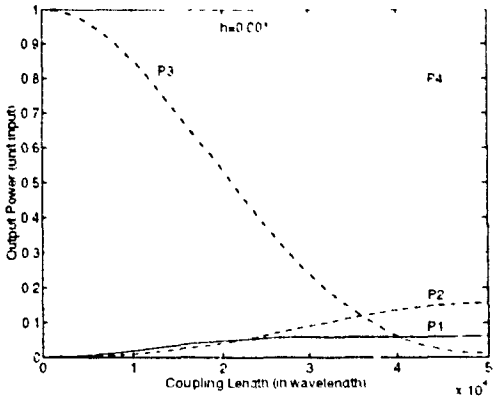

(a)

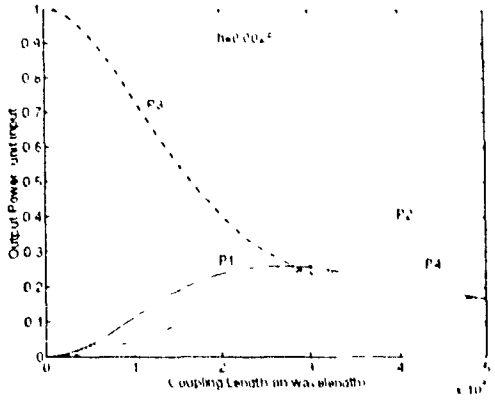

(b)

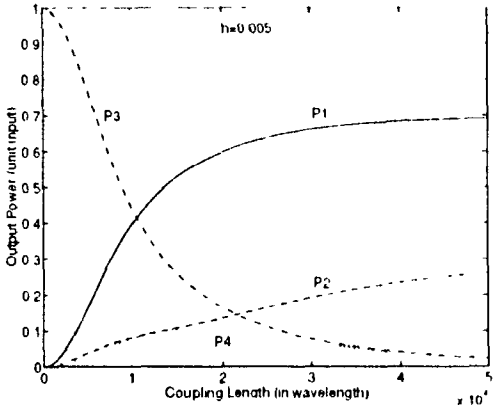

(c)

Fig. 2.15 Normalized power distributions in a grating assisted coupler in Z cut $LiNbO_3$. $\Delta n_e = 0.12$, $\Delta n_o = -0.04$, $d = w = s = \lambda$, $\Lambda = \lambda/2$: (a) $h = 0.001\lambda$, (b) $h = 0.0025\lambda$ and (c) $h = 0.005\lambda$

2.6 Computer Program Description

A computer analysis program which evaluates the properties of grating assisted optical couplers has been developed. This program is developed in a commercial software MATLAB environment which is for high-performance numeric computation and visualization. MATLAB integrates numerical analysis, matrix computation and graphics in an easy-to-use environment where problem and solution are expressed just as they are written mathematically. MATLAB is an interactive system whose basic data element is a matrix that does not require dimensioning. This software is very suitable to be used in engineering calculations, such as the analysis of grating assisted coupler.

The schematic description of the program appears in Fig. 2.16. Logically, the program consists of three parts: menu (main topics and sub-topics) and data input, calculation modules, graphic and data output. The analysis is based on the assumptions that the substrate axes are those of the laboratory Cartesian coordinates, that the normal of the substrate surface is in the x direction, that the optical wave propagation direction is in the z direction, and that the cover medium is air ($n_0 = 1$).

At the present time, this program is available in MATLAB version 4.0 in UNIX using X-windows.

2.6.1 Data input and menu selection

The data input includes material data, geometrical and modal parameters. The index tensors of the substrate and guiding film layer are input in the **Material Data Input**

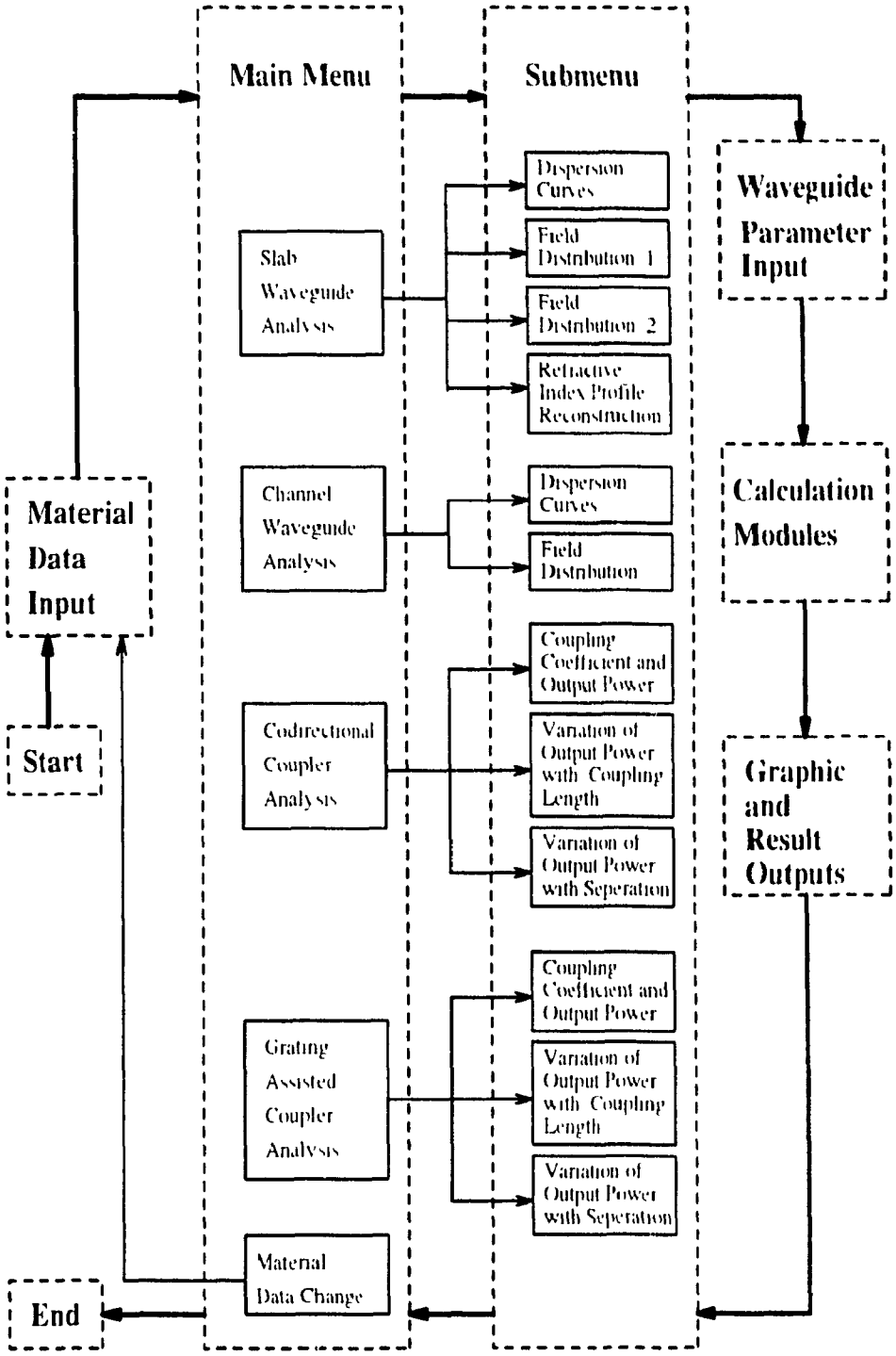

Fig. 2.16 Computer program organization

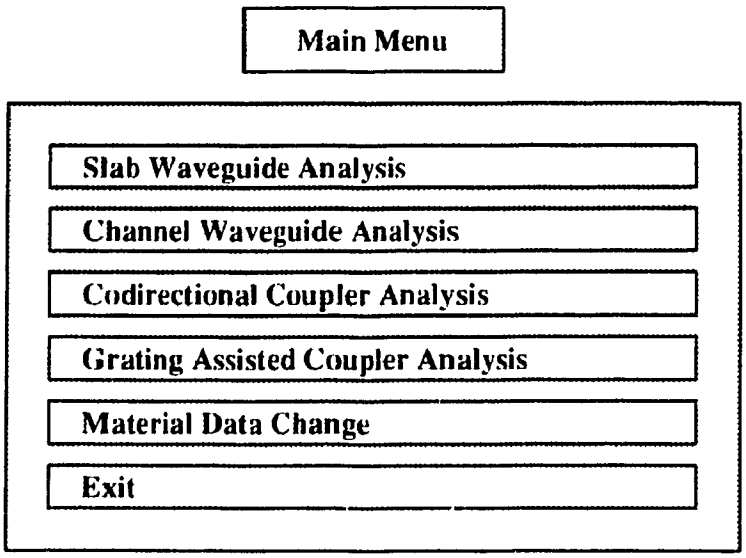

Fig. 2.17 Main input menu

block. This is done at the beginning of the executive program and the data can be changed by choosing **Material Data Change** in the main menu as shown in Fig. 2.17. Some common substrate materials for optical waveguides are stored in a library under this selection. If any other material is desired in the analysis, it is very simple to add a new M-file to include the new refractive index tensor into the library. Each input parameter can be individually updated (changed) on the screen.

The analysis topics are selected from the main-input and sub-input menus. Main input menu includes four selections of analysis topics, **Slab Waveguide Analysis, Channel Waveguide Analysis, Codirectional Coupler Analysis and Grating Assisted Coupler Analysis**, as shown in Fig. 2.17. Any selection among these four topics leads to a sub-input menu which offers as sub-topics properties available for analysis. The submenu for slab waveguide analysis is an example shown in Fig. 2.18. There are four

items in this submenu. The first one is for calculating the dispersion curves of the asymmetric slab waveguide. The field distribution is obtained from either the second or the third item. The second item is only to calculate one mode each time. The data of the mode order number and the waveguide parameters are fetched from the dispersion curve plots using mouse or the arrow keys. The dispersion curve plots must be obtained previously. The third item, which does calculation for several modes each time, uses waveguide parameters input from keyboard. The **Refractive Index Profile** is used to reconstruct the refractive index profile of a planar waveguide with a set of measured refractive index based on the inverse WKB method[40]. **Exit** returns the user to the main menu for other selections. The details of the other submenus are shown in Fig. 2.16.

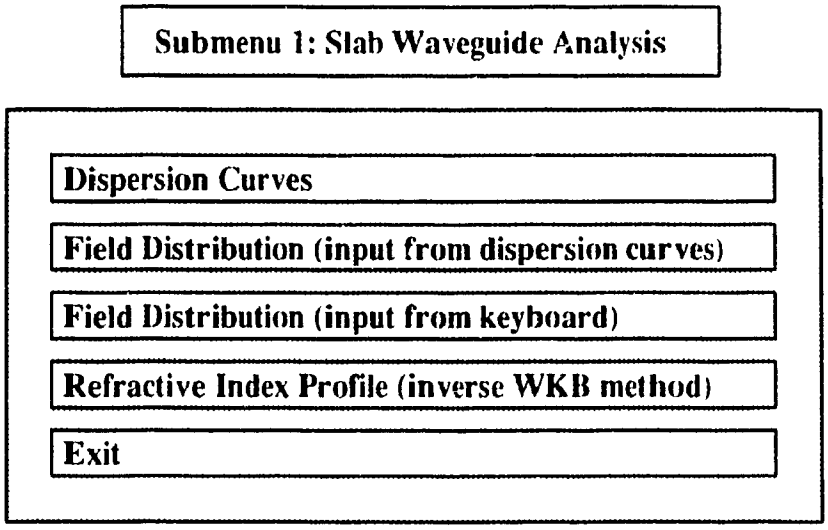

Fig. 2.18 Submenu 1 under *Slab Waveguide Analysis*

2.6.2 Calculation modules

Any submenu selection causes execution of the calculation modules after specifying the waveguide geometrical parameters. All these modules are based on the formulations given in the previous sections. For example, if the **Dispersion Curves** in Fig. 2.18 is selected, the effective indices are computed as a function of the normalized depth of the guiding layer (normalized wavelength parameter). This computation is based on the relations given in Section 2.1. Fig. 2.2 is an example for a dispersion curve calculation.

The selection of **Field Distribution** in the submenus, **Slab Waveguide Analysis** and **Channel Waveguide Analysis**, prompts computation of the field variation along the x direction (the normal direction) for slab waveguide or in the x-y plane (transverse cross section) for channel waveguide.

In all the calculations the length dimensional parameters are normalized to wavelength. Field distribution calculations correspond to unit power carried by the waveguides. In the codirectional coupler and grating assisted coupler analyses, the total input power is normalized to unity.

2.6.3 Graphics and data output

The results of all calculations are available both numerically and graphically. In **Dispersion Curves** calculations, both the dispersion curves and the cut-off point for each mode are displayed. The field distribution curves and the propagation constants as well

as the effective indices are displayed after the calculation after the selection of **Field Distribution**. In the analysis of couplers, the output results include the diagrams of output power variations with waveguide dimensions and the coupling coefficients.

After each diagram is obtained, the **Graphic Processing** menu, as shown in Fig. 2.19, gives a chance to add some necessary text to the current plots. The text is input from the keyboard and placed on the desired location with the mouse or the arrow keys. The plots can be saved to a file under a name specified by the user either with the extension name of ".ps" as a postscript file for later printing or with the extension name of ".eps" as a encapsulated postscript file which can be used in the word processing. Before the plot is being saved, the diagram size and location on the printed paper need to be specified following the explanation and the input prompt. **To Another Figure** lets the user work on other diagrams. The figure number appearing at the top-left of the menu is the current figure number. **Exit** brings the program back to the point where it was before the graphics calculation. If the current figure is not saved, it will be deleted from the workspace.

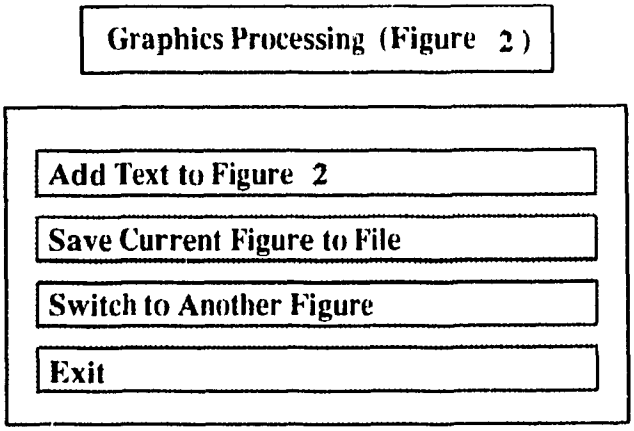

Fig. 2.19 Graphics processing menu

Chapter 3

EXPERIMENTAL PART

Fabrication & Characterization of Proton Exchanged Waveguide with Grating in $LiNbO_3$

The proton exchange process was invented in 1982 by J. Jackel et.al., and used for waveguide fabrication in $LiNbO_3$.[111] In this method, the metal ions in the crystalline substrate are partially replaced by hydrogen ions from some appropriate proton source. This approach can produce a large change in the refractive index, with a nearly step-like profile near the surface of the substrate. Comparing with Ti-indiffusion and ion exchange methods, proton exchange has some advantages such as greater index increase, lower processing temperature, simpler fabrication method, flexible control of the index profile and the surface index, etc.

In this chapter, the proton exchange method is reviewed, a two-step proton exchange process employed to produce waveguides and gratings in lithium niobate is presented, and the characterizations of the samples are described.

3.1 Fabrications

In this section, the proton exchange technique in $LiNbO_3$ is reviewed. The fabrication procedures and parameters of waveguide and grating made by proton exchange are presented.

3.1.1 Proton exchange technique in $LiNbO_3$

Of the several kinds of acids used as proton exchange source, benzoic acid (C_6H_5COOH) is the most widely used. It is a white powder at room temperature with a melting point of 121°C and boiling point of 250°C. The proton exchange process in $LiNbO_3$ is performed by immersing the $LiNbO_3$ substrate in molten benzoic acid kept at a fixed temperature, usually between 200°C - 300°C, for a desired exchange time. In equilibrium, the acid dissociates as

$$C_6H_5COOH \longleftrightarrow C_6H_5COO^- + H^+ \qquad (3.1)$$

The amount of dissociation and thus the number of protons depends only on temperature. The proton exchange process can be described by the following chemical equilibrium reaction

$$LiNbO_3 + C_6H_5COOH \longleftrightarrow Li_{1-x}H_xNbO_3 + (C_6H_5COOLi)_x \qquad (3.2)$$

where, usually, $x > 0.5$.[122] This process results in a higher index guiding layer near the crystal surface.

Observation shows that only the extraordinary refractive index in the guiding area

is modified ($\Delta n_e \approx 0.12$ at $\lambda = 0.6328\mu m$). The ordinary refractive index has a small but significant decrease ($\Delta n_o \approx -0.04$ at $\lambda = 0.6328\mu m$). These properties make polarization control available. As described in Chapter 2, only TM modes propagate in the waveguides in Z cut $LiNbO_3$ and TE modes in X and Y cut $LiNbO_3$ substrate. Applications of proton exchange in X-cut and Z-cut $LiNbO_3$ substrate to various devices has been successfully demonstrated[26,27,28]. The use of proton exchange to Y-cut substrate must be handled very carefully because of the potential surface damage to the substrate in pure benzoic acid.[29,30,31] This difficulty can be overcome by using diluted benzoic acid but longer processing times are required.[32] Another method to protect the surface of Y cut $LiNbO_3$ substrate is to use titanium indiffusion followed by proton exchange[30] or to shorten the processing time.

There are two techniques used in the fabrication of proton exchanged waveguide which can provide separate control over the index profile and the surface refractive index change.[29,32,33] These techniques can also be used to reduce the optical propagation loss.[34,35]

The first one is the use of diluted melts, which reduces the hydrogen ion concentration by adding various lithium salts to pure benzoic acid. With this method the index profiles obtained by a diluted proton source are step-like[33] and the extraordinary refractive index change can be reduced by an amount dependent on the percentage of the diluent. The change of the refractive index at the surface of the substrate: $\Delta n_e(0)$, depends on the concentration of lithium benzoate (*L.B.*), of the diluent. The $\Delta n_e(0)$ versus L.B. relation exhibits a jump at a specific value of *L.B.* For example, at $T = 300^{\circ}C$, this jump

occurs at *L.B.* = 2.6%. For lesser concentrations $\Delta n_e(0) \approx 0.10$ to 0.12 (at λ = 0.6328 μm), whereas for larger concentrations $\Delta n_e(0) \approx 0.025$ (at λ = 0.6328 μm).[136] For *L.B.* < 3% at *T* = 250°C, or for *L.B.* < 2.5% at 300°C the waveguide depth and the exchange time are related through

$$\log_{10}(d) = \alpha \log_{10}(t) + \beta \tag{3.3}$$

where α = 0.42, *d* is the depth in μm, *t* is the exchange time in minute, and the value of β when *L.B.* = 1% is -0.46 for *T* = 300°C and -0.72 for *T* = 250°C.[136] For *L.B.* ≥ 3% the above relationship must be replaced by

$$d = \sqrt{Dt} \tag{3.4}$$

where the diffusion coefficient *D* = 1.16 μm²/h for *L.B.* = 3% at *T* = 300°C, and *t* is the exchange time in hours.

The second method is annealing. Annealing can reduce the hydrogen concentration within the guiding layer, i.e., it can reduce the surface refractive index change, and it can increase the depth of the waveguides. Annealing will also change the index profile from step-like to graded profile. The modification of index profile is strongly dependent on the annealing time and temperature. With increasing annealing time the abrupt profile is gradually smoothened and the index change at the surface diminishes. Annealing is necessary to obtain a low loss, stable waveguide. Scattering losses are dependent on the orientation of the substrate; typical values being 2 dB/cm for Z cut waveguides and 5 dB/cm for X cut waveguides at λ = 0.6328μm.[137] Annealing can reduce the loss to about 1 dB/cm or lower. Annealing temperatures range usually

between 250°C and 400°C, while annealing times range from minutes to hours. When the temperature exceeds 300°C, annealing usually should be performed in the presence of flowing oxygen to prevent deoxidization of the substrate surface. The degree of annealing coupled with the initial depth of the proton exchange region determine the resulting waveguide refractive index profile.[38]

The effects of lithium benzoate concentration and annealing on proton exchange waveguide characteristics are also discussed by Hinkov and Ise.[33]

Since the molten benzoic acid is strongly noxious, proton exchange must be performed in a tightly closed pyrex glass tube, as shown in Fig. 3.1. The first step is putting the mixture of benzoic acid and lithium benzoate powders into a pyrex tube and melting it in a furnace. Next the sample (with mask for channel waveguide) is placed in the tube and the tube is then pumped down to vacuum and sealed. The glass tube is then preheated in a furnace. When the temperature stabilizes, the tube is turned upside down to start the proton exchange process. To stop the process, the tube is turned back into its original position. After the exchange, the sample is removed from the tube and the residual benzoic acid is cleaned off the sample with propanol.

3.1.2 Fabrication of proton exchanged waveguide

A waveguide has been produced in X cut Y propagation $LiNbO_3$ substrate. The procedure is summarized in Fig. 3.2. It includes six steps: substrate cleaning, Cr metal

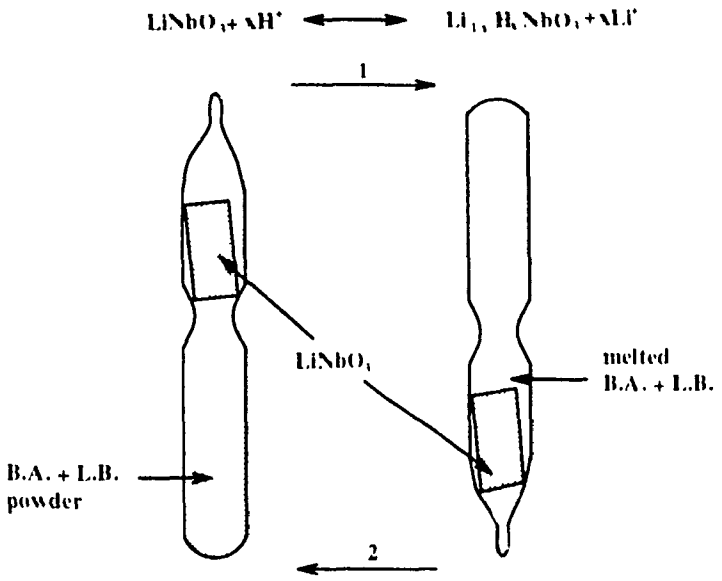

Fig. 3.1 Proton exchange technique

film coating, photolithography, proton exchange, annealing and polishing. The details are described below.

Substrate cleaning:

Well polished optical grade X cut $LiNbO_3$ substrates (10mm × 8mm × 1mm) were cleaned carefully with the standard cleaning procedure that includes four steps:

- Clean the substrate in heated trichloroethylene (TCE) for about 10 minutes and rinse thoroughly in deionized (D.I.) water.
- Repeat the above procedure with acetone.
- Repeat the above procedure with propanol.
- Dry the substrate with N_2 gas.

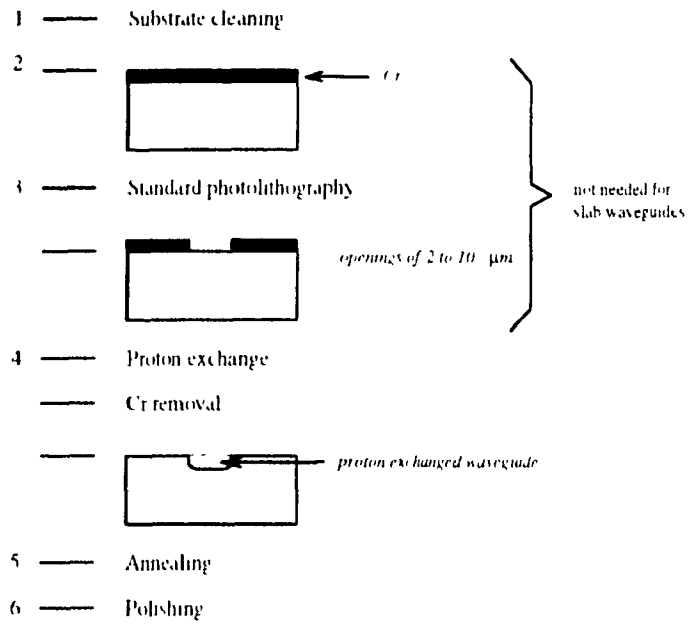

Fig. 3.2 Fabrication procedures of proton exchanged waveguide

Cr film coating:

The cleaned substrate is loaded into an E_Beam vacuum system to deposit a layer of Cr film with a thickness of about 800 Å. The vacuum chamber should be pumped down to 2×10^{-6} torr. The evaporating voltage is 4,000 Volts and the current is slowly increased to about 50 - 80 mA which leads to the proper evaporating rate of about 5 - 10 Å/s.

Photolithography:

The channel waveguide mask is made by standard photolithography. The process parameters are:

- Application of "1400-17" photoresist with spinning rate of 4000 rpm for

30 seconds

- baking at 90°C for 30 minutes
- exposing to light for 5 seconds
- developing for 45 seconds in "Developer 345"

The two steps described above, namely Cr film coating and photolithograph are not needed for slab waveguide fabrication.

Proton exchange:

The fabrication of the proton exchanged waveguide was performed in melted diluted benzoic acid by the procedures mentioned in Section 3.1.1. The lithium benzoate concentration used was 1%. Proton exchange was carried out at 200°C and 300°C for 1 to 3 hours. After the processing the samples were slowly cooled to room temperature, and then removed from their glass enclosure. The residual benzoic acid was removed with propanol. The Cr film was subsequently removed in the etchant

$$Ce(SO_4)_2 \cdot 2(NH_4)_2SO_2 \cdot 2H_2O\ (16.45g) + HCLO_4\ (4.3ml) + H_2O = 100\ ml \qquad (3.5)$$

Annealing:

Afterwards the waveguide was annealed at 300°C and 400°C with 3 hours. During the annealing processing, flowing dry oxygen was used to prevent deoxidization. The flowing rate of the oxygen gas was 5 cm^3/s. The fabrication parameters are summarized in Table 3.1.

Table 3.1: Waveguide fabrication parameters

No.	Proton-exchanging			Annealing	
	T (°C)	t (h)	$L.B.$(%)	T (°C)	t (h)
gs1	200	2.5	1		
gs2	300	3	1		
gs7	300	1	1	400	3
gs10	300	1	1	400	3
gs12	300	1	1	400	3
gc4	300	40 min	1	400	3
gc6	300	1	1	400	3
gc8	300	1	1		

Polishing:

The two ends of the sample were carefully polished. Rough polishing was carried out with 3 μm polishing liquid for 20 - 30 minutes. Fine polishing was carried out with 0.05 μm polishing liquid for 1 hour.

3.1.3 Fabrication of proton exchanged grating

A grating was implanted onto the waveguide. The procedures of grating fabrication is shown in Fig. 3.3. It consists of substrate cleaning, Cr metal film coating, grating mask pattern fabrication by photolithography, proton exchange and chromium film removal. The first two steps are the same as those in the waveguide fabrication. Here

only the last few steps are discussed.

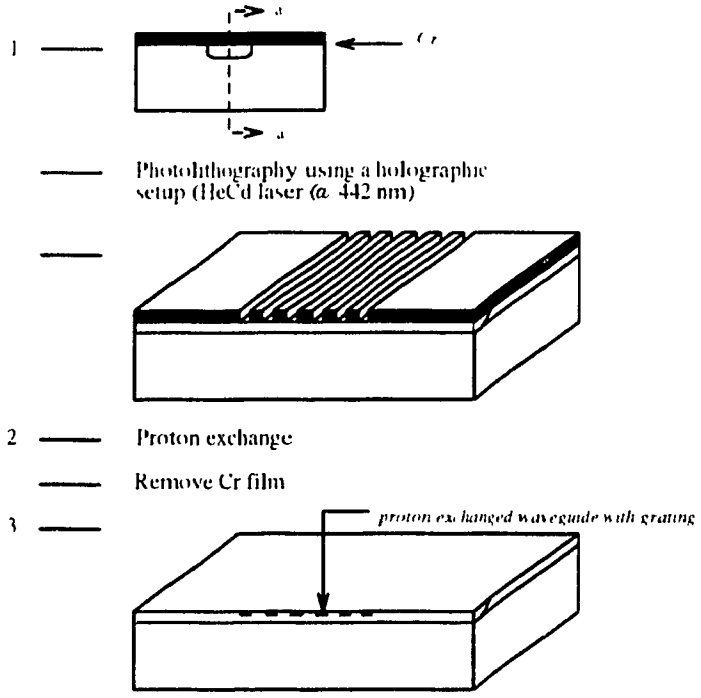

Fig. 3.3 Procedures of grating fabrication

The grating mask pattern was made using a holographic setup and a two layer photoresist processing. Fig. 3.4 is the scheme of the holographic setup. The light source is a HeCd laser, operating at λ_0 = 442 nm. The period of the interference pattern is determined by the angle ϕ between the two interfering beams according to the formula

$$\Lambda = \frac{\lambda_0}{2\sin\phi} \tag{3.6}$$

The substrates were first coated with a thin (~800Å) Cr film and subsequently coated with two layers of photoresist, the first of which is doped with coumarin to prevent reflection from the Cr film. The samples were then placed in the holographic setup and were

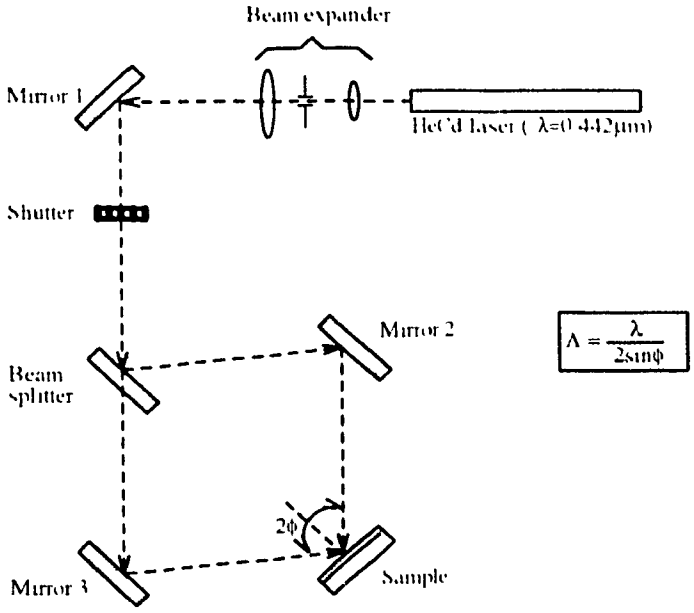

Fig. 3.4 Holographic setup

exposed to the interference pattern. Then the exposed samples were developed in "Developer 345". After development, the exposed photoresist was removed and the grating pattern was imposed on the photoresist layers. After that the gratings were transferred to the Cr mask by chemical etching. Afterwards, the photoresist was removed completely. Finally, another proton exchange was implemented through the openings created in the metal mask. The fabrication parameters are summarized in Table 3.2. The temperature used was 260°C, the lithium benzoate concentrations applied were 1% and 3%. Processing time was 10 - 20 min. For comparison, some of the gratings were made by plasma etching (using 96% CF_4 and 4% O_2). The procedures and processing parameters are summarized in Fig. 3.5.

Table 3.2: Grating fabrication parameters

No.	Proton exchanging			Plasma etching
	T (°C)	t (min)	$L.B.(\%)$	t (min)
gs1				10
gs2				11
gs7	260	10	1	
gs10	260	15	1	
gs12	260	10	1	
gc4				10
gc6	260	15	1	
gc8	260	15	1	

1. Doped photoresist layer

- photoresist (1400-4) : coumarin = 5 ml : 80 mg
- spinning: 7,000 - 10,000 rpm, 40 s
  bake: 120°C; 1 h

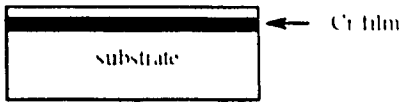

2. Second photoresist layer

- photoresist 1400-4 : 1400-17 = 2 : 1
- spinning 4,000 - 6,000 rpm, 40 s
  bake 90°C - 95°C, 0.5 h

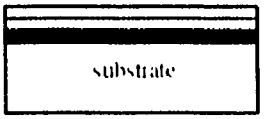

3. Exposure

- exposure 1 - 1.5 s

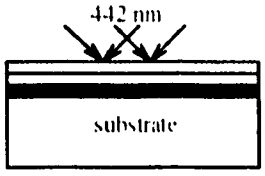

4. Development

- develop sample in "Developer 354" 45 - 60 s
- rinse sample in D.I. water

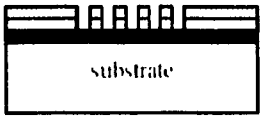

5. Chemical etching

- $Ce(SO_4)_2 \cdot 2(NH_4)_2SO_4 \cdot 2H_2O$ (16.45g) + $HClO_4$ (4.3ml) + H_2O = 100 ml

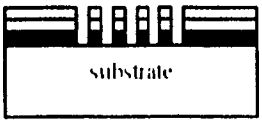

6. Photoresist removal

Fig. 3.5 Holographic fabrication procedure of a grating mask

3.2 Characterization

The samples of proton exchanged waveguides with grating are characterized. The measurement set-up and method are described. The inverse WKB method for refractive index profile reconstruction is reviewed. The results obtained from those methods are presented. The light intensity diffracted out into the air by the grating is about 0.5% of that in the waveguide.

3.2.1 Refractive index measurement of slab waveguide by prism coupling

The prism coupling technique is used to characterize slab waveguides using a high-index prism to excite a guided wave through phase matching between the incident wave and a guided mode. The schematic of the setup for the measurement of refractive

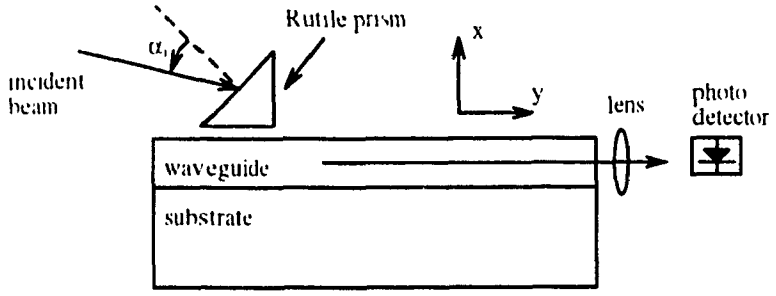

Fig.3.6 Measurement setup for Prism coupling

index of slab waveguide is shown in Fig. 3.6. A rutile (TiO_2) prism is used to couple the optical beam of a HeNe laser source (λ_0 = 0.6328μm) into the waveguide at an oblique angle α_1 measured from the normal of prism. A standing wave distribution within the

prism and an exponentially decaying field in the gap region between prism and waveguide are created. The entire field distribution propagates along the z direction. If the prism is close enough to the waveguide, the tail of the prism mode overlaps the tail of the waveguide mode and strong coupling occurs. When the phase matching requirement is satisfied for waveguide mode i, the corresponding effective index value is obtained by[109]

$$n_{eff} = n_p \sin\left[\sin^{-1}\left[\frac{\sin \alpha_i}{n_p}\right] + \theta_p\right] \qquad (3.7)$$

where $n_p = 2.8625$ is the refractive index of the rutile prism, $\theta_p = 45°$ is the toe angle of the prism and $i = 0, 1, 2, 3,...$ is the waveguide mode number. By varying the incident angle α_i the coupling can be optimized for each mode separately. At optimum coupling the output at the end of the waveguide, measured by a photodetector, is maximum.

The measured results for a prism coupled slab waveguide are listed in the proper rows of Table 3.3. Because only the extraordinary index was increased in the guiding area, those samples only support TE mode(s). Sample gs1 only supports one mode because it was made with lower processing temperature, while sample gs2 supports seven modes due to the higher processing temperature. The higher processing temperature is used, the higher diffusion rate is obtained and the larger waveguide depth is obtained.

Table 3.3: Effective refractive indices of slab waveguides measured using prism coupling and grating diffraction

Sample	Mode								Measurement
	0	1	2	3	4	5	6	7	
gs1	2.2462								prism coupling
	2.2444								2nd order diffr.
	2.2463								3rd order diffr
gs2	2.3026	2.2936	2.2816	2.2641	2.2426	2.2169			prism coupling
	2.3069	2.2981	2.2856	2.2685	2.2449	2.2184			2nd order diffr
	2.3052	2.2957	2.2826	2.2667	2.2442	2.2171			3rd order diffr.
gs7	2.2552	2.2348	2.2234	2.2148	2.2085	2.2047	2.2030		prism coupling
					2.2187	2.2147	2.2114		2nd order diffr.
gs10	2.2325	2.2261	2.2206	2.2153	2.2110	2.2076	2.2047	2.2031	prism coupling
				2.2198	2.2150	2.2108	2.2097		2nd order diffr.
gs12	2.2381	2.2303	2.2238	2.2180	2.2128	2.2087	2.2056	2.2024	prism coupling
	2.2441	2.2366	2.2294	2.2213	2.2170	2.2105	2.2090	2.2085	1st order diffr.

3.2.2 WKB evaluation of the refractive index profile

Using the effective refractive indices associated with the guided modes , obtained in the last section, the refractive index profile of the planar multimode waveguide is reconstructed by the inverse WKB method proposed by White and Heidrich.[40] In this method, a set of effective indices, $n_{eff,m}$ (m = 1, 2, 3, ..., M) for a waveguide which has M modes, is given, and the estimation of the refractive index profile $n(x)$, i.e. the index vs. waveguide depth function, is in the form of M straight line segments which connect the M+1 points ($[x_0, n_{eff,0}]$, $[x_1, n_{eff,1}]$, ..., $[x_M, n_{eff,M}]$) as shown in Fig. 3.7. To simplify the writing in the following discussion, n_m is used to instead of $n_{eff,m}$. The profile $n(x)$ decreases monotonically, with $n_0 = n(0)$ at $x_0 = 0$. The surface index n_0 is chosen so as

to produce the smoothest profile. The mode numbering system used here is shifted by one from that used in previous sections and n_0 is used to refer to the surface index.

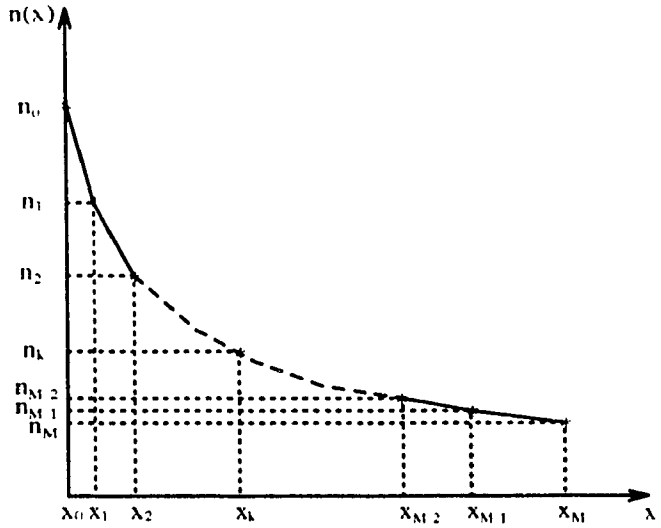

Fig. 3.7 The numbering system of a refractive index profile which is built by M straight segments connecting M+1 points.

Since a mode is a standing wave pattern in the transverse direction, the total phase change of the propagating wave must be an integral multiple of 2π. In the WKB approximation, the effective index n_m of the mth order guided mode is determined by

$$2k_0\int_0^{x_m}\sqrt{n^2(x)-n_m^2}\,dx - 2\phi_1 - 2\phi_2 = 2(m-1)\pi \qquad (3.8)$$

where x_m is defined by $n(x_m) = n_m$, $-2\phi_1$ and $-2\phi_2$ represent the phase shift at the waveguide-air interface and at the turning point where the light beam changes the propagation direction, respectively. Note that m-1 is used in (3.8) because m starts from 1. It is assumed that the phase shift $2\phi_1 \approx 2 \times (\pi/2)$ at the waveguide surface ($x = 0$) and $2\phi_2 \approx 2 \times (\pi/4)$ at the turning points ($x = x_m$).[40,41] So (3.8) can be reduced to

$$\int_0^{x_m} \sqrt{n^2(x) - n_m}\,dx = \frac{4m-1}{8} \tag{3.9}$$

where $n(x)$ is normalized to the free space wavelength λ_0. To evaluate x_m, the integration at the l.h.s. of (3.9) can be expressed as a sum of the integrals in each sub-period (x_{k-1}, x_k),

$$\sum_{k=1}^{m} \int_{x_{k-1}}^{x_k} \sqrt{n^2(x) - n_m^2}\,dx = \frac{4m-1}{8} \tag{3.10}$$

The term in the square root is split into two terms,

$$\sum_{k=1}^{m} \int_{x_{k-1}}^{x_k} \sqrt{n(x) + n_m}\,\sqrt{n(x) - n_m}\,dx = \frac{4m-1}{8} \tag{3.11}$$

Since $n(x)$ is assumed to be a piecewise linear function connecting the given values of n_m, a linear function in the sub-period (x_{k-1}, x_k) is expressed as

$$n(x) \approx n_k + \frac{n_k - n_{k-1}}{x_k - x_{k-1}}(x - x_k) \qquad \text{for } x_{k-1} \le x \le x_k \tag{3.12}$$

To approximate the first factor under the integral in (3.11) we use the midpoint value to replace the function value in the sub-period (x_{k-1}, x_k) as shown in Fig. 3.8 so that

$$n(x) + n_m \approx \frac{n_{k-1} + n_k}{2} + n_m \qquad \text{for } x_{k-1} \le x <= x_k \tag{3.13}$$

Upon substitution of (3.12) and (3.13) into (3.11), the equation can be reduced to

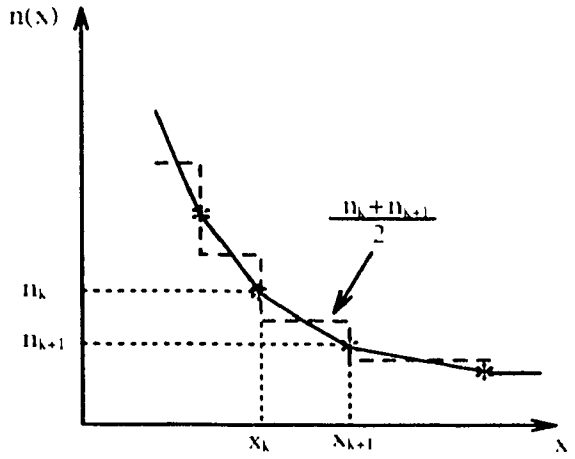

Fig. 3.8 Approximation of a refractive index profile which a midpoints is used to replace the function value in each sub-period.

$$\sum_{k=1}^{m}\left(\frac{n_k+n_{k-1}}{2}+n_m\right)^{\frac{1}{2}}\int_{x_{k-1}}^{x_k}\sqrt{(n_k-n_m)+\frac{n_k-n_{k-1}}{x_k-x_{k-1}}(x-x_k)}\,dx=\frac{4m-1}{8} \qquad \textbf{(3.14)}$$

The solution for x_m is obtained by carrying out the integration in (3.14) and by grouping the proper terms. Thus

$$\begin{aligned} x_m = x_{m-1}+&\left[\frac{3}{2}\left(\frac{n_{m-1}+3n_m}{2}\right)^{-1/2}(n_{m-1}-n_m)^{-1/2}\right] \\ &\times\left\{\left(\frac{4m-1}{8}\right)-\frac{2}{3}\sum_{k=1}^{m-1}\left(\frac{n_{k-1}+n_k}{2}+n_m\right)^{1/2}\left(\frac{x_k-x_{k-1}}{n_k-n_{k-1}}\right)\left[(n_k-n_m)^{3/2}-(n_{k-1}-n_m)^{3/2}\right]\right\} \end{aligned} \qquad \textbf{(3.15)}$$

for $m = 2, 3, ..., M$, and

$$x_1 = \frac{9}{16}\left(\frac{n_0+3n_1}{2}\right)^{-1/2}(n_0-n_1)^{-1/2} \qquad \textbf{(3.16)}$$

The calculation can be started from (3.16) to obtain x_1, and x_m can be obtained based on the previously determined values x_{m-1}. All the depth values x_m for the M modes can be

obtained by repeating this calculation procedure and the function $n(z)$ is finally determined as approximated in (3.12).

It should be noted that n_0 is still unknown so far. The principle of the determination of n_0 is to take the value for n_0 that gives the smoothest profile, i.e., that value which minimizes the sum of the M-1 triangle areas described by the set of M+1 points. The mth triangle consists of the three points $[(n_m, x_m), (n_{m+1}, x_{m+1}), (n_{m+2}, x_{m+2})]$, $m = 0, 1, 2,..., M$-2. This can be expressed to find the minimum value of

$$\sum_{m=0}^{M-2} \frac{1}{2}\left[x_m(n_{m+1}-n_{m+2}) - x_{m+1}(n_m-n_{m+2}) + x_{m+2}(n_m-n_{m+1})\right] \qquad (3.17)$$

for a given n_0 (by iterative trial and error). The major effect of this procedure is the straightening of the initial segments of the curve. Since diffusion tends to smooth out index changes, there is physical justification for this assumption.

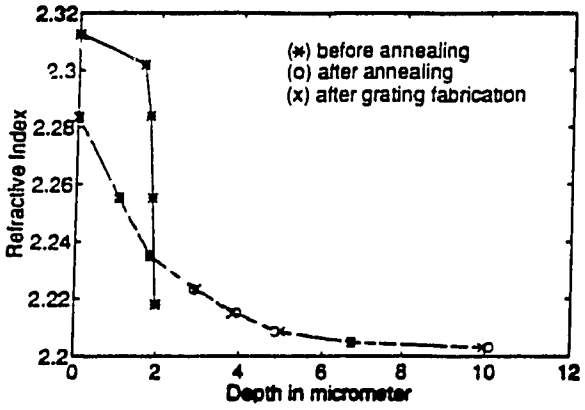

Fig. 3.9 Refractive index profile of sample gs7

We applied the WKB method to evaluate the index profile of the fabricated waveguides. Fig. 3.9 illustrates the result obtained for sample gs7. From this figure, we can see that after the proton exchange process the profile is step-like while it is smoothly

graded after the annealing process. Annealing increases the number of propagating modes from 4 to 7 since the waveguide depth is increased after this process.

The inverse WKB method described above gives good results provided that the guide supports several modes. If the waveguide supports less than three modes, the approximation in this method decreases in accuracy because the profile function $n(x)$ is sensitive to the chosen value n_0 for the lowest order modes and it is difficult to use the minimization method in (3.17) to give a good approximation for few points.

Hertel and Menzler presented an improved inverse WKB method[11]. In this method, they have taken into account one more effective index point — bulk index n_{bulk}, and the profile form near the surface and its approach towards the bulk value. Then an interpolation algorithm is used to construct a polynomial function which passes through the points. Considering one more index point is able to reconstruct the refractive index profile within experimental accuracy even the waveguide only supports three or two modes.

A method that can estimate the refractive index profile of a monomode graded index planar optical waveguide is presented by Kaul and Thyagarajan.[12] The principle of this method is that instead of measuring the different effective indices corresponding to the various modes propagating in a multimode guide, here one measures the fundamental mode index for the single mode guide at several wavelength. The index profile is then determined from these data.

3.2.3 Grating assisted waveguide

The periodicity of the fabricated gratings were determined using a HeNe laser (0.633μm) and a HeCd laser (0.442μm). Light was directed onto the surface of the sample and the diffraction angles were recorded, as shown in Fig. 3.10. The period was calculated from the expression[43]

$$\Lambda = \frac{\lambda}{\sin\theta_1 - \sin\phi} \qquad (3.18)$$

where ϕ is the angle between the incident beam and normal, θ_1 is the angle between the first order diffracted beam and normal and λ is the wavelength. Note that ϕ is negative

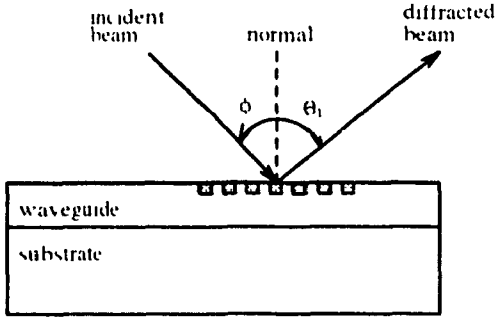

Fig. 3.10 Measurement of grating periodicity

when the incident and diffracted beams are on the same side of the normal. The measured values are reported in Table 3.4

Table 3.4: Calculated grating periodicity

Sample	Λ (μm)	Fabrication process
gs1	0.922	slab waveguide, no annealing, plasma etched grating
gs2	0.922	
gs4	0.922	slab waveguide, annealed, p-exchanged grating
gs7	0.923	
gs10	0.908	
gs12	0.294	
gc4	0.915	channel waveguide, annealed, plasma etched grating
gc6	0.292	channel waveguide, annealed, p-exchanged grating
gc8	0.292	channel waveguide, no annealing, p-exchanged grating

To characterize the grating assisted slab waveguides, the refractive indices were computed from the measured values of the diffraction angle. Light from a HeNe laser was coupled into the waveguides using a rutile prism and the beams diffracted by the grating were observed on a screen, as shown in Fig. 3.11. The angles between the various diffracted beams and the substrate normal, θ_m, were measured and the effective indices of the corresponding waveguide modes were determined from the phase matching condition[43,44]

$$n_{eff} = \sin \theta_m + \frac{m \lambda}{\Lambda} \qquad (3.19)$$

where m = 1, 2, 3, ... is the diffraction order. The results are summarized in Table 3.3. The indices obtained by the measurement of grating diffraction are comparable to those obtained by prism coupling. The difference is caused by uncertainties in the grating period Λ, and in the diffraction angle θ_m. For proton exchanged slab waveguides gs7 and

gs10, only part of the modes can be observed due to the weak diffraction.

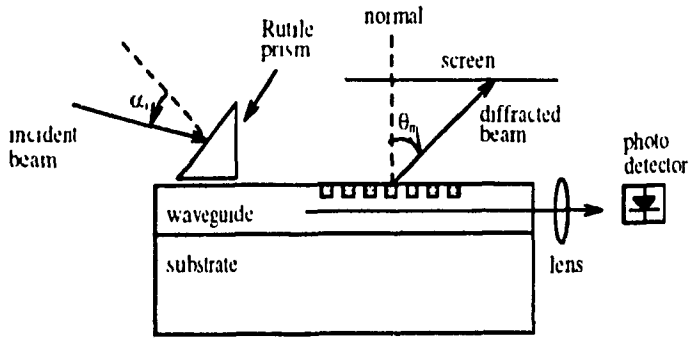

Fig. 3.11 Measurement of refractive index using grating on a slab waveguide; prism coupling

The same measurement technique was applied to channel waveguides. Light from a HeNe laser was coupled into the waveguide through one of the polished ends and the diffraction angles were measured as described above. The measurement setup is shown in Fig. 3.12. Table 3.5 summarizes the results. The range of angles represents the difference in diffractive angles corresponding to the lowest and highest order modes.

Table 3.5: Diffraction measurement results for channel waveguides

No.	Diffraction angle range	Index range (n_{eff})
gc4	6.789° - 8.381°	2.2041 - 2.2317
gc6	1.960° - 3.525°	2.2036 - 2.2308
gc8	3.096° - 7.567°	2.2226 - 2.3003

To estimate the efficiency of the grating, light from a HeNe laser was fed into the waveguide through one of the polished ends as shown in Fig. 3.13. The diffraction efficiency is obtained by measuring the intensity I_d of the beam diffracted by the grating

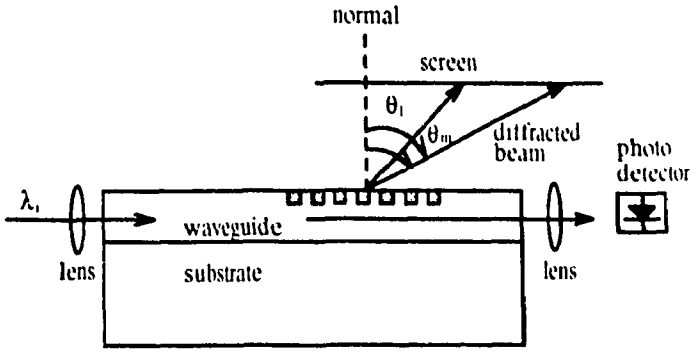

Fig. 3.12 Measurement of the refractive index using grating on a channel waveguide; butt coupling

and the intensity I_o of the beam output from the waveguide. The intensity of the beams were measured using a calibrated detector. The spot of the diffracted beam is very small, no lens is used in the intensity measurement. The ratio I_d/I_o gives the efficiency. Approximately one half percent of the guided light was found to diffract into air for the proton-exchanged grating.

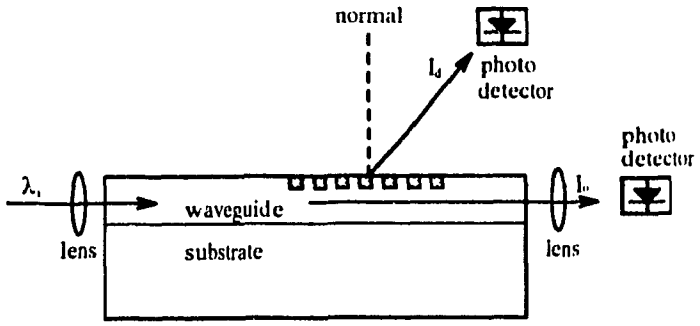

Fig. 3.13 Measurement of grating diffraction efficiency

The gratings of sample gs1 and gs2 were made by plasma etching, while those of gs7, gs10 and gs12 were made by proton exchange. The diffraction efficiency of plasma etched grating (the coupling between propagating and radiation modes) is much higher

than that in the proton exchanged gratings, due to the larger Δn_g. For samples gs1 and gs2, all the radiation modes can be observed from the 2nd and 3rd order diffraction, while only 3 and 4 modes can be observed from the 2nd order diffraction for gs7 and gs10, respectively. First order diffraction is normally stronger than the higher order diffraction. The diffraction observed in sample gs12 is first order, whereas those in gs7 and gs10 were second order. All the diffraction modes can be observed in gs12. From these measured results, we can see that the diffraction efficiency can be improved in two ways. The first one is increasing the index difference between the grating area and the waveguiding area. This may be obtained by reducing the refractive index using longer time and higher temperature in the annealing process during waveguide fabrication, and by increasing the refractive index of the grating using pure benzoic acid for proton exchange. The second way is using a first order diffractive grating.

Chapter 4

CONCLUSIONS

In this thesis, the channel waveguide and the grating assisted coupler have been analyzed and numerically evaluated using a computer program developed in MATLAB. The operation of a grating assisted waveguide fabricated in X cut $LiNbO_3$ substrate with the proton exchange technique has been successfully demonstrated.

In Chapter 2, the theoretical part, we derived the relations between the device properties and device geometry parameters. In Section 2.1 we presented the dispersion relations and field distributions for TE and TM modes in a slab waveguides consisting of three biaxial layers. The range of waveguide depths for which a single mode is supported by a slab waveguide over a $LiNbO_3$ substrate can be obtained from the refractive indices of the guiding film and substrate. Following Marcatili's method in Section 2 we analyzed the properties of wave propagation in channel waveguides. The dispersion relations and field distributions for E^x_{pq} and E^y_{pq} modes were obtained. The coupling coefficients in codirectional couplers were obtained in Section 3, while in Section 4 the coupling coefficients of grating assisted waveguides were derived. The coupling coefficients were found to be proportional to the index change in the grating area. In Section 5, a matrix representation was given to describe the power exchange in

a grating assisted codirectional coupler. The coupling coefficient matrix was derived and constraints imposed by symmetry wave examined.

A computer program was used to demonstrate the behaviour of wave propagation in slab waveguide, channel waveguide, codirectional coupler and grating assisted coupler for specified geometrical parameters. The computer program can be used to compute the optimal device parameters. The dispersion curves and the field distributions of slab and channel waveguides, and the coupling coefficients of a codirectional coupler or a grating assisted coupler were evaluated for given waveguide parameters, i.e. waveguide depth, width, guide separation of coupling length of a coupler. Variations of output power in a codirectional coupler and in a grating assisted coupler were simulated. A coupler that has two dissimilar waveguides can also be analyzed by this computer program.

A shallow grating was considered in the analysis. The numerical analysis of the grating assisted coupler reveals the dependence of direct Bragg coupling and exchange Bragg coupling on the waveguide parameters. The direct Bragg coupling increases with increasing grating depth. As the depth of grating increases, the exchange Bragg coupling tends to increase.

The experimental part in Chapter 3 reports on grating assisted proton exchanged waveguides which were successfully fabricated using two step proton exchange technique. The proton exchange was carried out in diluted benzoic acid. An annealing technique is used to decrease the surface index change and to obtain low loss waveguides. The grating pattern with submicrometer periodicity was made using a holographic setup.

The diffraction angles and diffraction efficiency were measured. The calculation

of refractive indices from the diffractive angles in slab waveguides showed the results were comparable to those obtained by prism coupling measurement. Using this method, it was found that the surface refractive index increase caused by annealing the grating assisted channel waveguide was 0.03. The diffraction efficiency was found to be approximately 0.5%. This value is small due to the small index difference between the guide and the grating, and because the grating is very shallow.

The grating assisted waveguides have a fully planar structure, it allows the integration of surface mounted components, such as detectors. These components can be used to selectively tap different wavelengths guided by the waveguide.

References

[1] S.E. Miller, "Integrated optics: an introduction," The Bell System Technical Journal, Vol. 48, No. 7, (1969) pp. 2059 - 2068

[2] M.L. Dakss, L. Kuhn, P.F. Heidrich, B.A. Scott, "Grating coupler for efficient excitation of optical guided waves in thin films," Applied Physics Letters, Vol. 16, No. 12, (1970) pp. 523 - 525

[3] H. Kogelnik, T.P. Sosnowski, "Holographic thin film couplers," The Bell System Technical Journal, Vol. 49, No. 7, (1970) pp. 1602 - 1608

[4] D.C. Flanders, H. Kogelnik, R.V. Schmidt, C.V. Shank, "Grating filters for thin film optical waveguides," Applied Physics Letters, Vol. 24, No. 4, (1974) pp. 194 - 196

[5] M.J. Li, S.I. Najafi, W.J. Wang, J.R. Simard, J. Albert, K.O. Hill and A. Leung, "Fabrication and characterization of ion-exchanged glass channel waveguides with etched and diffused grating taps," SPIE Proceedings, Vol. 1334, (1990) pp. 148 - 152

[6] H. Zhang, M.J. Li, O. Schwelb, S.I. Najafi, "Fully planar proton-exchanged lithium niobate waveguides with grating," SPIE Proceedings, Vol. 1583, (1991) pp. 83 - 89

[7] C.H. Von Helmolt, "Integrated optic strip waveguide phase modulator driven by a SAW," Journal of Lightwave Technology, Vol. 5, No. 2, (1987) pp. 218 -228

[8] H. Kogelnik and C.V. Shank, "Coupled-wave theory of distributed feedback laser," Journal of Applied Physics, Vol. 43, No. 5, (1972) pp. 2327 - 2335

[9] D. Marcuse, "Directional couplers made of nonidentical asymmetrical slabs Part II: grating assisted couplers," Journal of Lightwave Technology, Vol. 5, No. 2, (1987) pp. 268 - 273

[10] D. Marcuse, *Theory of Dielectric Optical Waveguides* (Second Edition), Academic Press, Inc., 1991

[11] J. Jackel, C.E. Rice, and J.J. Veselka, "Proton-exchange for high index waveguides in $LiNbO_3$," Applied Physics Letters, Vol. 41, No. 7, (1982) pp. 607 - 608

[12] E.A.J. Marcatili, "Dielectric rectangular waveguide and directional coupler for integrated optics," The Bell System Technical Journal, Vol. 48, No. 7, (1969) pp. 2071 - 2102

[13] J.E. Goell, "A circular-harmonic computer analysis of rectangular dielectric waveguides," The Bell System Technical Journal, Vol. 48, No. 7, (1969) pp. 2133 - 2160

[14] W. Schlosser and H.G. Unger, "Partially filled waveguides and surface

waveguides of rectangular cross-section," *Advances in Microwaves*, New York, Academic Press, (1966) pp. 319 - 387

[15] A. Sharma, P.K. Mishra and A.K. Ghatak, "Single-mode optical waveguides and directional couplers with rectangular cross section: a simple and accurate method of analysis," Journal of Lightwave Technology, Vol. 6, No. 6, (1988) pp. 1119 - 1124

[16] R.M. Knox and P.P. Toulios, "Integrated circuits for the millimeter through optical frequency region," in *Proceeding of Symposium on Submillimeter Waves*, J. Fox, (Ed.) Brooklyn: Polytechnic Press, pp. 497 - 516

[17] S. Akiba and H.A. Haus, "Variational analysis of optical waveguides with rectangular cross section," Applied Optics, Vol. 21, No. 5, (1982) pp. 804 - 808

[18] A. Kunar, K. Thyayarajan, and A.K. Ghatak, "Analysis of rectangular-core dielectric waveguides: An accurate perturbation approach," Optics Letters, Vol. 8, (1983) pp. 63 - 65

[19] H.A. Haus, W. Huang, and N.M. Whitaker, "Optical waveguide dispersion characteristic from the scaler wave equation," Journal of Lightwave Technology, Vol. 5, No. 12, (1987) pp. 1748 - 1754

[20] Pochi Yeh, *Optical Waves in Layered Media*, John Wiley & Sons, Inc (1988)

[21] A. Yariv and P. Yeh, *Optical Waves in Crystals*, John Wiley & Sons, Inc., New York, N.Y., (1984)

[22] H. Nishihara, M. Haruna, T. Suhara, *Optical Integrated Circuits*, McGraw-Hill Book Company, (1989)

[23] T. Tamir (Ed), *Guided-Wave Optoelectronics* (second Edition), Springer-Verlag, (1990)

[24] D.Marcuse, "Directional couplers made of nonidentical asymmetric slabs, Part II: grating assisted couplers," Journal of Lightwave Technology, Vol. 5, No. 2, (1987) pp. 268 - 273

[25] Y. Cai, T. Mizumoto, Y. Naito, "Improved perturbation feedback method for the analysis of rectangular dielectric waveguides," Journal of Lightwave Technology, Vol. 9, No. 10, (1991) pp. 1231 - 1237

[26] T. Suhara, S. Fujiwara, and H. Nishihara, "Proton-exchanged fresnal lenses in Ti:$LiNbO_3$ waveguides," Applied Optics, Vol. 25, No. 19, (1986) pp. 3379 - 3383

[27] T. Findakly and M. Bramson, "High-performance integrated-optical chip for a broad range of fiber-optic gyro applications," Optics Letters, Vol. 15, No. 12, (1990) pp. 673 - 675

[28] M. De Micheli, J. Botineau, S. Neveu, P. Sibillot, D.B. Ostrowsky, M. Papuchon, "Extension of second-harmonic phase-matching range in lithium niobate guide," Optics Letters, Vol. 8, No. 2, (1983) pp. 116 - 118

[29] J L. Jackel, C.E. Rice and J.J. Veselka, "Composition control in proton-exchanged $LiNbO_3$," Electronics Letters, Vol. 19, No. 10, (1983) pp. 387 - 388

[30] M. Goodwin and C. Stewart, "Proton-exchanged optical waveguides in Y-cut lithium niobate," Electronics Letters, Vol. 19, No. 6, (1983) pp. 22? - 225

[31] A. Campari, C. Ferrari, et. al., "Strain and surface damage induced by proton

exchange in Y-cut $LiNbO_3$," Journal of Applied Physics, Vol. 58, No. 12, (1985) pp. 4521 - 4524

[32] M. De Micheli, J. Botineau, S. Neveu, P. Sibillot, D.B. Strowsky, and M. Papuchon, "Independent control of index and profiles in proton exchanged $LiNbO_3$ guides," Optics Letters, Vol. 8, (1983) pp. 114 - 115

[33] V. Hinkov and E. Ise, "Control of birefringence in Ti:$LiNbO_3$ optical waveguide by proton exchange of lithium ions," Journal of Lightwave Technology, Vol. 4, No. 4, (1986) pp. 444 - 448

[34] P.G. Suchoski, T. Findakly, and F.J. Leonberger, "Stable low loss proton exchange $LiNbO_3$ waveguides with low electro-optic degradation," Optics Letters, Vol. 13, No.11, (1986) pp. 1050 - 1052

[35] A. Loni, G. Hay, R.M. De La Rue, and J.M. Winfield, "Proton-exchanged $LiNbO_3$ waveguides: the effects of post-exchange annealing and buffered melts as determined by infrared spectroscopy, optical waveguide measurements, and hydrogen isotropic exchange," Journal of Lightwave Technology, Vol. 7, No. 6, (1989) pp. 911 - 919

[36] M.J. Li, M. Demichelli, D.B. Ostrowski and M. Papuchon, "High index low loss $LiNbO_3$ waveguides," Optical Communications, Vol.62, No.1, (1987) pp. 17-20

[37] A. Loni, "Proton-exchanged $LiNbO_3$ waveguides come of age," Laser Focus World, Vol. 27, No. 4, (1991) pp. 183 - 188

[38] N. Goto and G.L. Yip, "Characterization of proton-exchange and annealed $LiNbO_3$ waveguides with pyrophosphoric acid," Applied Optics, Vol. 28, No.

1, (1989) pp. 60 - 65

[39] S.I. Najafi, R. Srivastava and V. Ramaswamy, "Wavelength dependent propagation characterization and mode cutoff in silver ion exchanged planar waveguides," Applied Optics, Vol. 25, No. 11, (1986) pp. 1848 - 1843

[40] J.M. White and P.F. Heidrich, "Optical waveguide refractive index profile determined from measurement of mode indices: a simple analysis," Applied Optics, Vol. 15, No. 1, (1976) pp. 151 - 155

[41] P. Hertel and H.P. Menzler, "Improved inverse WKB Procedure to reconstruct refractive index profiles of dielectric planar waveguides," Applied Physics B, Photophysics and Laser Chemistry, Vol. 44, (1987) pp. 75 - 80

[42] A.N. Kaul and K. Thyagarajan, "Inverse WKB method for refractive index profile estimation of monomode graded index planar optical waveguides," Optics Communications, Vol. 48, No. 5, (1984) pp. 313 - 316

[43] M.C. Hutley, *diffraction Grating*, New York, Academic Pres., (1982)

[44] M.J. Li, W.J. Wang, S.I. Najafi, J. Albert and K.O. Hill, "Glass waveguides with grating," *Proceedings First International Workshop in Photonics Networks, Components and Applications*, World Scientific, New Jersey, (1991) pp. 218 - 222

[45] S. Akiba and H.A. Haus, "Variational analysis of optical waveguides with rectangular cross section," Applied Optics, Vol. 21, No. 5, (1982) pp. 804 - 807

Appendix

Wave equations of E^x_{pq} and E^y_{pq} modes in channel waveguides

In Marcatili's method, the solution of a rectangular channel waveguide is assumed to be the superposition of the solutions of two orthogonal slab waveguides. The wave equations of these two slab guides can be derived and obtained from Maxwell's equations. A structure of a channel waveguide with three *biaxially anisotropic* regions in the *principal* axes coordinate system as in Fig. 2.3 is considered here. The permittivity tensor of each region is *diagonal*,

$$[\varepsilon] = \varepsilon_0 \begin{bmatrix} \varepsilon_{xx} & 0 & 0 \\ 0 & \varepsilon_{yy} & 0 \\ 0 & 0 & \varepsilon_{zz} \end{bmatrix} = \varepsilon_0 \begin{bmatrix} n_{xx}^2 & 0 & 0 \\ 0 & n_{yy}^2 & 0 \\ 0 & 0 & n_{zz}^2 \end{bmatrix} \tag{A.1}$$

where ε_{ii} (i = x, y, z) are relative permittivity and n_{ii} (i = x, y, z) are refractive indices in x, y, z directions, respectively. A plane wave propagating along the z axis can be described by the characteristic equation

$$\begin{bmatrix} k_0^2 n_{xx}^2 - k_y^2 - k_z^2 & k_x k_y & k_x k_z \\ k_y k_x & k_0^2 n_{yy}^2 - k_x^2 - k_z^2 & k_y k_z \\ k_z k_x & k_z k_y & k_0^2 n_{zz}^2 - k_x^2 - k_y^2 \end{bmatrix} \begin{bmatrix} E_x \\ E_y \\ E_z \end{bmatrix} = 0 \qquad \text{(A.2)}$$

where k_x, k_y and k_z are the propagation constants in the x, y and z directions, respectively. The dispersion relation can be found by setting the determinant of the matrix in (A.2) to zero. Thus

$$\det \begin{vmatrix} k_0^2 n_{xx}^2 - k_y^2 - k_z^2 & k_x k_y & k_x k_z \\ k_y k_x & k_0^2 n_{yy}^2 - k_x^2 - k_z^2 & k_y k_z \\ k_z k_x & k_z k_y & k_0^2 n_{zz}^2 - k_x^2 - k_y^2 \end{vmatrix} = 0 \qquad \text{(A.3)}$$

Expanding (A1.3) one obtains a solution for k_z in terms of k_x and k_y

$$k_z^2 = \frac{1}{2n_{zz}^2}\left\{-\left(n_{xx}^2+n_{zz}^2\right)k_x^2 - \left(n_{yy}^2+n_{zz}^2\right)k_y^2 + \left(n_{xx}^2+n_{yy}^2\right)k_0^2 n_{zz}^2 \right. \qquad \text{(A.4)}$$
$$\left. \pm \left[\left(n_{xx}^2-n_{zz}^2\right)k_x^2 + \left(n_{yy}^2-n_{zz}^2\right)k_y^2 - k_0^2 n_{zz}^2\left(n_{xx}^2-n_{yy}^2\right)\right]\right\}$$

The dispersion relation for TE mode is obtained by taking the plus sign in (A.4). The result is

$$\left(k_z^2\right)_{TE} = k_0^2 n_{yy}^2 - k_x^2 - k_y^2 \qquad \text{(A.5)}$$

The dispersion relation for TM mode is obtained by taking the minus sign in (A.4). The result is

$$\left(k_z^2\right)_{TM} = k_0^2 n_{xx}^2 - \frac{n_{xx}^2}{n_{zz}^2} k_x^2 - \frac{n_{yy}^2}{n_{zz}^2} k_y^2 \qquad \text{(A.6)}$$

We shall assume wave propagation in the z direction, $\partial/\partial z = -j\beta$, and a $e^{j\omega t}$ harmonic time dependence, $\partial/\partial t = j\omega$. With these assumptions, the time independent Maxwell equations in a nonmagnetic dielectric can be expanded as

$$\frac{\partial E_z}{\partial y} + j\beta E_y = -j\omega\mu_0 H_x \qquad \text{(A.7)}$$

$$j\beta E_x + \frac{\partial E_z}{\partial x} = j\omega\mu_0 H_y \tag{A.8}$$

$$\frac{\partial E_y}{\partial x} - \frac{\partial E_x}{\partial y} = -j\omega\mu_0 H_z \tag{A.9}$$

$$\frac{\partial H_z}{\partial y} + j\beta H_y = j\omega\varepsilon_0\varepsilon_{xx}E_x \tag{A.10}$$

$$j\beta H_x + \frac{\partial H_z}{\partial x} = -j\omega\varepsilon_0\varepsilon_{yy}E_y \tag{A.11}$$

$$\frac{\partial H_y}{\partial x} - \frac{\partial H_x}{\partial y} = j\omega\varepsilon_0\varepsilon_{zz}E_z \tag{A.12}$$

The field expressions given by E_x and E_y are obtained from (A.9)

$$H_z = \frac{1}{j\omega\mu_0}\left(\frac{\partial E_x}{\partial y} - \frac{\partial E_y}{\partial x}\right) \tag{A.13}$$

from (A.10) and (A.13)

$$H_y = \frac{\omega\varepsilon_0 n_{xx}^2}{\beta}E_x + \frac{1}{\beta\omega\mu_0}\left(\frac{\partial^2 E_x}{\partial y^2} - \frac{\partial^2 E_y}{\partial x\partial y}\right) \tag{A.14}$$

from (A.11) and (A.14)

$$H_x = -\frac{\omega\varepsilon_0 n_{yy}^2}{\beta}E_y + \frac{1}{\beta\omega\mu_0}\left(\frac{\partial^2 E_x}{\partial x\partial y} - \frac{\partial^2 E_y}{\partial x^2}\right) \tag{A.15}$$

and from (A.11) and (A.14), (A.15)

$$E_z = \frac{n_{xx}^2}{j\beta n_{zz}^2}\frac{\partial E_x}{\partial x} + \frac{n_{yy}^2}{j\beta n_{zz}^2}\frac{\partial E_y}{\partial y} \tag{A.16}$$

Two groups of the field expressions can be found, one is the E^x_{pq} modes which is polarized predominantly in the x direction, the principal transverse field components are E_x and H_y with $E_y \approx 0$. The

other one is called E^{y}_{pq} which is polarized predominantly in the y direction, and its principal field components being E_y and H_x with $E_x \approx 0$. In both cases the subscripts referring to the x and y directions, respectively. It is important to note that E^{x}_{pq} and E^{y}_{pq} are hybrid modes. When the waveguide width is infinite, the rays progress in the z direction and the guided modes correspond to TM and TE modes. When the waveguide width is finite, the rays progress at a certain angle to the z axis and the guided modes are hybrid modes that combine the TE mode and TM mode.

E^{x}_{pq} modes

For E^{x}_{pq} modes, we can let $E_y = 0$, and obtain the field expressions from (A.13) - (A.16) those depend on E_x

$$E_z = \frac{n_{xx}^2}{j\beta n_{zz}^2}\frac{\partial E_x}{\partial x} \tag{A.17}$$

$$H_y = \frac{1}{\beta\omega\mu_0}\left(k_0^2 n_{xx}^2 E_x + \frac{\partial^2 E_x}{\partial y^2}\right) \tag{A.18}$$

$$H_z = \frac{1}{j\omega\mu_0}\frac{\partial E_x}{\partial y} \tag{A.19}$$

$$H_x = \frac{1}{\beta\omega\mu_0}\frac{\partial^2 E}{\partial x \partial y} \tag{A.20}$$

When the waveguide width is infinite, $\partial/\partial y = 0$, this leads TM mode which has three nonzero electromagnetic field components H_y, E_x and E_z. Substituting (A.17) and (A.19) into (A.8) we obtain the Helmholtz equation for E_x

$$\frac{n_{xx}^2}{n_{zz}^2}\frac{\partial^2 E_x}{\partial x^2} + \frac{\partial^2 E_x}{\partial y^2} + \left(k_0^2 n_{xx}^2 - \beta^2\right)E_x = 0 \tag{A.21}$$

Because the Marcatili's approximation is used in the analysis of channel waveguide, the channel waveguide

is subdivided into two slab guides as shown in Fig. 2.5. Let

$$n_{xx}^2 = \left(n_{xx}^x\right)^2 + \left(n_{xx}^y\right)^2 - n_{fxx}^2 \tag{A.22}$$

$$n_{zz}^2 = \left(n_{zz}^x\right)^2 + \left(n_{zz}^y\right)^2 - n_{fzz}^2 \tag{A.23}$$

From (A.6) the propagation constant is

$$\beta^2 = k_0^2 n_{xx}^2 - \frac{n_{xx}^2}{n_{zz}^2} k_x^2 - \frac{n_{yy}^2}{n_{zz}^2} k_y^2 \tag{A.24}$$

k_x and k_y are obtained which are depended on propagation constants in x and y slab guides by letting k_y = 0 in x guide

$$k_x^2 = k_0^2 n_{zz}^2 - \frac{n_{zz}^2}{n_{xx}^2}(\beta^x)^2 \tag{A.25}$$

and letting k_x = 0 in y slab guide

$$k_y^2 = k_0^2 \left(n_{xx}^y\right)^2 \frac{\left(n_{zz}^y\right)^2}{\left(n_{yy}^y\right)^2} - \frac{\left(n_{zz}^y\right)^2}{\left(n_{yv}^y\right)^2}(\beta^y)^2 \tag{A.26}$$

Substituting (A.25) and (A.26) into (A.24)

$$\beta^2 = (\beta^x)^2 + (\beta^y)^2 - k_0^2 n_{fxx}^2 \tag{A.27}$$

where superscripts x and y refer to x and y slab guides. Substituting (A.22) - (A.24) into (A.21),

$$\frac{\left(n_{xx}^x\right)^2 + \left(n_{xx}^y\right)^2 - n_{fxx}^2}{\left(n_{zz}^x\right)^2 + \left(n_{zz}^y\right)^2 - n_{fzz}^2} \frac{\partial^2 E_x}{\partial x^2} + \frac{\partial^2 E_x}{\partial y^2} + \left[k_0^2 \left(n_{xx}^x\right)^2 - \beta_x^2\right] E_x + \left[k_0^2 \left(n_{xx}^y\right)^2 - \beta_y^2\right] E_x = 0 \tag{A.28}$$

Considering that the increase of the index is small compared to the value of the index, i.e. that $n^2_{xx} >> (n^2_{xx} - n^2_{fxx})$, $n^2_{zz} >> (n^2_{zz} - n^2_{fzz})$, (A.26) is rewritten as

$$\frac{(n_{xx}^x)^2}{(n_{zz}^x)^2}\left\{\frac{\partial^2 E_x}{\partial x^2}+\frac{(n_{zz}^x)^2}{(n_{xx}^x)^2}\left[k_0^2(n_{xx}^x)^2-(\beta^x)^2\right]E_x\right\}+\frac{\partial^2 E_x}{\partial y^2}+\left[k_0^2(n_{xx}^y)^2-(\beta^y)^2\right]E_x=0 \qquad \text{(A.29)}$$

By using separation of variables,

$$E_x(x,y) = e_x^x(x)\,e_x^y(y) \qquad \text{(A.30)}$$

and setting the two terms of (A.29) to equal to zero separately, we get the reduced Helmholtz equations for $e_x^x(x)$ and $e_x^y(y)$, namely

$$\left[\frac{d^2}{dx^2}+\left(k_0^2(n_{zz}^x)^2-\frac{(n_{zz}^x)^2}{(n_{xx}^x)^2}(\beta^x)^2\right)\right]e_x^x(x) = 0 \quad \text{(in x slab)} \qquad \text{(A.31)}$$

and

$$\left[\frac{d^2}{dy^2}+\left(k_0^2(n_{xx}^y)^2-(\beta^y)^2\right)\right]e_x^y(y) = 0 \quad \text{(in y slab)} \qquad \text{(A.32)}$$

The propagation constant of channel waveguide can be found either from (A.6) or (A.27) above.

E^y_{pq} modes

For E^y_{pq} modes, following the similar procedures, we can let $E_x = 0$ and obtain the expressions from (A.13) - (A.16)

$$H_x = -\frac{1}{\beta\omega\mu_0}\left(k_0^2 n_{yy}^2 E_y+\frac{\partial^2 E_y}{\partial x^2}\right) \qquad \text{(A.33)}$$

$$H_y = -\frac{1}{\beta\omega\mu_0}\frac{\partial^2 E_y}{\partial x\partial y} \qquad \text{(A.34)}$$

$$H_z = -\frac{1}{j\omega\mu_0}\frac{\partial E_y}{\partial x} \tag{A.35}$$

$$E_z = \frac{n_{yy}^2}{j\beta n_{zz}^2}\frac{\partial E_y}{\partial y} \tag{A.36}$$

When the waveguide width is infinite, $\partial/\partial y = 0$, this leads TE mode which has three nonzero electromagnetic field components E_y, H_x and H_z. Substituting (A.33), (A.36) into (A.8) yields the Helmholtz equation

$$\frac{\partial^2 E_y}{\partial x^2} + \frac{n_{yy}^2}{n_{zz}^2}\frac{\partial^2 E_y}{\partial y^2} + \left(k_0^2 n_{yy}^2 - \beta^2\right)E_y = 0 \tag{A.37}$$

Using variable and index separation, and letting

$$\beta^2 = (\beta^x)^2 + (\beta^y)^2 - k_0^2 n_{fyy}^2 \tag{A.38}$$

we get the reduced Helmholtz equations for $e_y^x(x)$ and $e_y^y(y)$, namely

$$\left[\frac{d^2}{dx^2} + \left(k_0^2\left(n_{yy}^x\right)^2 - (\beta^x)^2\right)\right]e_y^x(y) = 0 \qquad \text{(in x slab)} \tag{A.39}$$

and

$$\left[\frac{d^2}{dy^2} + \left(k_0^2\left(n_{zz}^y\right)^2 - \frac{\left(n_{zz}^y\right)^2}{\left(n_{xx}^y\right)^2}(\beta^y)^2\right)\right]e_y^y(x) = 0 \qquad \text{(in y slab)} \tag{A.40}$$